The Molecular Mechanisms That Underlie Neuron Morphogenesis

by

Macy W. Veling

A dissertation submitted in partial fulfillment
of the requirements for the degree of
Doctor of Philosophy
(Cellular and Molecular Biology)
in the University of Michigan
2019

Doctoral Committee:

Associate Professor Bing Ye, Chair
Associate Professor Scott Barolo
Assistant Professor Dawen Cai
Associate Professor Catherine Collins
Associate Professor Cheng-Yu Lee

Macy W. Veling

wenqianz@umich.edu

ORCID iD: 0000-0001-8518-8724

© Macy W. Veling 2019

Dedication

To my beloved husband and our family.

Acknowledgements

I would like to thank my mentor, Dr. Bing Ye, for his guidance, patient and support throughout my Ph.D. training period. Bing is an excellent mentor who taught me how to pursue the highest standards of research from bench work, to grant writing, to manuscript preparation, to public presentation and so on. He always patiently listened to my opinions and guided me through many challenges I have faced in the past several years. I truly appreciated your mentorship for making me an independent researcher. Thank you Bing!

I would like to thank my committee members, Drs. Scott Barolo, Dawen Cai, Catherine Collins, and Cheng-yu Lee. Thank you all for being so helpful and supportive. I sincerely appreciate you all for providing me feedback and positive motivation during my committee meeting in the past years. Your invaluable contribution shed light on me and kept me go on forward to achieve my goal. Thank you Scott for always keeping me posed about student rights and events on and outside campus. Thank you Cathy for your advice at the joint lab meetings I present. Thank you Dawen for being a great collaborator and letting me use your lab equipment often. Thank you Cheng-yu for sharing your lab space, reagents, and letting me show up at your office with random questions all the time. Thank you very much!

I would like to thank past and present members of the Bing Ye Lab for their inputs in experimental planning and troubleshooting, and for their help in taking care of my samples while I was traveling.

I would like to thank my program CMB for their support in academics and personals.

I would like to thank my best friends, Anabel Flores Arenas, Brittany Flores, Sierrah Grigsby, Yajia Zhang, Xiaoxue Zhang, Hao Liu, Ruonan Li, Yujia Hu, Takuya Kaneko, and those back home, for their support in science and in life during my time at the University of Michigan.

I would like to thank my past research PI and mentors from University of Massachusetts Amherst, Dr. Daniel Hebert, who sparked my interest in research and has always been supportive since then. Dr. Kristina Giorda, who taught me how to work at the bench and encouraged me when experiments didn't work. I would not have a chance to pursue a Ph.D. without their guidance and support.

I would like to thank my now husband Mike for all the hard work he has done to keep us moving forward in science and in life. Besides being a good husband, Mike is my life time mentor and an excellent collaborator. When I struggled in research, he always had provided professional advices to help me solve problems. I am so glad that science is one of our common interests that keep us together despite we have different cultural backgrounds and long distance for six years. Lastly, I would like to thank my parents, my parents-in-law and our relatives who have been greatly supportive to me and Mike all the time. I am so thankful to have you all be part of my life.

The work for my dissertation was supported by NIH grants R01MH091186, R01MH112669, R21MH106151, T32GM007315 and F31NS100391; Rackham graduate student research grant, Rackham 2016 Spring/Summer Award, Rackham and CMB conference grants, and T21RS 2019 conference travel award.

Table of Contents

Dedication ..... **ii**

Acknowledgements ..... **iii**

List of Figures ..... **vii**

Abstract ..... **ix**

Chapter 1 Introduction **1**

1.1 The development of *Drosophila* peripheral nervous system **1**

1.1.1 Sensory organ formation in Drosophila *2*

1.1.2 Timing of proneural genes expression is essential for proper lineage formation *5*

1.1.3 Multispectral labeling tools for studying lineage in Drosophila *6*

1.2 The cell biology of dendritic branching and regulation **9**

1.2.1 Microtubule organization in neurons *10*

1.2.2 Dynein-dependent and Golgi outposts trafficking controls dendritic branching *11*

1.2.3 Transcriptional controls of dendritic morphologies *12*

1.3 The cell biology of axonal branching and regulation **15**

1.3.1 Actin organization in axon *15*

1.3.2 Membrane trafficking controls axon growth *17*

1.3.3 Extracellular cues in axon branching *19*

Chapter 2 The Krüpple-like factor Dar1 determines multipolar neuron morphology **24**

2.1 Abstract **24**

2.2 Introduction **25**

2.3 Results and Discussion 26

2.4 Materials and Methods 35

Chapter 3 Identification of neuronal lineages in the *Drosophila* peripheral nervous system with a novel multi-spectral lineage tracing system 47

3.1 Abstract 47

3.2 Introduction 48

3.3 Results and Discussion 50

3.4 Materials and Methods 61

Chapter 4 Functional interactions between Down syndrome genes in axon development .. 82

4.1 Abstract 82

4.2 Introduction 82

4.3 Results and discussion 84

4.4 Materials and Methods 87

Chapter 5 Conclusions and future directions 99

Bibliography 114

List of Figures

Figure 2.1 Dar1 is required for multipolar neuronal morphology but not cell fates in postmitotic neurons. 40

Figure 2.2 Dar1 requires the dynein complex to induce multipolar morphology of neurons. 42

Figure 2.3 Nuclear positioning complex is required for multipolar morphology of neurons. 44

Figure 2.4 Dar1 requires nuclear positioning complex to induce multipolar morphology of neurons. 46

Figure 3.1 Design and color-coding principles of *nBitbow*. 69

Figure 3.2 Labeling and lineage tracing efficacy of *nBitbow* in *Drosophila* nervous system. 71

Figure 3.3 *nBitbow* efficiently identifies neuronal lineages of *Drosophila* PNS neurons. 73

Figure 3.4 PNS lineage maps revealed by *nBitbow* at different developmental times. 74

Figure 3.5 Lineage tracing by *nBitbow* confirms some previously reported lineages. 75

Figure 3.6 Lineage tracing by *nBitbow* rejects some previously reported lineages. 77

Figure 3.7 *nBitbow* provides an efficient way to compare the birth-time of neurons in different lineages. 78

Figure 3.8 Multipolar neurons arising from different lineages express the morphological terminal selector gene *dar1* through different combinations of *cis*-regulatory elements. 80

Figure 3.9 Identification of the cis-regulatory elements of *dar1* expression by using GFP reporters. 81

Figure 4.1 Appl promotes axon terminal growth in C4da sensory neurons. 91

Figure 4.2 Co-overexpression of Dscam and Appl shows additive effect on C4da presynaptic arbor growth. 93
Figure 4.3 Appl requires Dscam to promote presynaptic arbor growth. 94
Figure 4.4 Dscam does not require Appl to promote presynaptic arbor growth..... 95
Figure 4.5 Appl overexpression increases endogenous Dscam levels in neurons. 96
Figure 4.6 Dscam overexpression does not affect Appl levels in neurons. 97
Figure 4.7 Appl does not regulate *dscam* transcript levels. 98
Figure 5.1 Proposed model of how dendrite-nucleus coupling occurs to promote formation of multipolar morphology in neurons..... 110
Figure 5.2 Lineage tracing of Basin neurons. 111
Figure 5.3 Dscam expression level driven by the Gal4/UAS system with 1:1 ratio. 112
Figure 5.4 Working model of axon development in normal and Appl overexpression conditions. 113

Abstract

Morphological development of neurons is critical for neural circuit formation. Interestingly, the morphologies of all neurons belong to several common types that are conserved across animal species. These basic morphologies, including multipolar, bipolar, and unipolar, are defined by the number of primary dendrites connected from the cell body. The mechanisms that determine basic morphologies among neurons from different lineages remain unknown. Besides dendrites, neurons typically have a single axon that projects away from the somatodendritic compartment. Although the developmental processes of dendrite and axon and their regulations share many similarities, the morphogenesis of each of these compartments involves differential regulations by genes. Dysregulated levels of these genes could cause morphological changes of neurons, and therefore may lead to neurological disorders. For example, trisomy 21, the causative genetic disorder in Down syndrome (DS), leads to upregulation of the expression of many genes, some of which affect the same aspect of axon morphogenesis. It is unclear whether these DS genes interact with each other to cause neuronal defects in DS, and if so, how. Here, my dissertation aims to address three aspects of neuronal morphogenesis. First, I demonstrate the *dar1* gene as a key determinant of the multipolar morphology of neurons. Second, I elucidate the lineage relationships of all multipolar neurons in the *Drosophila* peripheral nervous system (PNS) with a new multicolor labeling system, which enables me to investigate how neurons from different lineages control the same basic morphological program. Lastly, I illustrate that two cell adhesion DS proteins, each of which contributes to the same morphological changes in axon, interact in the genetic and cellular levels, suggesting a potential mechanism behind the morphological

abnormality in DS neurons. Taken together, these findings provide new understandings in the basic morphological types selection in dendritic morphogenesis and the abnormality in axonal morphogenesis caused by dysregulation of functional similar DS factors. This observation also highlights the polygenic nature of DS, clearly demonstrating that multiple DS related genes converge onto the same morphological features. Also, this study delivers a new multicolor labeling system with high efficiency and accuracy for studying lineages, which is suitable in other tissue systems, in addition to the complete *Drosophila* PNS lineage map, which can be applied to study biological questions in the lineage related context.

Chapter 1 Introduction

The nervous system is a network of nerve and specialized cells that coordinates sensory information and actions by transferring signals to and from different parts of the body. Disruption of the neural circuit caused by developmental defects, diseases, or injury, can lead to severe impacts in life quality and style. In order to develop clinical supports and treatments to fight against neural disorders or repair damaged nervous system, it is crucial to first understand the basics of nervous system development. One option is to understand the lineage patterning and cell type specification during development because lineage is the fundamental frame work that builds a nervous system. Another option is to understand the differential regulations of both the dendritic and axonal compartments inside a single neuron. Formation of proper morphology in each compartment is what allows neurons to integrate themselves into a fully functional nervous system.

1.1 The development of *Drosophila* peripheral nervous system

The nervous system of both vertebrates and invertebrates consist of the central nervous system (CNS) and the peripheral nervous system (PNS). Although the nervous system of vertebrates contain more multipolar neurons whereas invertebrates contain more unipolar neurons, the neuronal organization, cell type, and function in CNS and PNS are evolutionary similar between the two types (Ramón y Cajal, 1995; Schmidt-Rhaesa et al., 2015). This makes invertebrate, such as *Drosophila*, a great model for investigating nervous system development because the number

of neurons and the size of nervous system are smaller, in additional to the wide choices in tools for genetic manipulations.

1.1.1 Sensory organ formation in Drosophila

The insect sensory nervous system is used to receive and pass sensory information from environment to the CNS, and to promote appropriate larval and adult behaviors, which is essential for survival in the wild. In *Drosophila*, the PNS is organized into repeated sets of hemi-segments (e.g. 3 thoracic and 8 abdominal segments on each side) on the body wall. In each hemi-segment, the number, types, and location of neurons are identical (Singhania and Grueber, 2014). The PNS is made up of different types of sensory organs, including external sensory (es) organ with or without multidendritic (md) neurons, chordotonal (ch) organ, and those involve md neurons only. During embryogenesis, many sensory organ precursor cells (SOPs) delaminated from ectoderm undergo a few round of asymmetric cell division to eventually give birth to different types of sensory neurons and other non-neuronal cells (Ghysen and Dambly-Chaudiere, 1989).

Formation of SOPs is best studied in the es organs, and it involves two key steps. First of all, proneural fields are established by a group of ectodermal cells expressing the bHLH family proneural genes, *achaete* (*ac*), *scute* (*sc*), *lethal of scute* (*l'sc*) and *asense* (*ase*), of the Achaete-Scute Complex (AS-C) (Campuzano and Modolell, 1992; Ghysen and Dambly-Chaudiere, 1989; Romani et al., 1989). These four genes form the AS-C complex, and have overlapping but distinct loss of function phenotypes (Brand et al., 1993; Domínguez and Campuzano, 1993; Hinz et al., 1994; Jan and Jan, 1994; Rodriguez et al., 1990). Of these four genes, *ac* and *sc* are the essential ones for es organ formation. For example, loss of both *ac* and *sc* causes failure of major

es organs formation in adult flies. By contrast, ectopic es organs are formed when Ac or Sc is misexpressed (Rodriguez et al., 1990). This provides an example showing the redundancy of gene functions in SOP formation. As AS-C controls es organ formation, other studies demonstrate that the bHLH gene *atonal* (*ato*) is necessary and sufficient for only ch organ formation (Jarman et al., 1993; Jarman et al., 1994). Disrupting both AS-C complex and *ato* gene functions causes loss of nearly all SOP organs except a few md neurons in each PNS hemi-segment, suggesting additional proneural factor(s) is needed for these md neurons. Later studies reveal that the bHLH gene *absent MD neurons and olfactory sensilla* (*amos*) is required for a few md neurons formation that do not involve in es organs lineage. These findings elucidate that different proneural factors influent specific organ fate determination at the first sign of SOP formation, and yet other proneural factors may be used to specify cell type formation within a SOP lineage (see below).

While proneural field formation of es organs is controlled by AS-C, the immediate step of Notch (N) receptor – Delta (Dl) ligand interaction is essential for promoting one cell to become the SOP among other cells in the field. This N-Dl cell-cell interaction mediates lateral inhibition through a N signal and proneural feedback regulatory loops to promote SOP cell fate choice in one cell among others (Artavanis-Tsakonas and Simpson, 1991; Ghysen et al., 1993; Heitzler and Simpson, 1991; Parks and Muskavitch, 1993). This process occurs as competing cells within the proneural field express similar protein levels of AS-C, N, and Dl at the initial stage. As one cell accumulates higher AS-C protein levels than the neighboring cells over time, this cell will end up with a higher Dl protein level, which is induced by the AS-C complex. As this cell has more Dl ligands that can provide more binding to the N receptors in the neighboring cells, this cell will signal the surrounding cells through the N signaling cascade to therefore

increasing expression of the AS-C suppressor, Enhancer of split Complex E(spl)-C, thus results in the loss of AS-C over time in these surrounding cells. Hence, this proneural feedback loop leads to one cell with higher AS-C level to become an SOP and the surrounding cells with lower AS-C level to retain their original cell identity (Cabrera, 1990; Heitzler et al., 1996; Schweisguth et al., 1996).

Subsequently, the SOP must undergo a series of stereotyped cell division to give rise to es neuron and accessory cells that associated to the sensory organ (Brewster and Bodmer, 1995, 1996). There are two types of embryonic es organ lineages, and both are controlled by the AS-C complex. The first type is that an es SOP gives birth to total four cells including an es neurons, a thecogen/glial cell (known as sheath cell), a trichogen cell (known as shaft cell), and a tormogen cell (known as socket cell). The second type is an es SOP gives birth to total five cells including the same four cells and an extra md neuron (Lai and Orgogozo, 2004). As demonstrated in many studies, the es organ SOP first divides into two progenitor cells PIIa and PIIb. As the PIIa divides into one tormogen cell and one trichogen cell, the PIIb gives arise to one PIIIb progenitor cell, which in the end becomes one es neuron and one thecogen/glial cell, and another cell as a md neuron or it undergoes apoptosis. Nevertheless, both es lineage types have conserved PIIa pattern with differences starting from the PIIb cell division (Fichelson and Gho, 2003; Lai and Orgogozo, 2004; Moore et al., 2002; Orgogozo et al., 2001). Some ch SOPs show similar division pattern as es organs, though they produce different cell types than those in the es organs (Brewster and Bodmer, 1995, 1996). However, many md lineages and some ch lineages, remain unclear, and thus leaving open questions in the neuronal lineages of *Drosophila* PNS. Therefore, this gap in knowledge of PNS lineages prevents studies from doing full comparison of, for

instance, specific neuronal property development in neurons between every lineage in the whole PNS.

1.1.2 Timing of proneural genes expression is essential for proper lineage formation

Proper expression of different proneural genes at different cell division steps are essential for controlling the final fates of neurons and accessory cells in a single lineage. For examples, a homeoprotein transcription factor Cut is essential for es organ formation. In wild type es organs, Cut is expressed as early as in the first SOP stage of the lineage, and it is absence in any ch organs. Loss of *cut* function in es organ converts the entire es organ to a ch organ, whereas Cut overexpression driven by an early ch SOP-specific driver converts the ch organ to an es organ (Blochlinger et al., 1988; Blochlinger et al., 1990; Blochlinger et al., 1991). These observations indicate that Cut regulates the entire es organ fate selection starting from the very beginning of the SOP lineage. *Prospero* (*pros*), another homeoprotein transcription factor, is essential for cell fate determination in part of the es lineage. Pros is first observed expression in the PIIb just prior to its division and is absence in the PIIa of an es lineage (Manning and Doe, 1999). Loss of *pros* function in es organ sometimes converts the PIIb to a “PIIa”-like fate, leading to two identical sets of PIIa daughter cells in the lineage, or sometimes one daughter cell from the PIIb becomes a different cell type without affecting the identity of its sibling cell (Manning and Doe, 1999). On the other hand, Pros overexpression driven by an early es SOP-specific driver converts the PIIa to a “PIIb”-like fate, but the identity of the two daughter cells divided from this “PIIb” is the same, therefore resulting in two asymmetric daughter cells (e.g. one neuron and one sheath cell) from the normal PIIb are and two symmetric daughter cells (e.g. two sheath cells) from the new “PIIb” in a lineage. (Manning and Doe, 1999). These observations indicate that Pros determines

asymmetric cell fate of sibling cells within a SOP lineage, and additional factor(s) may be required to control the final asymmetric division of the “PIIb”. The PRDM family transcription factor *Hamlet* (*ham*) is first expressed in the PIIIb and its two daughter cells, one es neuron and one thecogen/glial cell (Moore et al., 2002). Loss of *ham* converts the es neuron to a md neuron fate and the thecogen/glial cell to a PIIa daughter cell fate. Interestingly, when Ham overexpression is driven by an early es SOP-specific driver, it converts the PIIa to a “PIIIb”-like fate and the single md to an es fate (Moore et al., 2004). However, when Ham overexpression is driven by a PIIb-specific driver, it only converts the md neuron to a es neuron fate. On the other hand, when Ham overexpression is driven by a post-mitotic neuronal driver, it does not alter the md fate except switching the md neuron morphology to a es neuron morphology (Moore et al., 2002). These results indicate that Ham determines the PIIIb-derived fate in the es lineage, and Ham can change neuronal morphology by changing neuronal fate or simply by changing the morphology of the neuron, depending on its expression timing in a lineage.

Taken together, these studies demonstrate that the process of PNS development requires local proneural field formation to promote a single SOP selection, which is mediated by cell-cell competition through a lateral inhibition of N signaling and its proneural feedback regulatory loops among neighboring cells, immediately followed by temporal expression of different proneural genes at specific developmental stages to control proper asymmetric differentiation in a single sensory lineage.

1.1.3 Multispectral labeling tools for studying lineage in Drosophila

The concept of cell lineage has undergone evolution as modern genetic techniques make it possible to trace cell lineages not only based on their physical location but also their gene

expression patterns. The first genetic tool for fate mapping in *Drosophila* was based on experimental generation of flies whose tissues form a mosaic of male and female cells (Sturtevant, 1929). Subsequently, lineage tracing based on genetic recombination has become one of the most popular approaches. Two types of site-specific recombination systems FLP/*FRT* and CRE/*loxP*, in combination of a conditional reporter system (e.g. Gal4/UAS, LexA/LexAop), have been wildly used for cell-type specific manner (Duffy, 2002; Fischer et al., 1988; Golic and Lindquist, 1989; Lai and Lee, 2006; Siegal and Hartl, 1996). Previous identification of SOP lineages in the *Drosophila* PNS was done by heat-shock-induced FLP expression, by removing the FRT-Stop-FRT sequence between the actin promoter and the lacZ gene, to drive lacZ reporter expression in random lineages during early development (Brewster and Bodmer, 1995, 1996). However, the lineage determination with this method is restricted by the physical location of cells, making errors including false negative and false positive types for lineage conclusion are relatively high. For instances, if a cell migrates away from its original birth region, which has been observed in PNS neurons (Lhamo and Ismat, 2015; Salzberg et al., 1994), the cell would not be considered as related to other cells from the same cluster. On the other hand, if nearby cells are born at similar time points and happen often to express reporter at the same time, it would be concluded as lineage related even they are not necessarily to be related. Moreover, the efficiency of this labeling system is low, as more than 5000 embryos were used to map SOP lineages in the PNS (Brewster and Bodmer, 1995).

Modern multicolor labeling systems have further advanced the single reporter system by providing multiple reporters in the form of color variants and preserving the in-situ resolution of lineages, in which sequencing-based techniques would not be able to preserve the in-situ lineage inforamtion. *Brainbow*, the first multi-spectral labeling technology, creates stochastic labeling of

colors in neighboring cells or cell lineages by randomly expressing one of three or four fluorescent proteins (FPs) from a single cassette (Boulina et al., 2013b; Cai et al., 2013; Hadjieconomou et al., 2011; Hampel et al., 2011b; Livet et al., 2007; Pan et al., 2013). To uniquely label more cell lineages, more color variants are needed. Thus, *Brainbow* may not be suitable for studying lineages in a larger scale organism. One option to improve color diversity is to increase the number of *Brainbow* cassettes, and thus creating differential expression levels of FPs. For example, three *Brainbow* cassettes together can create up to 10 colors (Richier and Salecker, 2015a). However, cells do not necessarily express every FP at equal ratio, making color differentiation by FP intensity not always reliable (Cai et al., 2013). Therefore, this strategy is less suitable for studying lineages. Another option to increase color diversity is to use combinatorial labels of *Brainbow* cassettes that express in different subcellular localization of a cell. Genomic integration of two nuclear and two membrane tagged *Brainbows*, each of which carries three FPs, has been used to create up to 48 colors in chick and mouse embryonic brains (Garcia-Moreno et al., 2014; Loulier et al., 2014). This method relies on electroporation to deliver transposase and *Brainbow* cassettes into the cells, however, transposase can integrate various number of targeting cassettes in different cells, making it difficult to estimate the probability of each label combination for quantitative analysis. Generating transgenic animals would solve this problem. For example, the *Raeppli* system allows creation of up to 16 colors by crossing one nuclear and one membrane tagged transgenic flies, each of which carries four FPs (Kanca et al., 2014). But the *Raeppli* strategy requires FLP expression to activate integrase expression, which is necessary for random FP excisions to create color variants (Bateman et al., 2006a; Groth et al., 2004), meaning that this system requires extra time duration to generate color variants. Therefore, it may not be suitable for tracing lineages at the early developmental

stages. Given the limitation that each *Brainbow*-based strategy has, it is urge to create a new system to overcome the limitations including the generation of more color variants with simpler genetic design and the reliability of color differentiation for lineage identification.

In this dissertation, I introduce a new multicolor labeling system, the *nuclear Bitbow* (designed by the Cai lab at the University of Michigan). A single *Bitbow* cassette can generate up to 31 color variants through FLP activation. The *Bitbow* colors are recognized by the random recombination of five FPs that are independent to each other. To demonstrate the utility of *Bitbow* for lineage tracing, I mapped the whole neuronal lineages of the *Drosopihla* PNS. Moreover, I developed statistical methods, which not only consider the frequency of neurons matching colors but also the probability of seeing each color variants, for lineage identification. This work is significant by providing not only a new multicolor labeling system that works effectively for lineage identification, but also a refined PNS lineage map that allowed me to illustrate the complexity of morphological regulation in neurons from different lineages.

1.2 The cell biology of dendritic branching and regulation

A neuron is the basic building block of the nervous system. It is made of dendrite, soma, and axon compartments, and is polarized by receiving information on the soma and dendrites and passing it through axons (Ramón y Cajal, 1995). Understanding how dendrites and axons develop their branches and shapes is important to unravel how neurons integrate themselves into a functional neural circuit.

1.2.1 Microtubule organization in neurons

One cellular hallmark that makes axon different from dendrites in a neuron is the uniform distribution of microtubules, which is the primary building block of dendrites. The best-studied microtubule arrangement is organized by the centrioles. However, in developing or mature *Drosophila* sensory neurons, it seems that the centrosome is not required in maintaining microtubule organization and nucleation, suggesting microtubule is organized independent from centrosome in these neurons (Nguyen et al., 2011). However, whether centrosome associated proteins involve in the microtubule organization and dynamic remains unknown. Microtubules have intrinsic polarity of plus-end and minus-end, with tubulin subunits being added to the growing plus-end side. Early studies in cultured hippocampal neurons reveal that the first process of neurite outgrowth is initiated by microtubule polarization with uniformly plus-end out (Baas et al., 1989). This process then rapidly grows into the axon. Subsequently, the later processes grow into dendrites, where the microtubule distribution contains a mix of both plus-end and minus-end at the proximal dendrites and mainly plus-end out at the distal dendrites (Stepanova et al., 2003; Stone et al., 2008). Invertebrate neurons share similar but not identical roles of microtubule distribution as in vertebrate neurons. The axon of invertebrate neurons has uniformly plus-end out microtubules (Stone et al., 2008). However, in proximal dendrites the microtubule distribution in invertebrate neurons is mainly minus-end out (Ori-McKenney et al., 2012; Stone et al., 2008). These observations suggest that a minus-end out microtubule orientation in dendrites and a plus-end out in axon are the common features, and are evolutionarily conserved in both vertebrate and invertebrate systems.

1.2.2 Dynein-dependent and Golgi outposts trafficking controls dendritic branching

The unique microtubule orientation allows specific microtubule motor proteins to transport cargos in a specific direction. Dynein is the major minus-end-directed microtubule motor protein in dendrites that transports cargos from the soma (Schroer et al., 1989). A dynein complex is made of several subunits including the dynein heavy chain (DHC), dynein light chain (DLC) and light intermediate chain (Dlic). Disruption of dynein complex and dynein cargos affects dendritic morphology. For example, the *Drosophila* dendritic arborization (da) neurons, a subtype of md sensory neurons in the PNS, generally have dendritic branches concentrated at the distal region and less at the proximal region. Disruption of Dlic function in these neurons results in an abnormal shift of dendritic branches from distal region to proximal region. Moreover, disrupting both Dlic and Rab5 proteins, a GTPase that controls the entry of endocytosed cargos into the early endosome, prevent the hyperbranching phenotype seen in *Dlic* mutant neurons (Satoh et al., 2008). This suggests that the endocytic pathway also involves in the dendritic branching process.

The secretory pathway, which refers to the endoplasmic reticulum (ER), Golgi apparatus and the vesicles traveling in between them, contributes important roles in dendritic morphogenesis. In neurons, the somatic Golgi apparatus reorganizes small, isolated stacks of Golgi, called Golgi outposts, are found predominately in dendrites. Such Golgi outposts are functionally conserved for dendritic branching mechanism in both vertebrate and invertebrate (Horton et al., 2005; Ye et al., 2007). For examples, the homolog of mammalian Sec23, Sar1, and Rab1 in *Drosophila* Class IV da (C4da) neurons control dendritic arborization. These proteins are the essential components of Coat protein complex II (COPII) vesicles that mediate ER-Golgi transport. Disruption of these proteins in C4da neurons leads to failure of dendritic branching but has no effect on axonal growth, suggesting the Golgi trafficking is predominately

important for dendritic growth. Moreover, the directional movement of dendritic Golgi outposts has been found to correlate with the dynamics of dendritic outgrowth and retraction. Redistribution of Golgi outposts by disrupting the Lava lamp (Lva)-mediated interaction of Golgi and dynein complex impairs dendritic branching, suggesting the dendritic branching machinery is Golgi transport-dependent. In addition, Golgi outposts contain γ-tubulin and centrosome protein CP309 that both are necessary for Golgi outposts-mediated microtubule nucleation (Ori-McKenney et al., 2012). Disrupting γ-tubulin or CP309 function does not affect the localization of Golgi outposts in dendrites but decreases the overall complexity of dendritic arbor. This elucidates that Golgi outposts direct acentrosomal microtubule nucleation to control dendritic branching.

1.2.3 Transcriptional controls of dendritic morphologies

The morphology of dendritic arbors in different neurons can be diversified but the overall shape can be very consistent. Hence, neurons with similar dendritic arbor shape are often be classified into the same type. In the PNS of *Drosophila*, individual da type sensory neurons are categorized into one of the four classes: class I, II, III, or IV (e.g. C1da, C2da, C3da or C4da), in the order that the complexity of dendritic arbors increases (Grueber et al., 2002). Different transcriptional programs have been found to control da-type-specific morphologies. For examples, the C2H2 zinc finger transcription factor Abrupt is expressed in C1da neurons. Loss of *abrupt* function in C1da neurons leads to increased dendritic arbors, whereas misexpression of Abrupt in other da types results in reduction of dendritic arbor size and branch numbers (Li et al., 2004; Sugimura et al., 2004). By contrast, the transcription factor Cut is absent in C1da but expressed in all other da types with different expression levels, as it is expressed low in C2da, intermediate in C4da, and

high in C3da (Grueber et al., 2003). Loss of *cut* function in C2da or C4da neurons leads to simplification of dendritic arbors, whereas misexpression of Cut in post-mitotic C1da neurons increases the arbor complexity to the extent of C3da-like morphology. This suggests that the expression level of Cut acts as a bidirectional switch to determine the complexity of dendritic arbors among different da types. The function of Cut in dendritic morphogenesis is opposite to the way of transcription factor Ham does, in which Ham alters neuronal fate to cause morphological change (Moore et al., 2002; Moore et al., 2004). Despite the fact that Cut is expressed in both SOP cells and differentiated neurons, the loss- and gain-of-function of *cut* at either SOP cell or post-mitotic neurons demonstrate the functions of Cut in es organ fate identity or the later development of dendritic morphogenesis is developmental stage dependent (Blochlinger et al., 1988; Blochlinger et al., 1990; Blochlinger et al., 1991, 1993; Brewster et al., 2001; Grueber et al., 2003). Moreover, Cut directs the secretory trafficking machinery, via Cyclic-AMP response element binding protein A (CrebA), to positively regulating many COPII secretory pathway proteins, including Sec23 and Sar1, respectively (Fox et al., 2010; Iyer et al., 2013). Again, this demonstrated that the secretory trafficking pathway plays essential roles in dendrite branching, and in part, is controlled by Cut in specific groups of da neurons.

The class-type morphological patterns of da neurons is determined by the combination of intrinsic transcriptional factors (Corty et al., 2009; Dong et al., 2015; Gao, 2007; Grueber and Jan, 2004; Jan and Jan, 2010). For examples, the transcription factor Knot/Collier is selectively expressed in C4da, which is required for their complex dendritic arbor morphology (Crozatier and Vincent, 2008; Hattori et al., 2007). Misexpression of Knot in other da types increases their arbor complexity to gain C4da-like morphology. However, loss of *knot* or *cut* function alone in C4da neurons shows reduction of dendritic branching in both cases, but the phenotypes are

qualitative different, presumably both Knot and Cut may act in combination to promote the proper dendritic arbor morphology in these neurons. Interestingly, Knot and Cut are found to control dendritic arbor cytoskeleton through predominantly parallel pathways, at which Cut promotes actin-based short dendrite extension (known as dendrite spikes) and Knot promotes microtubule-based dendritic arborization. In addition, Knot mediates dendritic branching by inducing expression of the microtubule severing protein Spastin and by repressing the activity of Cut from growing spikes (Jinushi-Nakao et al., 2007). These results suggest that different transcriptional factors function in combination, each of which controls distinct dendritic branching features, to promote da-type-specific morphological patterns. Unlike Abrupt, Cut or Knot, the bHLH transcription factor Spineless is expressed in all PNS neurons including all da types. Spineless has been found to regulate dendritic arborization in all da neurons. However, loss of *spineless* function in different da types exhibits distinct morphological phenotypes by either increasing or decreasing the arbor complexity (Kim et al., 2006). This suggests that other transcription programs may be necessary to control the specific activity of Spineless.

As neurons have various of dendritic morphologies, Santiago Ramón y Cajal, who is considered by many to be the father of modern neuroscience, discovered that all neurons share common morphologies which are universally conserved across different animal species (Ramón y Cajal, 1995). These common morphologies are determined by the number of primary dendrites connected from the soma, as more than one primary dendrites called multipolar neuron, equal to one called bipolar, and having a neurite extended out from soma which then bifurcates into one axon and one dendrite called unipolar. Although Cajal had documented his observation of common morphologies, it was unknown whether any transcriptional programs control the selection of basic morphologies in neurons. In *Drosophila*, multipolar neurons, including md

neurons and its subtypes da, bipolar dendrite (bd), and tracheal dendrite (td) neurons, only present in the PNS. Interestingly, we previously observed that the Krüppel-like transcription factor Dar1, which was found to promote microtubule-based dendrite branching by suppressing the transcription level of Spastin in da neurons (Ye et al., 2011), is selectively expressed in all multipolar neurons.

Given the unique expression pattern of Dar1 in multipolar neurons, we asked whether Dar1 plays role in the basic morphology formation of neurons. My collaborator Dr. Xing Wang showed that Dar1 is necessary and sufficient for the multipolar morphology of neurons. Moreover, we showed that this transcriptional program controlling the basic morphological selection occurs after neuronal fate specification, and loss of *dar1* in da neurons does not alter neuronal fate, except these neurons gradually convert their multipolar shape to bipolar. Furthermore, I demonstrated that specific groups of Dynein proteins and the Nuclear positioning complex involve in the formation of multipolar shape, and Dar1 requires these proteins to promote multipolar morphology in neurons, suggesting a coupling mechanism between primary dendrites and nucleus is required for multipolar shape. Taken together, our findings demonstrated a novel transcriptional program and a coupling mechanism that is important for basic morphological determination in neurons.

1.3 The cell biology of axonal branching and regulation

1.3.1 Actin organization in axon

Actin organization and dynamic are important for neuronal polarization, axon elongation and branching. Actin exists in monomeric (G-actin) or polymerized (F-actin) form that the monomers can spontaneously self-assembly into isolated actin filaments. In neurons, actin filaments

polymerize at the plus-end (barbed end) and depolarize at the minus-end (pointed end), and they do assembly into different higher structural networks, including lamellipodia, filopodia, actin arcs, and cortical actin juxtaposed to the membrane (Lowery and Van Vactor, 2009). In the growth cone of neuron, the plus-end F-actin filament is oriented distally whereas the minus-end is oriented proximally. The growth cone is highly dynamic and being constantly remodeled, which is driven by the actin retrograde flow and protrusion resulted from the total kinetics of polarization and depolarization, in order to direct the movement of growing axon (Lowery and Van Vactor, 2009).

This dynamic process is regulated by different actin-associated proteins that control different events, which is evolutionary conserved in vertebrate and invertebrate (Luo, 2002). One event is actin nucleation. For examples, the first identified factor is the Arp2/3 complex, which initiates axon polymerization from existing filaments to allow actin network generation (Korobova and Svitkina, 2008). Knocking down of Arp2/3 complex by siRNA in cultured rat hippocampal neurons and neuroblastoma cells impair lemellipodia and filopodia formation in the growth cone. Moreover, the activity of Arp2/3 complex is controlled by the elongation factors Ena/WASP which links to extracellular signaling to promote actin polymerization (Chen et al., 2014; Rohatgi et al., 1999). Furthermore, Ena/VASP forms complex with the actin monomer binding protein Profilin at the filament tip to presumably stabilize and facilitate filament growth (Bear and Gertler, 2009; Hopmann and Miller, 2002; Verheyen and Cooley, 1994). Formin, another actin nucleation factor that promotes filaments assembly, is independent from the Arp2/3 complex function. Disrupting Formin function in neurons reduces filopodia number and length, suggesting Formin is required for filament elongation (Evangelista et al., 2002; Matusek et al., 2008; Pring et al., 2003). Another important event for promoting actin polymerization is actin

filament capping. For example, Ena/VASP functions to block the actin capping protein activity, and thus allowing actin filament polymerization to promote axonal growth (Bear et al., 2002; Iwasa and Mullins, 2007; Krause et al., 2003). In addition, the event of disassembly of old F-actin is also important for recycling free actin monomers in order to promote new filament formation. This process is regulated by the actin depolymerizing factor and Cofilin to mediate the severing of old F-actin filaments, and thus to increase the pool of free actin monomers (Gehler et al., 2004). Taken together, these studies demonstrate that actin dynamic is essential for promoting axon growth, and this process of actin filament assembly and disassembly is regulated by distinct factors that act on specific steps.

1.3.2 Membrane trafficking controls axon growth

An additional hallmark that specify axon from dendrites is the presence of a dense F-actin filter barrier at the axon initiation site (AIS) (Lewis Jr et al., 2009; Lewis et al., 2011; Watanabe et al., 2012). In particular, this filter barrier requires the microtubule plus-end directed protein EB3 to connect the microtubules and the actin filaments at the AIS (Leterrier et al., 2011). Moreover, this filter barrier has been suggested for the selection and diffusion of macromolecules and the transport of specific vesicular carriers into axon growth cone to promote axon elongation and branching (Bennett and Baines, 2001; Galiano et al., 2012; Song et al., 2009; Xu et al., 2013).

Unlike dendrites, Golgi outposts has not been found in the axons of both vertebrate and invertebrate neurons, thus membrane components synthesized in the ER for axon development must be transported between the post-Golgi apparatus and the axon through membrane trafficking pathway (Sann et al., 2009; Ye et al., 2007). The Rab GTPase family proteins play essential roles for intracellular trafficking, in both non-neuron and neuronal cells, and have been

found to function in axon specification and outgrowth (Hutagalung and Novick, 2011; Villarroel-Campos et al., 2016). In hippocampus neurons, Rab33a is upregulated during axon outgrowth, and it is preferentially accumulated in the axon by mediating synaptophysin-positive anterograde vesicle transport (Nakazawa et al., 2012). RNAi knock-down of Rab33a inhibits axon formation and outgrowth, by preventing membrane exocytosis of synaptophysin-positive vesicles at the growth cone region. Similarly, another small GTPase Rab10, has shown a polarized distribution in cultured hippocampus neurons (Wang et al., 2011). Rab10 is initially enriched in the axonal growth cone and lately in the distal part of axons, but it is always low or not detected in dendrites. Expression of a dominant-negative form or knocking down with RNAi of Rab10 reduces axonal growth or even leads to absence of axon formation, suggesting Rab10-mediated anterograde trafficking is required for axonal growth.

The unique plus-end microtubule orientation in axons specifies the plus-end directed microtubule motor Kinesin-1 to promote axon growth by accelerating anterograde transport (Vale et al., 1985). Kinesin-1 composes of the kinesin heavy chain (KHC) and kinesin light chain (KLC) subunits (de Cuevas et al., 1992; Gauger and Goldstein, 1993). Disrupting *Klc* function in *Drosophila* motor neurons causes fast axon transport defects, resulting in axonal swellings (Gindhart et al., 1998; Hurd and Saxton, 1996). Similarly, loss of *Khc* function, in *Drosophila* optic lobe neurons, prevents axon outgrowth to some extent (Winding et al., 2016), suggesting Kinesin-1 is necessary for axon development. Moreover, Kinesin-1 is regulated by autoinhibition, which is in part controlled by the JNK pathway kinases (Blasius et al., 2007; Horiuchi et al., 2007; Verhey and Hammond, 2009). Disruption of Kinesin-1 autoinhibition in *Drosophila* da neurons not only leads to Golgi outposts mis-located into the axons, but also enriches Kinesin-1 accumulation in axon terminals (Kelliher et al., 2018). In cultured cerebellar

granule neurons (CGNs), Kinesin-1 is preferentially accumulated in subsets of axonal terminals, and inhibition of Kinesin-1 function enhances retraction of arbor terminals, thus reducing axon terminal growth (Seno et al., 2016). Taken together, these studies demonstrate that both the membrane trafficking pathway and the microtubule plus-end motor protein for fast axonal transport are required for axon growth, and such mechanisms are commonly used in both vertebrate and invertebrate systems.

1.3.3 Extracellular cues in axon branching

Different neurons can use different neurotrophic factors, or a combination of these factors, to promote axon branching and arborization in mouse neurons (Goldberg, 2003). For examples, in mouse the dorsal root ganglion (DRG) neurons use the Brain-derived neurotrophic factor (BDNF) together with the nerve growth factor (NGF) to promote more axon branching than either one alone (Lindsay, 1988; Lindsay et al., 1985). On the other hand, the retinal ganglion cells (RGC) use the combination of BDNF and the ciliary neurotrophic factor (CNTF) to promote more axon growth than either one alone (Goldberg et al., 2002). Although NGF and neurotrophic factors are not present in *Drosophila* or *C. elegans*, these examples demonstrate how axon is regulated by these extracellular factors, and also elucidate the difference between vertebrate and inveterate.

Adhesion and guidance molecules are also involved in axon elongation and branching regulation. For example, the transmembrane receptor Roundabout (Robo) and its ligand Slit are first identified in *Drosophila* as important axon guidance molecule in the CNS, and the function of Slit/Robo in repulsion of axons away from the midline is evolutionary conserved in both vertebrate and invertebrate (Brose et al., 1999; Dickinson and Duncan, 2010; Li et al., 1999;

Rothberg et al., 1988; Seeger et al., 1993). The binding of Slit to Robo causes reorganization of the actin cytoskeleton in axon. Several adaptor proteins that regulate actin polymerization, including Abelson tyrosine kinase (Abl), enabled (Ena), Rho GTPase activating protein (srGAP), Dreadlocks (Dock), and son of sevenless (SOS), interact the cytosolic domain of Robo (Bashaw et al., 2000; Wong et al., 2001; Yang and Bashaw, 2006). Loss of *slit*, *robo*, or *sos* function leads to midline crossing of FasII-positive axons in the ventral nerve core (VNC) of *Drosophila*, whereas loss of *sos* together with *slit* or *robo* causes even stronger midline crossing phenotype, suggesting SOS interacts with Slit and Robo pathway to control axon repulsion at the midline (Yang and Bashaw, 2006). Moreover, Slit/Robo have shown differential regulation of axon arborization in different neuronal types. In mouse brain, Slit/Robo promotes axon elongation and arborization in both DRG and trigeminal ganglion (TG) neurons, but inhibits axon arborization in RGC, suggesting the function of Slit/Robo is cell type dependent.

Cell adhesion can be achieved by binding to factors either in the extracellular matrix (ECM) or by homophilic interaction with surface molecule on other cells. For example, ECM is a complex structure of macromolecules that provides a scaffold for cell adhesion, migration and morphogenesis (Kiryushko et al., 2004). ECM-associated molecules include heparin-binding growth-associated molecules, adhesive glycoproteins, and glycosaminoglycans (Bovolenta and Fernaud-Espinosa, 2000; Giancotti, 1997; Jones and Jones, 2000; Miyamoto et al., 1996; Rauvala and Peng, 1997; Sherman et al., 2002). These ECM molecules are often expressed strongly in the developing brain and they are preferred substrates for inducing neuritogenesis, including axonal and dendritic growths (Bixby and Harris, 1991; Kiryushko et al., 2004). Besides ECM, homophilic interaction of cell adhesion molecules (CAMs) also play important roles in axon growth. For examples, the N-cadherin (CadN), which belongs to the cadherin

superfamily transmembrane protein, is expressed in the nervous system and contributes to axon patterning in *Drosophila* CNS neurons (Iwai et al., 1997). In photoreceptor cells (R cells), CadN is required for R cells to regulate target-specificity by mediating an attractive interaction between R cells and lamina neurons in the targeted area (Lee et al., 2001; Prakash et al., 2005). In olfactory projection neurons, CadN controls axon terminal branching, and loss of *cadN* function results in normal axon growth and guidance to targeted region but reduced axon arborization (Zhu and Luo, 2004). These observations suggest that the function of CadN in axon growth, guidance, or branching is cell-type-specific.

The Down syndrome cell adhesion molecule (Dscam), an Ig superfamily transmembrane protein, has been found to regulate axon guidance and branching (Yamakawa et al., 1998). The *Dscam* gene is located on the human chromosome 21 within the Down syndrome critical region. Studies have shown that Dscam is overexpressed in Down syndrome (DS) mouse brain, and its overexpression may contribute to morphological defects in neurons and impair learning and memory formation in DS adults (Agarwala et al., 2001; Barlow et al., 2001). In *Drosophila*, Dscam generates hundreds and thousands of isoforms and exhibit exquisite binding specificity (Hattori et al., 2008). It exhibits unique homophilic adhesion that mediates repulsion in dendrites or axon to avoid each other in the same class type neurons, and thus allowing these neurons to maximize their synaptic field coverage (Chen et al., 2006; Matthews et al., 2007; Millard et al., 2007). Recent study has demonstrated that Dscam controls axon terminal size in gene-dosage-dependent manner, as loss of *dscam* function reduces axon terminal size and Dscam overexpression leads to terminal overgrowth (Kim et al., 2013). In mice, L1-CAM and neural CAM (NCAM), which are the best studied Ig-CAMs, also control axonal development. Mice lacking L1 show abnormal development of major axonal tracts in the brain and impairment of

learning, which shared similarity to the behavioral abnormalities in human with L1 mutation (Kamiguchi et al., 1998). Besides, mice expressing the extracellular domain of NCAM show abnormal axon arborization in interneurons, which has been linked to human brain disorders including Alzheimer's diseases, bipolar disorder, schizophrenia (Brennaman and Maness, 2010). Taken together, these studies elucidate that Ig-CAM proteins play essential roles in axon morphogenesis, and malfunction or dysregulation of these proteins may contribute to intellectual disability in different brain disorders.

The transmembrane glycoprotein amyloid precursor protein (APP) has been suggested to act as adhesion molecule to regulate axon terminal growth (Sosa et al., 2017). The *APP* gene is also located on human chromosome 21, and is overexpressed in DS mouse brain and human fetal DS brain (Sosa et al., 2013). APP has long been implicated in Alzheimer's diseases (AD), and according to the National Down syndrome society and other studies, DS adults generally develop AD in earlier age than the standard AD adults, and APP is presumably one of the major risk factors contributes to the AD defects (Zigman et al., 2008). However, the functional and physiological roles of APP in neuronal development is not well understood, as compared to the pathogenesis of APP in aging. Recent studies in mouse and *Drosophila* models have demonstrated that disrupting APP or the *Drosophila* homolog of APP (Appl) function in neurons causes axon terminal growth defects, whereas overexpression of APP or Appl leads to axon overgrowth (Leyssen et al., 2005; Mora et al., 2013; Soldano et al., 2013). Moreover, the function of APP in controlling axon morphology is gene-dosage dependent, as similar to Dscam, suggesting APP may contribute to neuronal defects in DS (Sosa et al., 2013). These observations suggest that multiple DS genes maybe functionally similar to act on axon development. Despite the fact that many DS genes are overexpressed at the same time in DS brain, little is known

whether different DS genes work together to govern the same morphological aspect in neuron development.

We pursued to investigate this question by examining whether these two DS genes (*Dscam* and *Appl*) interact to control axon terminal growth in *Drosophila*, and if so, how. This work was inspired from the initial idea from my collaborator Dr. Gabriella Sterne, who observed co-expression of these two genes causes synergistic overgrowth in axon terminal of *Drosophila* sensory neurons. Given such interesting observation, I first confirmed that the function of Appl in axon terminal growth is as similar as Dscam function in the same neuronal type. Next, genetic evidences suggest that Appl requires Dscam, whereas Dscam does not require Appl, to promote axon terminal growth. Furthermore, I found that Appl overexpression alters Dscam protein level through post-transcriptional regulation. Taken together, our findings demonstrate that two DS proteins indeed functionally interact to each other, in which one can affect the other one to modulate axon terminal growth. This also raise the necessity to investigate risk factor interactions in disease with dysregulation of multiple genes.

Chapter 2 The Krüpple-like factor Dar1 determines multipolar neuron morphology

- Journal of Neuroscience, 2015

Co-authored with Xin Wang, Jung Hwan Kim, Ann Marie Macara, Gabriella Sterne, Tao Yang, and Bing Ye.

2.1 Abstract

Neurons typically assume multipolar, bipolar, or unipolar morphologies. Little is known about the mechanisms underlying the development of these basic morphological types. Here, we show that the Krüppel-like transcription factor Dar1 determines the multipolar morphology of postmitotic neurons in *Drosophila*. Dar1 is specifically expressed in multipolar neurons and loss of *dar1* gradually converts multipolar neurons into the bipolar or unipolar morphology without changing neuronal identity. Conversely, misexpression of Dar1 or its mammalian homolog in unipolar and bipolar neurons causes them to assume multipolar morphologies. Dar1 regulates the expression of several dynein genes and *nuclear distribution protein C* (*nudC*), which is an essential component of a specialized dynein complex that positions the nucleus in a cell. We further show that these genes are required for Dar1-induced multipolar neuron morphology. *Dar1* likely functions as a terminal selector gene for the basic layout of neuron morphology by regulating both dendrite extension and the dendrite–nucleus coupling.

2.2 Introduction

Ramon y Cajal placed neurons into three major morphological types based on the number of dendrites connected to the soma (i.e., primary dendrites): unipolar, bipolar, and multipolar and this classification system is universally applicable to different species throughout evolution (Ramón y Cajal, 1995). Multipolar neurons, like mammalian pyramidal neurons, develop more than one primary dendrite. In contrast, bipolar neurons are defined as having a single primary dendrite that may (e.g., cerebellar Purkinje cells) or may not (e.g., photoreceptors) branch out into an elaborate dendritic arbor. Finally, unipolar neurons such as DRG neurons in vertebrates and the majority of CNS neurons in invertebrates extend a single primary neurite, which usually bifurcates into dendritic and axonal branches.

Multipolar morphology separates the dendritic arbor into distinct fields around the soma (Spruston, 2008), which has an impact, not only on the passive current spread and processing of electrical signals in the neuron (Rall, 1964), but also on the types of synaptic or sensory inputs that the neuron receives (Spruston, 2008). In addition, the three basic morphologies of neurons are relevant to the distinct organizational principles used in both the nervous systems of different animal species and in different parts of a single nervous system. Although all three morphological types are found in different species throughout evolution, the majority of neurons in invertebrates are unipolar, whereas the majority of those in vertebrates are multipolar (Grueber et al., 2005; Strausfeld, 1976; Stuart et al., 1999). In the insect CNS, unipolar neurons extend a single process from the soma to a synapse-enriched neuropil and then bifurcate into dendrites that arborize locally and an axon that typically projects to other neuropil areas or target tissues (Strausfeld, 1976). Unipolar organization of neuronal processes allows the formation of synaptic connections away from the location of the neuronal cell body, so it is likely an alternative

strategy for neuronal migration, which is rare in the insect CNS (Harris, 2001) but common in the vertebrate CNS (Hatten, 1999).

Despite the importance of these fundamental organizations of neuronal processes, very little progress has been made toward understanding the molecular and cellular programs that lead postmitotic neurons to develop multipolar, bipolar, or unipolar morphologies since their description a century ago.

In this study, we show that the transcription factor Dar1 determines the multipolar morphology of postmitotic neurons in *Drosophila*. Dar1 is selectively expressed in postmitotic multipolar neurons and is required for these neurons to assume the multipolar morphology. Ectopic expression in unipolar or bipolar neurons leads to multipolar morphology. Dar1 regulates the expression of several dynein genes and *nudC*, which is an essential component of a specialized dynein complex that positions the nucleus in a cell. We further show that this evolutionarily conserved complex is required for multipolar morphology of neurons. These results suggest that *dar1* likely functions as a terminal selector gene for the basic layout of neuron morphology.

2.3 Results and Discussion

Dar1 is required for multipolar morphology in postmitotic neurons

The *Drosophila* nervous system offers a simple platform for studying the mechanisms that underlie the basic morphological types of neurons. In *Drosophila*, the CNS neurons are predominantly unipolar (Grueber et al., 2005; Strausfeld, 1976; Stuart et al., 1999), whereas the PNS neurons are either multipolar or bipolar (Orgogozo and Grueber, 2005). In the PNS, the da

neurons are multipolar (Grueber et al., 2002), whereas the es and chordotonal (ch) neurons are bipolar (Orgogozo and Grueber, 2005).

We previously identified the *dendritic arbor reduction 1* (*dar1*) gene, which encodes a member of the Krüppel-like factor (KLF) family of transcriptional regulators, as a specific regulator of dendritic, but not axonal, growth (Ye et al., 2011). In neurons that lack *dar1* function, total length and branch number of dendrites in da neurons are reduced. Conversely, overexpressing Dar1 in these neurons increases dendrite length and branch number. Strikingly, in the embryonic and larval nervous system, Dar1 was exclusively expressed in multipolar neurons and was undetectable in bipolar and unipolar neurons (Fig. 2.1A, B) (Ye et al., 2011). As a comparison, other transcription factors known to regulate dendritic development in multidendritic (md) neurons, such as Knot, Cut, Abrupt, and Spineless, are expressed either in a subset of or in all PNS and CNS neurons (data not shown) (Crozatier and Vincent, 2008; Grueber et al., 2003; Hattori et al., 2007; Jinushi-Nakao et al., 2007; Kim et al., 2006; Sugimura et al., 2004). The unique and selective expression of Dar1 in multipolar neurons led us to hypothesize that Dar1 determines the multipolar layout of neuronal dendrites.

To test this hypothesis, we first introduced *dar1*-null mutations into single da, es, and ch neurons using the MARCM technique (Fig. 2.1C, D) (Lee and Luo, 1999). The wild-type class I-IV (C1– 4) da neurons typically extend two or three primary dendrites from the soma. In sharp contrast, the majority of *dar1* mutant neurons became bipolar with a single primary dendrite and an axon. Loss of *dar1* even converted some C1da neurons into unipolar morphology (Fig. 2.1C), which was not observed in wild-type neurons. Consistent with the observation that Dar1 is absent in bipolar neurons (Fig. 2.1A) (Ye et al., 2011), bipolar es neurons with *dar1* mutations were unchanged, projecting a single primary dendrite, as was seen in wild-type es neurons (data

not shown). Two different null alleles of *dar1*, $dar1^{3232}$ and $dar1^{3010}$, exhibited similar defects (Fig. 2.1E, F), suggesting that the loss of multipolar morphology in mutant neurons is caused specifically by loss of *dar1*.

Despite their dendritic defects, the axons of mutant neurons were correctly targeted to the C4da neuron-specific neuropil and formed normal terminal branches (Fig. 2.1G) (Yang et al., 2014; Ye et al., 2011). Moreover, Dar1 is expressed in postmitotic neurons after the expression of the neuronal marker Elav started (Fig. 2.1H). Furthermore, neuronal type-specific markers, including Knot (Hattori et al., 2007; Jinushi-Nakao et al., 2007), Cut (Grueber et al., 2003), Abrupt (Sugimura et al., 2004), and Spineless (Kim et al., 2006), were expressed appropriately in $dar1^{-/-}$ da neurons (Fig. 2.1I and data not shown). Therefore, *dar1* functions in postmitotic neurons and loss of *dar1* does not change the type of neurons.

Together, these results demonstrate that Dar1 is required for the multipolar morphology in *Drosophila* neurons.

Misexpression of Dar1 in unipolar neurons induces multipolar morphology

Next, we investigated whether misexpressing Dar1 in unipolar neurons would cause them to assume a multipolar morphology. We overexpressed Dar1 in a small subset of unipolar motor neurons labeled by the *RN2-Gal4* driver ($RN2^+$ neurons) (Fujioka et al., 2003; Ghabrial et al., 2003) and examined their morphology. Dar1-overexpressing $RN2^+$ neurons extended ectopic neurites directly from the soma and consequently became multipolar (Fig. 2.2A, B). The ectopic primary neurites induced by Dar1 misexpression in these neurons were positive for Nod::*β*Gal, a marker that labels subsets of dendritic branches (Zheng et al., 2008). Similarly, misexpression of Dar1 caused the unipolar PDF neurons in adult brain and the bipolar es neurons in larval PNS to

assume multipolar morphology (Fig. 2.2C–E and data not shown). Moreover, overexpressing the mouse homolog of Dar1, KLF7, in larval $RN2^{+}$ neurons and adult PDF neurons also led to a dramatic increase in the number of primary dendrites (Fig. 2.2B–E), suggesting an evolutionarily conserved function of Dar1 and KLF7.

dar1 requires dynein genes to determine multipolar morphology of neurons

How might Dar1 determine multipolar organizations of neuronal processes? To answer this question, we first conducted microarray analysis to identify genes with expression that was regulated by Dar1. Transcripts were extracted from wild-type and $dar1^{-/-}$ PNS neurons purified with FACS and used for microarray analysis. GO-based functional annotation (Huang et al., 2008) of the differentially expressed genes showed that cellular components that were significantly enriched in $dar1^{-/-}$ neurons are mostly related to microtubules (Fig. 2.2F). Strikingly, the transcript levels of several genes in the dynein complex were consistently reduced in *dar1* mutant neurons, which was confirmed by qRT-PCR (Fig. 2.2G). We thus examined the role of the dynein complex in forming the multiple morphology of neurons by suppressing dynein functions with a temperature-sensitive mutant of the dynein intermediate chain *short wing* (*sw*), sw^{ts} (Boylan and Hays, 2002). Rearing $sw^{ts/+}$ larvae at nonpermissive temperatures led to the appearance of bipolar-shaped C1da neurons (Fig. 2.2H), which are virtually absent in wild-type controls, without altering the number of dendritic branches (data not shown).

Next, we tested whether Dar1 requires the dynein complex to induce primary dendrite formation by introducing a heterozygous sw^{ts} mutation in $RN2^{+}$ and PDF neurons that misexpressed Dar1. In animals raised at a nonpermissive temperature, the sw^{ts} mutation potently

reduced the supernumerary primary dendrites induced by Dar1 misexpression (Fig. 2.2I, J), suggesting that *dar1* requires the dynein complex to induce multipolar morphology of neurons.

We showed previously that Dar1 regulates dendrite branching by suppressing the expression of Spastin (Ye et al., 2011). We thus examined the possible role of Spastin in determining the basic layout of neuronal morphology. Although overexpressing Spastin reduced dendritic growth as previously reported, it did not alter the multipolar morphological type of da neurons (Fig. 2.2K, L). These results suggest that the roles of Dar1 in dendrite branching and in determining the multipolar layout of da neurons are mediated by distinct mechanisms. Consistent with this notion, whereas dendritic branching was reduced in neurons lacking the transcription factor Cut (Grueber et al., 2003) or the E3 ubiquitin ligase Highwire (Wang et al., 2013), these neurons still formed the normal number of primary dendrites despite having simplified higher-order branches (data not shown). Therefore, factors regulating dendritic growth or branching are not necessarily determinants of the multipolar morphology.

Nuclear positioning complex is required for the multipolar morphology of neurons

Loss of *dar1* gradually converted multipolar neurons into bipolar or unipolar morphologies. At early stages of development, *dar1* mutant neurons are multipolar despite appreciable defects in dendritic growth (Fig. 2.3A). These multipolar neurons gradually became bipolar, whereas the overall pattern of the dendritic arbors remained unaffected (Fig. 2.3A, B), indicating that loss of *dar1* led to defective coupling between the primary dendrites and the cell nucleus.

Previous studies have demonstrated that a specialized dynein complex is important for positioning the nucleus in the cell. The genes encoding the factors in the nuclear positioning complex, termed *nuclear distribution* (*nud*) genes, were first identified in filamentous fungi and

later found to be well conserved evolutionarily (Morris, 2000). For example, in mammals, the NudF homolog called LIS1 and the NudE homolog called NudE-like protein (or NUDEL) are required for coupling the leading process of the migrating neurons with its centrosome and nucleus (Ayala et al., 2007; Hippenmeyer et al., 2010; Niethammer et al., 2000; Reiner et al., 1993; Shu et al., 2004; Tsai et al., 2007; Tsai et al., 2005; Zhang et al., 2009). Interestingly, our microarray analysis also showed a significant reduction in the levels of the *nudC* gene, which encodes an essential component of the nuclear positioning complex (Morris, 2000) (data not shown). qRT-PCR further confirmed that *nudC* transcripts were dramatically reduced in $dar1^{-/-}$ da neurons (Fig. 2.3C). We thus examined the role of the nuclear positioning complex in the multipolar layout of neuronal morphology.

Knocking down the *Drosophila* homolog of NudC, NudE, or introducing mutations in *nudC* in da neurons by MARCM transformed the multipolar da neurons into bipolar morphology (Fig. 2.3D, E). Strikingly, whereas the overall morphology and branch numbers of the dendritic arbors were indistinguishable between the mutant and wild-type neurons (Fig. 2.3F), the nuclei of mutant neurons were several micrometers distant from the dendritic arbors (Fig. 2.3D). These results suggest that regulators of nuclear positioning are essential for the multipolar layout of neuronal dendrites in *Drosophila*.

To determine whether regulators of nuclear positioning are essential for mediating Dar1's function in determining the multipolar morphology of neurons, we performed epistasis analysis between *dar1* and *nudE*. NudE overexpression in $dar1^{-/-}$ da neurons partially rescued the increased number of bipolar da neurons caused by loss of *dar1* (Fig. 2.4A, B). Moreover, significantly fewer Dar1-overexpressing $RN2^{+}$ and PDF neurons displayed multipolar morphology when *nudE* ($nudE^{11R2/+}$) or *nudC* (NudC RNAi) function is reduced (Fig. 2.4C–F).

These results suggest that Dar1 likely acts via the nuclear positioning complex to induce multipolar morphology of neurons.

Discussion

The universal morphological organization of neuronal dendrites and axons—in the form of the unipolar, bipolar, and multipolar morphologies—is important for information processing in neurons and for the wiring of neural circuits. It has generally been assumed that the formation of the basic morphological types of neurons is determined by the number of dendrites growing out from the cell body (the "outgrowth model"). In this study, we show that this model alone is insufficient to explain the formation of multipolar morphology. We introduce nuclear positioning as a factor in determining the multipolar neuron morphology (Fig. 2.4G) and propose that Dar1 determines multipolar morphology by regulating both dendrite extension and primary dendrite–nucleus coupling.

Neuronal fate versus neuronal morphogenesis

We report a novel, instructive role for Dar1 in determining the multipolar morphology of postmitotic neurons without changing cell fate. First, despite the dendritic defects, axon morphology (Ye et al., 2011) and targeting (Fig. 2.1G) are unchanged in *dar1* mutant neurons. Second, ectopic expression of Dar1 in postmitotic neurons leads to supernumerary primary dendrites (Fig. 2.2A–E). Third, the remaining dendrites in *dar1*$^{-/-}$ neurons still follow the branching pattern assumed by wild-type neurons (Fig. 2.1C, D) (Ye et al., 2011). Fourth, *dar1* mutations do not affect the expression of neuron type-specific markers (Fig. 2.1I and data not shown).

Based on extensive studies in *C. elegans*, Hobert proposed the concept of terminal selector genes (Hobert, 2008). A terminal selector gene is required for determining specific aspects of a neuron's identity by regulating the expression of genes responsible for these characteristics such as those encoding neurotransmitter receptors, enzymes in a neurotransmitter synthesis pathway, and structural proteins. Loss of a terminal selector gene results in the loss of a specific aspect of the neuron type without affecting the overall neuronal identity. Dar1 plays such a function in the basic layout of neuronal morphology and thus is likely a "terminal selector gene" for neuronal morphology.

Role of dendrite outgrowth and dendrite–nucleus coupling in generating basic morphological types of neurons

Based on the findings in this study, we propose that generating neuronal multipolar morphology requires, not only dendritic extension, but also a coupling mechanism between the nucleus and the dendrites (Fig. 2.4G). Dar1 promotes both dendritic growth and dendrite–nucleus coupling. Therefore, its misexpression converts unipolar neurons into neurons with multipolar morphology (Fig. 2.2A–E).

The results presented here raise the interesting possibility that a specialized dynein complex in multipolar neurons with components that are transcriptionally regulated by Dar1 couples the nucleus with the primary dendrites. If the primary dendrite–nucleus coupling is weakened, then the nucleus may move to a different location in relation to the dendrites and axons. We speculate that there might also be an active or passive force that pulls the nucleus toward the axon, opposing the force that couples the primary dendrites and the nucleus. Consistent with this model, the remaining single primary dendrites of all bipolar-shaped da

neurons— caused by loss of *dar1*, reduced functions of dynein, or nuclear positioning complex—are those that project in the direction opposite the axon. This observation again rules out the possibility that the reduction in number of primary dendrites of *dar1*$^{-/-}$ da neurons is the result of reduction in dendrite growth. If that were the case, then the remaining single primary dendrites would likely project in random directions and not solely away from the axon. Further studies are needed to determine the cellular and molecular basis of the dendrite–nucleus coupling.

Several prior studies have demonstrated that neurons switch between different morphological types during development (Altman, 1972; Nadarajah et al., 2001; Ramón y Cajal, 1995; Sotelo and Dusart, 2009). These observations suggest that the acquisition of basic morphological types in many neurons includes intermediate morphologies with nucleus–primary dendrite relationships that are different from those seen in the mature neurons. It will be interesting to investigate whether the activity of the nuclear positioning complex and its regulators play a role in these developmental changes in morphological type.

In summary, this study offers a novel model for understanding the establishment of the three basic morphological types of neurons. Starting from genetic analysis of the KLF transcription factor Dar1, we not only uncover an instructive factor that determines the multipolar morphology of neurons, but also provide a mechanistic model showing that the position of the nucleus is critical for establishing multipolar neuron morphology. This study also demonstrates, for the first time to our knowledge, that the basic morphological types are determined by intrinsic molecular mechanisms in postmitotic neurons rather than in precursor cells. The model presented here may also be applied to explaining the changes in basic

morphological type during neuron development (Altman, 1972; Matsuda et al., 1996). This study therefore opens the door for a unifying theory of basic structural organization in neurons.

2.4 Materials and Methods

Fly stocks and cDNA constructs

Fly stocks include: *dar1*^{3232}, FRT^{2A} (Ye et al., 2011); *dar1*^{3010}, FRT^{2A} (Ye et al., 2011); *Ct*^{C145}, FRT^{19A} (Grueber et al., 2003); *hiw*$^{\Delta N}$, FRT^{19A} (Wang et al., 2013); *UAS-Dar1* (Ye et al., 2011); *UAS-Nod::βGal* (Clark et al., 1994), *ppk-CD4::tdTomato* (Han et al., 2011); *RN2-Gal4* (Bloomington Stock Center #7475) (Fujioka et al., 2003); *PDF-Gal4* (Taghert et al., 2001); *UAS-Glued*^{DN} (Allen et al., 1999); *sw*^{ts} (Boylan and Hays, 2002); *UAS-NudE* (Arthur et al., 2015); *nudE*^{11R2}, FRT^{2A} (Hayashi et al., 2014); and *UAS-monomeric RFP* (Ye et al., 2007). The following RNAi lines were obtained from the Vienna *Drosophila* RNAi Center: v105898 (CG9492 RNAi), v23504 (CG8407 RNAi), v8737 (CG14763 RNAi), and v35154 (CG6971 RNAi). The following lines were obtained from the Bloomington Stock Center: NudE RNAi (BL41860), NudC RNAi (BL33382), and *NudC*^{PL00045}, FRT^{2A}. The DNA construct for making the *UAS-KLF7* transgenic lines was generated by inserting the mouse KLF7 cDNA (tagged with a V5-epitope at the C terminus) into the pUAST vector.

MARCM and flip-out analyses

The mosaic analysis with a repressible cell marker (MARCM) experiments were performed as described previously (Ye et al., 2011). For MARCM analysis of *dar1* mutations in different classes of dendritic arborization (da) neurons and external sensory (es) neurons, the *hs*-FLP; *Gal4*$^{21-7}$, *UAS-mCD8::GFP*; *tubP-Gal80*, FRT^{2A} virgins were mated with males of *dar1*^{3232},

FRT^{2A} or *dar1*^{3010}, FRT^{2A}. For MARCM analysis of *dar1* mutations with the C4da neuropil marker *ppk-CD4::tdTomato*, the *hs*-FLP; *ppk-Gal4*, *UAS-mCD8::GFP*; *tubP-Gal80*, FRT^{2A} virgins were mated with males of *ppk-CD4::tdTomato*; *dar1*^{3232}, FRT^{2A}. For MARCM analysis of NudE overexpression in *dar1*$^{-/-}$ neurons, the *hs*-FLP; *Gal4*$^{21\text{-}7}$, *UAS-mCD8::GFP*; *tubP-Gal80*, FRT^{2A} virgins were mated with males of *UAS-NudE*; *dar1*^{3232}, FRT^{2A} or *UAS-NudE*; *dar1*^{3010}, FRT^{2A}. For flip-out analysis of Dar1 overexpression in es neurons, the *UAS-Dar1* virgins were mated with males of *hs*-FLP; *Gal4*$^{21\text{-}7}$; *UAS-FRT-CD2stop-FRT-CD8::GFP*.

Immunostaining and confocal imaging

Third-instar larvae were dissected and immunostained as described previously (Ye et al., 2011). The primary antibodies include: mouse anti-GFP (Invitrogen, 1:1000), chick anti-GFP (Aves Laboratories, 1:1000), rabbit anti-RFP (Rockland, 1:1000), rat anti-Elav (Developmental Studies Hybridoma Bank, 1:500), guinea pig anti-Dar1 (1:1000) (Ye et al., 2011), guinea pig anti-Knot (gift from Adrian Moore, 1:1000), guinea pig anti-Spineless (1:1000) (Kim et al., 2006), rabbit anti-Abrupt (gift from Stephen Crews, 1:200), rat anti-Cut (1:1000) (Blochlinger et al., 1988), and mouse anti-βGAL (Developmental Studies Hybridoma Bank, 1:100). Confocal imaging was performed with a Leica TCS SP5 confocal microscope.

Microarray with purified Drosophila PNS neurons and microarray analysis

PNS neurons were labeled with *Gal4*$^{21\text{-}7}$, *UAS-mCD8::GFP* and were purified with FACS as described previously (Ye et al., 2011). For each microarray sample (n = 3 for wild-type or *dar1* mutant), total RNA was extracted from ~20,000 GFP-positive cells using Trizol (Invitrogen), followed by purification with the RNeasy Micro Kit (Qiagen). cDNA was synthesized and

amplified with WT-Ovation Pico RNA amplification System (NuGEN Technologies), followed by biotin labeling with the Encore Biotin Module (NuGEN Technologies). The biotin-labeled cDNA were hybridized to the *Drosophila* Genome 2.0 Array (Affymetrix).

To detect differentially expressed genes, Bayesian tests were used and implemented in the limma R package (Smyth Gordon, 2004). Genes with false discovery rate (FDR) < 0.05 were considered differentially expressed.

For functional annotation of differential expressed genes, we used the DAVID bioinformatics resource (Huang et al., 2008). Cellular component gene ontology (GO) terms with Benjamini FDR < 0.05 were considered as significantly enriched.

qRT-PCR

Total RNA was extracted from purified PNS neurons of embryos 16 hours after egg laying (AEL) using Trizol (Invitrogen). First-strand cDNA was synthesized using SuperScript III First-Strand Synthesis SuperMix (Invitrogen). cDNA from RNA extracted from approximately 250 neurons was used for each real-time reaction. qRT-PCR and the quantification were performed as described previously (Kim et al., 2013).

Primer sets used were as following: *chmp1*, 5'-AAAGGCCAAGAAGGCGATTC-3' and 5'-GGGCACTCATCCTGAGGTAGTT-3'; *CG9492*, 5'-AGATGGATGGACTTGTGCCT-3' and 5'-CGATCACTCCGCAATATAAATCCT-3'; *CG8407*, 5'-GCCATTGAACTGTCCATTACC-3', and 5'-ACCTCAAAGCCGAACCCT-3'; *CG14763*, 5'-ACAACTACGACAGATATCGCT-3' and 5'-CTGTAGGTCACAAATCCGTC-3'; *nudC* set 1, 5'-GACGATGAATCCGATAAGAGTG-3' and 5'-GAATCTTGAGCTCCACCTCC-3'; *nudC* set 2, 5'-AGGTGGAGCTCAAGATTCC-3' and 5'-TCGATGATGGGCGTTTGAC-3'.

Quantifications and statistical analysis.

The number of primary dendrites was counted in 3D *z*-stacks. $RN2^{+}$ neurons in which the primary dendrites overlapped with neurites of neighboring neurons were unquantifiable and were excluded. For pigment dispersing factor (PDF) neurons, neurites shorter than 10 μm were excluded. In all bar charts of quantification, values and error bars indicate mean ± SEM. Sample numbers are indicated either in the bars or in the legends. ANOVA was used for comparing three or more groups. Two-tailed unpaired Student's *t* test was used for comparing two groups. *p* values are indicated in the bar charts as follows: not significant (NS) $p > 0.05$, $*p < 0.05$, $**p < 0.01$, and $***p < 0.001$.

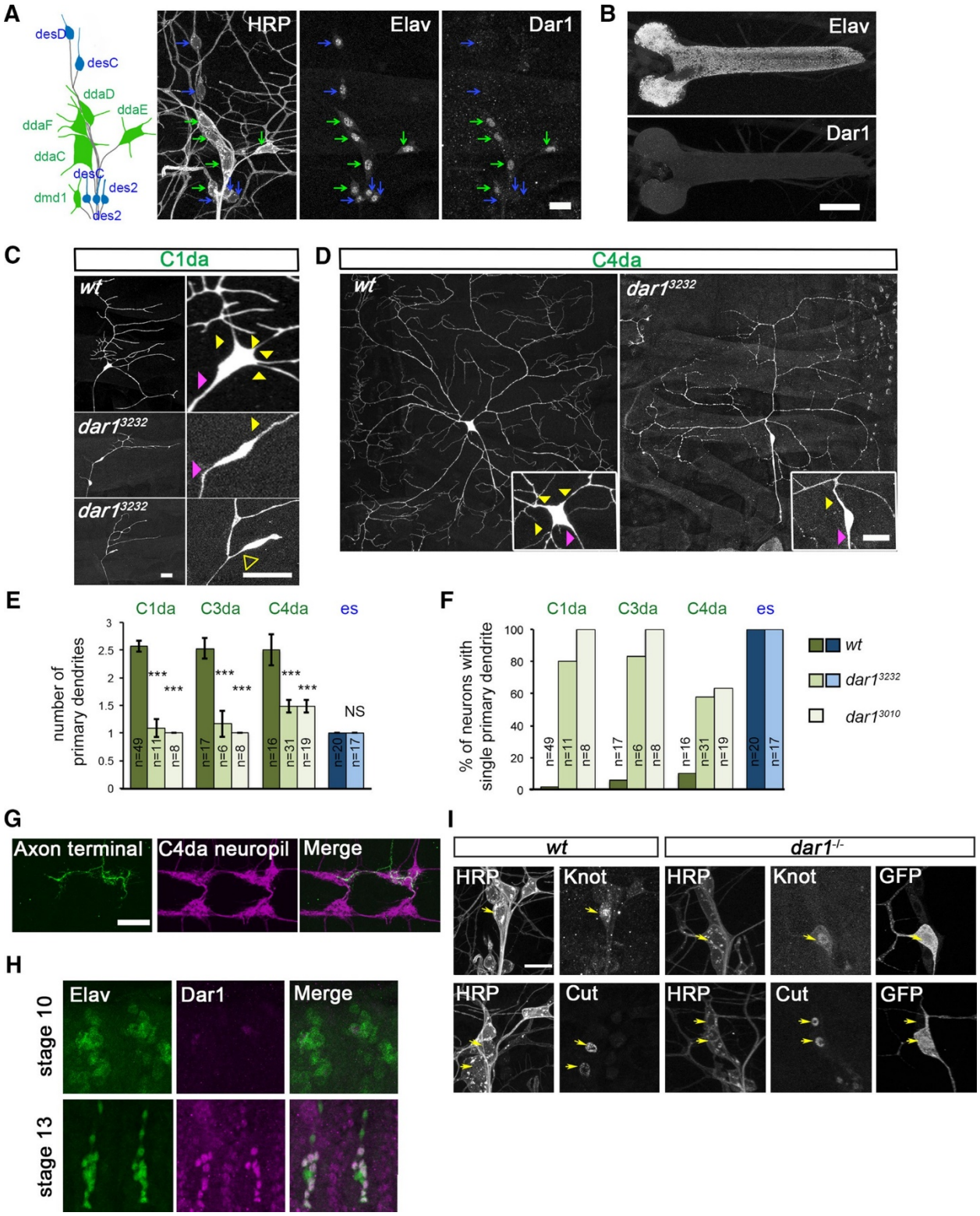
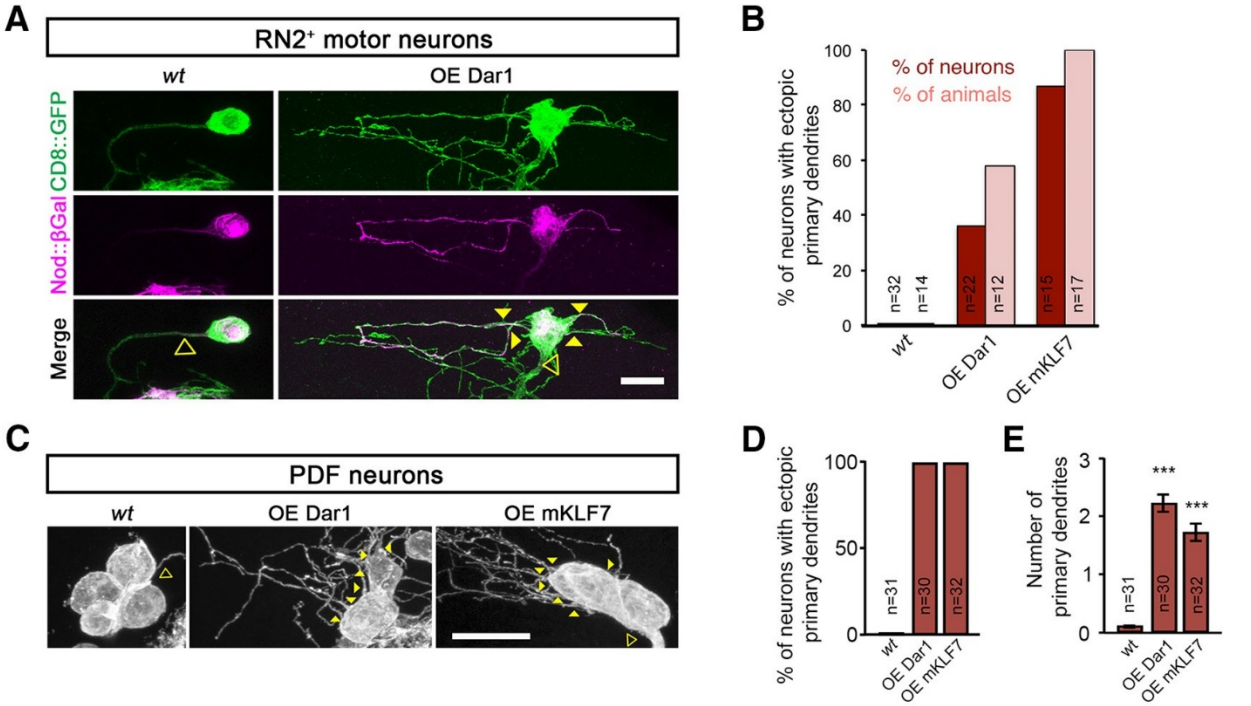

A
desD
desC
ddaD
ddaE
ddaF
ddaC
desC
des2
dmd1
des2
HRP
Elav
Dar1
B
Elav
Dar1
C
C1da
wt
dar1 3232
dar1 3232
D
C4da
wt
dar1 3232
E
C1da
C3da
C4da
es
number of primary dendrites
***
***
***
***
***
***
NS
n=49
n=11
n=8
n=17
n=6
n=8
n=16
n=31
n=19
n=20
n=17
F
C1da
C3da
C4da
es
% of neurons with single primary dendrite
wt
dar1 3232
dar1 3010
n=49
n=11
n=8
n=17
n=6
n=8
n=16
n=31
n=19
n=20
n=17
G
Axon terminal
C4da neuropil
Merge
H
stage 10
stage 13
Elav
Dar1
Merge
I
wt
dar1 -/-
HRP
Knot
HRP
Knot
GFP
HRP
Cut
HRP
Cut
GFP

Figure 2.1 Dar1 is required for multipolar neuronal morphology but not cell fates in postmitotic neurons.

(**A-B**) Dar1 is uniquely and selectively expressed in multipolar neurons in the *Drosophila* nervous system. (**A**) Dar1 is exclusively expressed in multipolar neurons in the PNS. The schematic shows larval PNS neurons in the dorsal cluster, including multipolar neurons (green) and bipolar neurons (blue). The images show PNS neurons labeled with antibodies against the pan-neuronal membrane marker HRP (left), the neuron-specific marker Elav (middle), and Dar1 (right). Green arrows indicate multipolar neurons and blue arrows indicate bipolar es neurons. Scale bar, 10μm. (**B**) Dar1 is absent in the CNS. Shown are larval VNC double-labeled for the pan-neuronal protein Elav and Dar1. Scale bar, 100 μm.
(**C**–**F**) Loss of *dar1* converts the multipolar da neurons into unipolar or bipolar morphology. (**C**) Shown are wild-type (top) and $dar1^{3232}$ (middle and bottom) MARCM clones of the class I (C1) da neurons ddaE. *Dar1* mutant ddaE neurons exhibit bipolar (middle) or unipolar (bottom) morphology. (**D**) Wild-type (left) and $dar1^{3232}$ (right) MARCM clones of the class IV (C4) da neurons ddaC. Yellow solid triangles are primary dendrites; magenta solid triangles, axons; open triangle, the primary neurite in unipolar neurons. Scale bar, 20 μm. (**E**) Bar chart showing quantification of the number of primary dendrites in wild-type, $dar1^{3232}$ and $dar1^{3010}$ MARCM multipolar (green) and bipolar (blue) neurons. (**F**) Bar chart of the percentage of neurons with single dendrites in wild-type, $dar1^{3232}$, and $dar1^{3010}$ MARCM multipolar (green) and bipolar (blue) neurons.
(**G**) Loss of *dar1* does not alter axon targeting of C4da neurons. The axon terminal of a representative $dar1^{3232}$ MARCM clone of the C4da ddaC neuron is shown. The axon terminal is labeled with CD8::GFP and the C4da neuropil is labeled with *ppk-CD4-tdTomato*.
(**H**) Dar1 is expressed postmitotically. Elav (green) and Dar1 (magenta) were stained in wild-type embryos. Although Elav is already expressed in peripheral neurons at stage 10 (top, left), Dar1 is only beginning to become visible at this stage (top, middle). By Stage 13, Dar1 is robustly expressed in identifiable da neurons (bottom, middle) that will henceforth become multipolar.
(**I**) Loss of *dar1* does not change the class identity of da neurons. Knot and Cut expression in $dar1^{-/-}$ MARCM clones remain identical to wild-type. A single $dar1^{-/-}$ ddaC neuron is marked by GFP expression. In the PNS dorsal cluster, Knot is expressed in C4da (ddaC) neurons, whereas Cut is expressed in C3da (ddaF is shown) and C4da (ddaC) neurons (yellow arrows). Anti-HRP antibody labels all PNS neurons and was used to help the identification of neurons based on the position of cell bodies in the cluster. Scale bar, 10 μm.



Gene Ontology TERM_Cellular Component	Fold enrichment	FDR
GO:0015630 microtubule cytoskeleton	2.39	0.005
GO:0030286 dynein complex	5.17	0.007
GO:0044430 cytoskeletal part	2.09	0.009
GO:0005856 cytoskeleton	1.88	0.017
GO:0005874 microtubule	3.04	0.018
GO:0005930 axoneme	8.25	0.018
GO:0044463 cell projection part	4.01	0.018
GO:0005875 microtubule associated complex	2.73	0.02
GO:0005858 axonemal dynein complex	9.63	0.029

Figure 2.2 Dar1 requires the dynein complex to induce multipolar morphology of neurons.

(**A**-**B**) Misexpression of Dar1 or mKLF7 converts the unipolar RN2^{+} motor neurons in larva VNC into multipolar morphology. (**A**) RN2^{+} neurons (Fujioka et al., 2003; Ghabrial et al., 2003) of wild-type and those overexpressing Dar1 (OE Dar1). Many of the ectopic primary neurites in RN2^{+} motor neurons are positive for Nod::*β*Gal, a marker that labels subsets of dendritic branches (Zheng et al., 2008). Yellow solid triangles are primary dendrites; open triangles, the primary neurites in unipolar neurons. Scale bar, 10 μm. (**B**) Bar chart showing the percentage of neurons and larvae with ectopic primary dendrites in RN2^{+} neurons of the indicated genotypes.
(**C**–**E**) Misexpression of Dar1 or mKLF7 converts the unipolar PDF neurons in adult brain into multipolar morphology. (**C**) Representative images wild-type, Dar1-overexpressing, and mKLF7-overexpressing (OE mKLF7) PDF neurons. Yellow solid triangles are primary dendrites; open triangles, the primary neurites in unipolar neurons. Scale bar, 10 μm. (**D**) and (**E**) Bar charts showing the percentage of neurons with ectopic primary dendrites and the number of primary dendrites in PDF neurons.
(**F**-**G**) Dar1 regulates the expression of dynein genes. (**F**) Significantly enriched GO terms (cellular components) of which the FDR is <0.05 between wild-type and *dar1* mutant microarrays. (**G**) Bar chart of quantifications of relative transcript levels of *chmp1* (control, n = 5), *CG9492* (n = 4), *CG8407* (n = 5), and CG14763 (n = 5) from *wt* and *dar1* mutant purified PNS neurons measured by qRT-PCR.
(**H**) The dynein complex is required for multipolar morphology of *Drosophila* da neurons. Multipolar C1da neurons (ddaE) became bipolar in a temperature-sensitive mutant of the dynein intermediate chain, *sw*$^{ts/+}$, at nonpermissive temperature (25°C). Yellow triangles are primary dendrites; magenta triangles, axons. Scale bar, 20 μm.
(**I**-**J**) Disrupting dynein function suppresses the appearance of ectopic primary dendrites induced by Dar1 misexpression. (**I**) Defective dynein function caused by *sw*$^{ts/+}$ (25°C) blocked the multipolar morphology induced by Dar1 overexpression in RN2^{+} and PDF neurons. Scale bar, 10 μm. (**J**) Bar chart showing quantification of percentages of RN2^{+} or PDF neurons with ectopic primary dendrites denoted genotypes in the indicated genotypes.
(**K**-**L**) Roles of Dar1 in dendrite branching and in determining the multipolar layout of da neurons are mediated by distinct mechanisms. (**K**) Wild-type and Spastin-overexpressing (OE Spastin) C1da (ddaE) neurons. Scale bar, 25 μm. (**L**) Quantifications of the percentage of multipolar C4da (ddaC) and C1da (ddaE) neurons. $p > 0.05$, NS, *t* test.

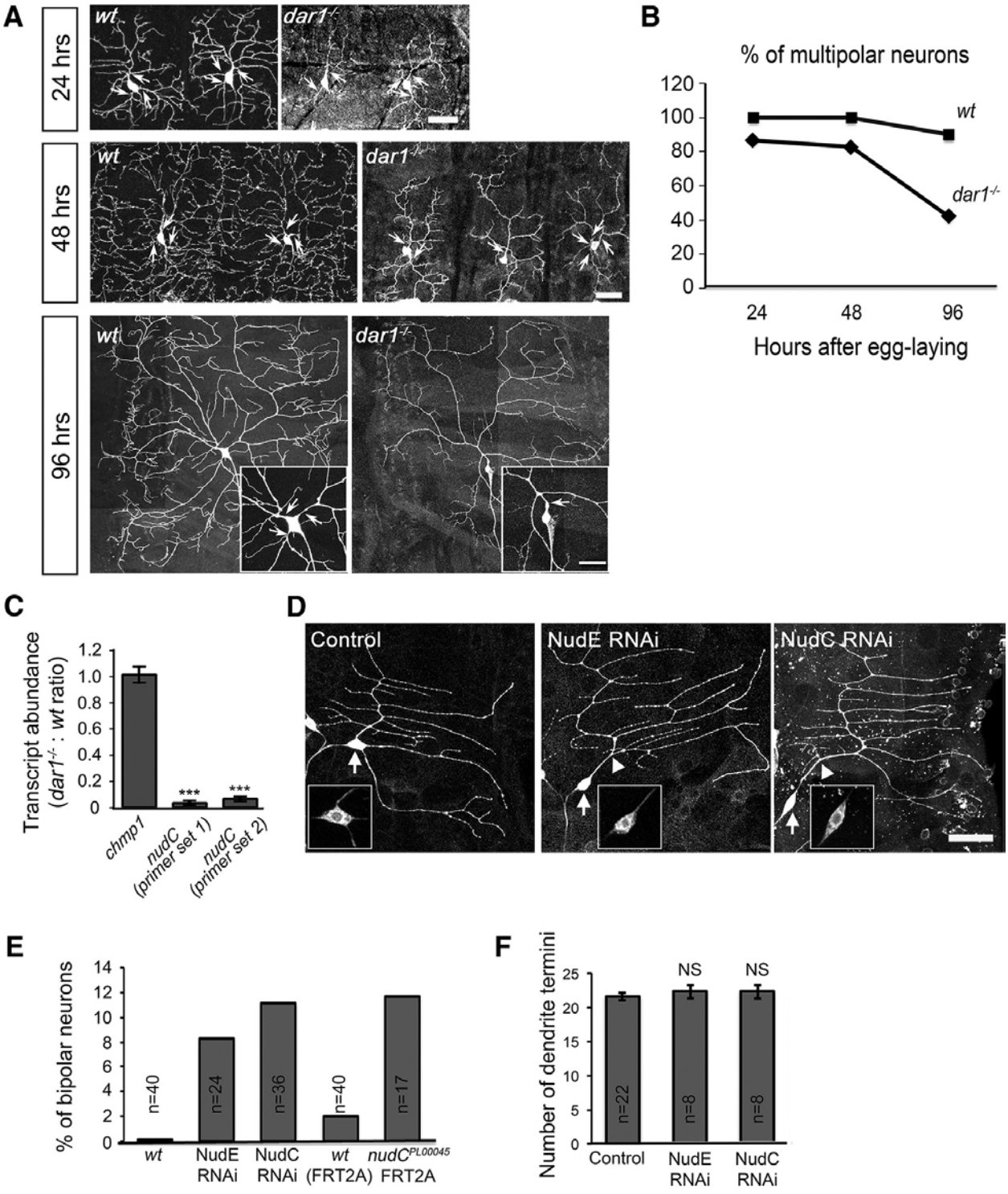
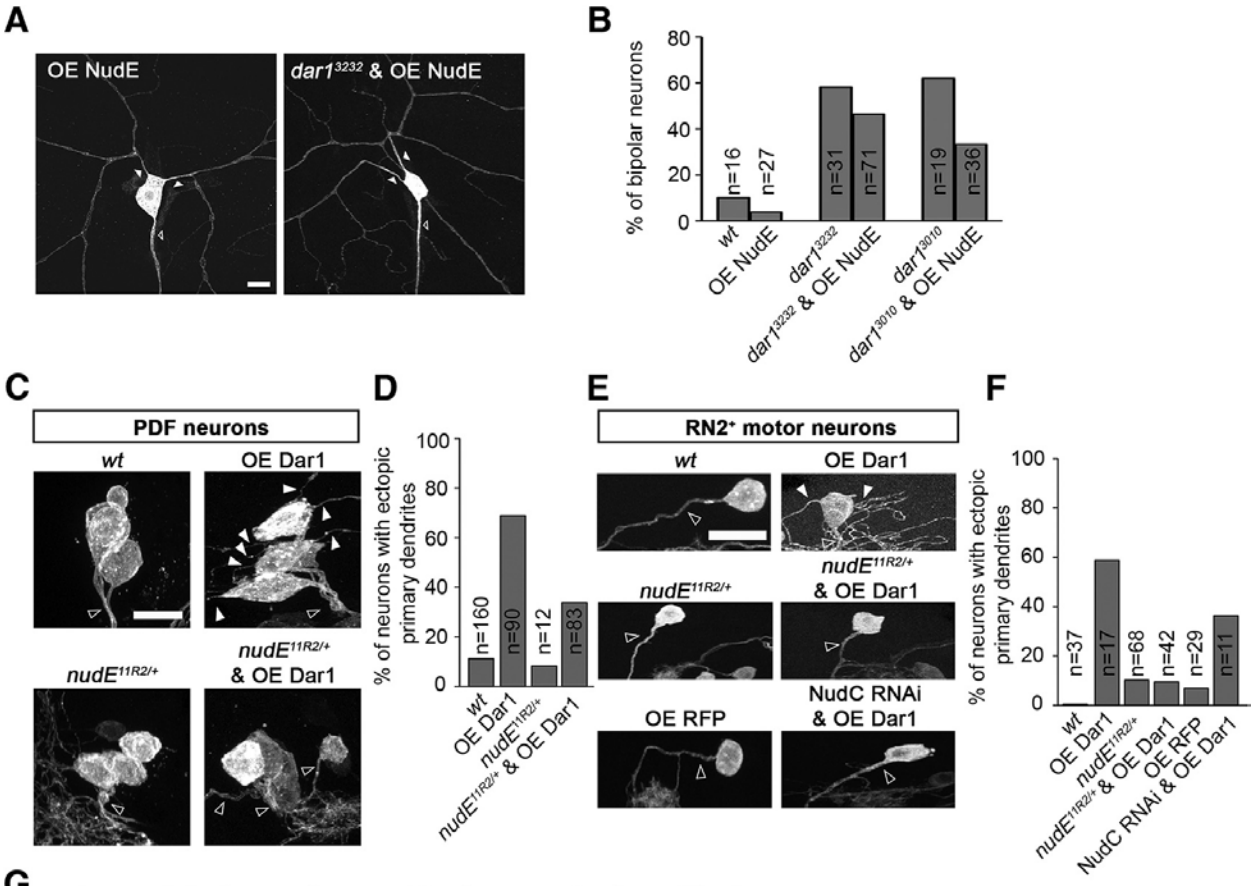

A
24 hrs
48 hrs
96 hrs
wt
dar1-/-
B
% of multipolar neurons
120
100
80
60
40
20
0
wt
dar1-/-
24
48
96
Hours after egg-laying
C
Transcript abundance
(dar1-/- : wt ratio)
1.2
1.0
0.8
0.6
0.4
0.2
0
***
***
chmp1
nudC (primer set 1)
nudC (primer set 2)
D
Control
NudE RNAi
NudC RNAi
E
% of bipolar neurons
14
12
10
8
6
4
2
0
n=40
n=24
n=36
n=40
n=17
wt
NudE RNAi
NudC RNAi
wt (FRT2A)
nudCPL00045 FRT2A
F
Number of dendrite termini
25
20
15
10
5
0
NS
NS
n=22
n=8
n=8
Control
NudE RNAi
NudC RNAi

Figure 2.3 Nuclear positioning complex is required for multipolar morphology of neurons.

(**A**-**B**) Loss of *dar1* causes multipolar neurons to gradually become bipolar during development. (**A**) Representative images of C4da (ddaC) neurons at different stages of larval development. At 24 hours AEL, all *dar1* mutant ddaCs are multipolar, although dendritic growth defects are already visible. At 96 hours AEL, many multipolar ddaCs become bipolar, whereas the overall dendritic pattern is maintained. (**B**) Line plot showing the percentage of multipolar ddaCs that are wild-type or *dar1* mutant at different developmental times.
(**C**) Quantification of relative transcript levels of *chmp1* and *nudC* from purified *wt* and $dar1^{-/-}$ PNS neurons. qRT-PCR with two distinct sets of *nudC* primers showed consistent reduction in PCR products in the cDNAs from $dar1^{3232}$ da neurons.
(**D**-**F**) Knocking down the *Drosophila* homologs of NudE and NudC caused C1da neurons (ddaE) to assume bipolar morphology. (**D**) Cell bodies (arrows) of some NudE or NudC knockdown neurons are connected with the dendritic arbors by a single primary dendrite, which does not occur in normal ddaE neurons. The first branch point of the dendritic arbor is indicated by a triangle. The inset in each panel shows the magnified view of cell body containing the nucleus. The neurons were labeled by the membrane marker mCD8::GFP, which is absent in the cell nucleus. Scale bar, 50 μm. (**E**) Bar chart showing the percentage of neurons with single primary dendrites of denoted genotypes. (**F**) Bar chart showing that the number of dendrite termini is unaffected in NudE or NudC knockdown neurons.


A
OE NudE
dar1^3232 & OE NudE
B
% of bipolar neurons
n=16
n=27
n=31
n=71
n=19
n=36
wt
OE NudE
dar1^3232
dar1^3232 & OE NudE
dar1^3010
dar1^3010 & OE NudE
C
PDF neurons
wt
OE Dar1
nudE^11R2/+
nudE^11R2/+ & OE Dar1
D
% of neurons with ectopic primary dendrites
n=160
n=90
n=12
n=83
E
RN2+ motor neurons
F
n=37
n=17
n=68
n=42
n=29
n=11
OE RFP
NudC RNAi & OE Dar1

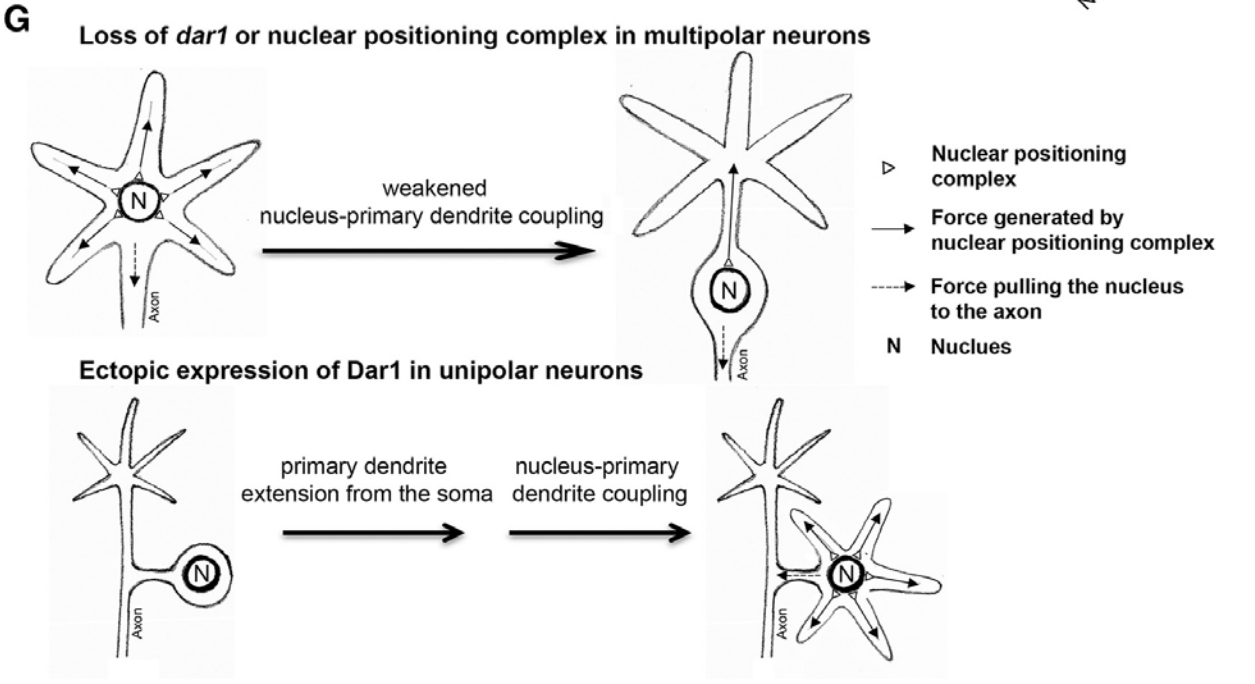

G
Loss of dar1 or nuclear positioning complex in multipolar neurons
N
Axon
weakened
nucleus-primary dendrite coupling
Nuclear positioning complex
Force generated by nuclear positioning complex
Force pulling the nucleus to the axon
N Nuclues
Ectopic expression of Dar1 in unipolar neurons
primary dendrite extension from the soma
nucleus-primary dendrite coupling

Figure 2.4 Dar1 requires nuclear positioning complex to induce multipolar morphology of neurons.

(**A**-**B**) NudE overexpression reduces the percentage of *dar1* mutant C4da neurons that assume the bipolar morphology. Results of wild-type, $dar1^{3232}$, and $dar1^{3010}$ neurons in **B** are the same as those in Figure 2.1F. The solid triangles indicate primary dendrites and open triangles indicate axons.
(**C**-**D**) Dar1 requires *nudE* to induce multipolar morphology in adult PDF neurons. (**C**) Representative images of PDF neurons that are wild-type, Dar1-overexpression, $nudE^{11R2/+}$, and $nudE^{11R2/+}$ with Dar1 overexpression. Solid triangles indicate primary dendrites and open triangles indicate the primary neurites in unipolar neurons. Scale bar, 10 μm. (**D**) Bar chart showing the percentage of neurons with ectopic primary dendrites in PDF neurons of denoted genotypes.
(**E**-**F**) Dar1 requires *nudE* to induce multipolar morphology in larval $RN2^{+}$ motor neurons. (**E**) Representative images of $RN2^{+}$ neurons that are wild-type, Dar1-overexpression, $nudE^{11R2/+}$, $nudE^{11R2/+}$ with Dar1-overexpression, RFP-overexpression, and NudC RNAi with Dar1-overexpression. Solid triangles indicate primary dendrites and open triangles indicate the primary neurites in unipolar neurons. Scale bar, 10 μm. (**F**) Bar chart showing the percentage of neurons with ectopic primary dendrites in $RN2^{+}$ neurons of denoted genotypes.
(**G**) Model explaining the roles of Dar1 in determining multipolar neuron morphology. The nuclear positioning complex couples the nucleus with primary dendrites. An opposing force may exist to pull the nucleus toward the axon. Top, When the coupling between nucleus and primary dendrites is weakened, as in the case of loss of *dar1* or loss of nuclear positioning complex components, the nucleus is pulled toward the axon, changing the morphology from multipolar to bipolar. Bottom, When Dar1 is misexpressed in a unipolar neuron, it promotes both dendritic extension from the cell body and coupling between the primary dendrites and the nucleus, leading to multipolar morphology.

Chapter 3 Identification of neuronal lineages in the *Drosophila* peripheral nervous system with a novel multi-spectral lineage tracing system

Co-authored with Ye Li, Michael T. Veling, Christopher Litts, Nigel Michki, Hao Liu, Dawen Cai, and Bing Ye.

3.1 Abstract

Elucidating cell lineages provides crucial understanding of development. Recently developed sequencing-based techniques enhance the scale of lineage tracing but eliminate the spatial information offered by conventional approaches. Multispectral labeling techniques, such as *Brainbow*, have the potential to identify lineage-related cells *in situ*. Here, we report *Lineage Tracker Bitbow*, a "digital" version of *Brainbow* that greatly expands the color diversity, and a suite of statistical methods for quantifying the lineage relationship of any two cells. Applying these tools to *Drosophila* peripheral nervous system, we determined lineage relationship between all neuronal pairs. Based on the refined lineage map, we explored whether distinct *cis*-regulatory elements are used in controlling the expression of a terminal selector gene in distinct lineage patterns. This study demonstrates *nBitbow* as an efficient tool for *in-situ* lineage mapping and its potential in studying molecular mechanisms in the lineage context.

3.2 Introduction

Cell lineage, which denotes the developmental history of a cell, is the conceptual framework of organism formation (Papaioannou, 2016; Stent, 1985). Modern genetic techniques have undergone evolutionary improvement, compared to early dye filling- or cell transplantation-based techniques for lineage tracing (Woodworth et al., 2017). For instance, sequencing-based methods can distinguish hundreds to thousands of uniquely barcoded lineages, though at the expense of the *in situ* spatial relationships of these lineages due to tissue disassembly (Raj et al., 2018; Schmidt et al., 2017; Spanjaard et al., 2018). In contrast, imaging-based methods, such as *Brainbow*, can preserve the spatial information *in situ* but their efficiencies are still limited by labeling diversities for unambiguous lineage tracing (Cai et al., 2013; Hadjieconomou et al., 2011; Livet et al., 2007; Pan et al., 2013). Hence, there is an urgent need to create novel labeling and detection methods that allow highly efficient lineage tracing while preserving spatial information.

Brainbow, a multi-spectral labeling technology, is designed to randomly express one of three or four fluorescent proteins (FPs) from a single cassette, thus creating stochastic labeling colors in neighboring cells or cell lineages (Cai et al., 2013; Hadjieconomou et al., 2011; Livet et al., 2007; Pan et al., 2013). When more color variants are needed, for example, to uniquely label many cell lineages, more than one *Brainbow* cassettes can be used to create differential expression levels of FPs. However, using color shades for lineage tracing is not always reliable. Distinguishing two color variants differing by subtle FP expression levels (e.g., color A generated from 2 YFP + 1 RFP + 1 CFP compares to color B generated from 1 YFP + 2 RFP + 1 CFP) can be challenging due to imaging noise (Cai et al., 2013). When applying *Brainbow* to trace cell lineages, daughter cells in the same lineage are assumed to inherit the same color

generated in the mother stem cell. However, protein synthesis levels in daughter cells can be quite different. A more robust color generation mechanism is highly desirable for efficient and reliable lineage tracing.

One way to generate more robust *Brainbow* lineage labels is to localize the same FPs to different sub-cellular compartments. Cytoplasmic membrane-targeted and nucleus-targeted FPs, expressed through genome integration by electroporated transposase, have been used to differentiate neighboring neuronal lineages in chick and mouse embryonic brains (Garcia-Moreno et al., 2014; Loulier et al., 2014). However, transposase integrates various number of targeting cassettes in different cells, making it difficult to estimate the probability of each label combination for quantitative analysis. Generating transgenic animals with a fixed number of labeling cassettes would solve this problem. For instance, the *Raeppli* strategy utilized 4 FPs to create up to 4 x 4 = 16 membrane and nucleus color combinations in transgenic *Drosophila* (Kanca et al., 2014). Another recombination mechanism, implemented in the *CLoNe* and the *MultiColor FlpOut* (*MCFO*) *Drosophila* lines, generates random colors by stochastic removal of the expression stops from each FP module (Garcia-Moreno et al., 2014; Nern et al., 2015). For instance, a *MCFO* fly integrates 3 different stop-“spaghetti monster GFPs” (smGFPs) modules into 3 distinct genomic loci and generates up to 2^3-1=7 smGFP combinations. However, further expanding the color pool requires inserting more FP modules to additional genomic loci to prevent inter-module recombination. In addition, the optimal color outcome can be difficult to obtain from *CLoNe* and *MCFO* animals. This is because while low FLP activity results in simple single-marker colors, high FLP activity often results in expressing all FPs in most of the cells (Nern et al., 2015). In conclusion, the small unique color pools generated by the above

mentioned methods result in frequent observations that neighboring cells or lineages are labeled by the same color.

To overcome the limitations discussed above, we introduced a novel "digital" format of *Brainbow* for robust lineage tracing, which we termed *Lineage Tracker Bitbow* (*nBitbow*). A single *nBitbow* cassette composites binary switches to independently determine an ON/OFF state of 5 FPs to generate up to 2^5-1=31 color variants. We applied *nBitbow* to trace neuronal lineages in the *Drosophila* peripheral nervous system (PNS). We chose the fly PNS as a model because (1) individual PNS neurons are identifiable by their soma locations and neurite patterns; (2) PNS neuronal lineages reported in previous studies can serve as references for result comparison (Brewster and Bodmer, 1995, 1996); and (3) previous neuronal lineage mapping in PNS was incomplete due to technical challenges. As there is a lack of statistical methods for color-based lineage tracing, we developed a lineage relatedness test to determine the likelihood of two cells being lineage-related based on their colors. Using this statistic test, we confirmed and rejected previously determined lineages, as well as revealed unknown lineages. Moreover, applying *nBitbow* labeling at different developmental time points, we revealed the proximate birth-timing of many PNS neuronal lineages. Based on the refined lineage map, we had the opportunity to examine whether distinct *cis*-regulatory elements are used in controlling the selective expression of *dendritic arborization 1* (*dar1*), a terminal selector gene for multipolar neurons derived through distinct lineage patterns (Cajal, 1995; Wang et al., 2015).

3.3 Results and Discussion

Lineage Tracker-Bitbow

As opposed to previous *Brainbow* designs that expand color variations by recombining multiple cassettes to mix different intensity levels in each spectral channel, *Bitbow*, a "digital" format of *Brainbow*, utilize several ("N") FPs, and randomly assign each to an ON or OFF expression state upon FLP-mediated recombination (Figure 3.1A). As a result, *Bitbow* generates "N-bit" (2^N-1, minus the all-OFF state) "colors" from a single cassette. We further optimized *Bitbow* for lineage tracing and generated a *Lineage Tracker-Bitbow* (*nBitbow*) cassette containing 5 FPs (mAmetrine, mTFP, mNeonGreen, mKusabira-Orange2 and tdKatushka2). Individual FP was fused to a human histone H2B (hH2B) for nuclear tagging. The cDNA of each nuclear-FP was positioned in the inverse direction and flanked by a pair of incompatible FRT sites, thus permitting spinning the FPs in forward or inverse orientation upon FLP recombination (Cai et al., 2013; Mcleod et al., 1986; Schlake and Bode, 1994; Turan et al., 2010; Volkert and Broach, 1986). Unlike previous *Brainbow* designs, recombination of each nuclear-FP in *nBitbow* was independent from each other, resulting in up to 2^5-1=31 unique colors by a single cassette (Figure 3.1B). Finally, a UAS sequence and a p10 baculovirus poly-adenylation sequence were placed upstream and downstream, respectively, to each of the five FP recombination units to allow strong FP expression when driven by a Gal4 driver (Pfeiffer et al., 2012). We chose the FPs whose native signals are bright and stable so that immunostaining is not required. In addition, spectral imaging and linear unmixing were applied and optimized for separating the five fluorescent signals to avoid signal bleed-through (Figure 3.1C).

To evaluate the labeling efficiency of *nBitbow* in the *Drosophila* larval PNS, we first combined a transgene encoding heat-shock-inducible flippase (*hsFLP*) and the pan-neuronal driver *elav-Gal4* to determine how often neurons expressed colors in the 3rd instar larvae. Without any heat-shock, an average of 2.89 ± 0.90% (mean ± standard error of mean) of PNS

neurons showed colors when the larvae were raised at 23 ℃ (Figure 3.2A), likely due to leaky FLP expression (Golic and Lindquist, 1989). Lowering the developmental temperature to 18 °C did not reduce this leaky FLP activity (data not shown). Induction of FLP expression by a 30 min heat-shock at 37 °C that started at the 3rd, 4th, or 5th hours (hr) after egg laying (AEL) led to significant increases of the number of PNS neurons that expressed colors (up to 18.62 ± 2.74 %) (Figure 3.2A). Heat-shock that started at 2nd hr AEL turned on color expression in similar number of neurons compared to the non-heat-shock condition (Figure 3.2A), possibly due to either low levels of FLP expression or poor accessibility of FLP to the *nBitbow* construct at very early stages of embryogenesis. Interestingly, we observed that the efficiency of turning on colors at the 6th hr AEL decreased to the level of non-heat-shock condition. This may indicate a lower efficiency of FLP recombination in the post-mitotic cells (detailed below).

As different FRT sites exhibit different efficiencies of FLP-induced recombination (Schlake and Bode, 1994; Turan et al., 2010), we quantified the expression frequency of individual FPs. mNeonGreen displayed the highest expression frequency, followed by mTFP, mKusabira-Orange2, tdKatushka2, and mAmetrine (Figure 3.2B). Next, we quantified the frequency of neurons expressing one, two, three, four, or all five FPs. We found that such frequency decreased exponentially from expressing one FP to five FPs, which suggests that the recombination of distinct FRT sites is independent of each other as the expression of one FP does not appear to increase the chance of expressing other FPs (Figure 3.2C). Finally, the expression frequencies of all the FP combinations (i.e., color variants) are quantified (Figure 3.2D) for our lineage relatedness test (detailed below). Despite that different combinations exhibited different frequencies, we observed 27 of the 31 expected colors after heat-shock-induced FLP expression.

One potential drawback of *nBitbow* for lineage tracing is that the "spinning" recombination design may cause color changes over time if the leaky FLP activity is persistent in a cell. As a result, cells with altered colors in the same lineage may be mis-identified as in distinct lineages. To evaluate whether *nBitbow* is reliable for lineage tracing, we performed the same heat-shock experiment and examined the color labeling in the central nervous system (CNS). Unlike the sensory organ precursors (SOPs) in the PNS, neuroblasts (NBs) in the CNS divide many more times to generate cell clusters with clear boundaries that can be easily separated from each other even with simple GFP labeling (Birkholz et al., 2015; Truman and Bate, 1988). We found that the vast majority of the cells in each cluster were labeled in the same *nBitbow* color (Figure 3.2E). We occasionally observed a few scattered cells labeled by different colors in a cluster, and rarely observed a cell cluster that was labeled by two distinctly colored clones (Figure 3.2F). This result indicates that the embryonic heat-shock induced *nBitbow* labeling mostly happens in neural stem/progenitor cells and that color changes caused by persistent FLP activity is minimal. Indeed, we also observed that *nBitbow* had the lowest labeling efficiency in the PNS when heat-shocked at the 6th hr AEL (Figure 3.2C), a stage that has more post-mitotic cells. Taken together, these results suggest that *nBitbow* provides more unique colors from a single cassette than previous variants of *Brainbow* and is reliable for lineage tracing in the *Drosophila* nervous system.

Identification of neuronal lineages in the *Drosophila* larval PNS by *nBitbow*

Drosophila PNS neurons are generated through lineages that repeat in the abdominal hemi-segments (Figure 3.3A) (Hartenstein and Campos-Ortega, 1984; Hartenstein et al., 1987). The SOPs in each hemi-segment are born and delaminated from ectoderm at approximately 3.5 to 7.5

hr AEL to eventually give rise to 45 PNS neurons (Bodmer et al., 1989; Ghysen and Okane, 1989; Younossi-Hartenstein and Hartenstein, 1997). We therefore induced *nBitbow* recombination in PNS neurons by heat-shock at 3-4 or 5-6 hr AEL and recorded their colors in 3rd instar larvae (Figure 3.3B). We expect to observe a significantly higher probability of two neurons being labeled in the same colors if they belong to the same lineage (i.e., inheriting the same colors from their SOP, Figure 3.3C) than if they belong to different lineages (i.e., acquiring the same colors by chance). Based on the Cohen's Kappa (κ) statistics, we designed a randomized lineage relatedness test to determine whether a pair of two neurons are lineage-related (Cohen, 1960; Dwass, 1957; Nichols and Holmes, 2007; Nichols and Holmes, 2002). Ranging from -1 to 1, $\kappa = 1$ indicates the two neurons are always labeled by the same colors, $\kappa = 0$ indicates the neurons are labeled by the same colors by chance, and $\kappa = -1$ indicates the two neurons are always labeled by different colors. We calculated the κ value of every pair of PNS neurons, and determined whether each κ value is significantly different against the probability of labeling the same neuron pair with the same colors by chance in a randomization test (Figure 3.3D, and see methods for further details). Finally, a $\leq 2\%$ false discovery rate (FDR) based on the Benjamini Hochberg method was applied to confirm any pair of neurons that are lineage-related (Benjamini and Hochberg, 1995).

Since some neurons are labeled at the 3rd instar larval stage without heat-shock, we first examined how this leaky FLP activity would affect the outcomes of our color-based lineage analysis. From the non-heat-shock experiments, our lineage relatedness test determined that all the neurons appear to be in distinct lineages (Figure 3.4, left panel). This indicates that the leaky FLP activity is unlikely to recombine the *nBitbow* cassette in any SOP until accumulating to a sufficiently high level to recombine in the post-mitotic neurons. This also suggests that our

lineage relatedness test is reliable to avoid the false-positive assignment of two cells being lineage related.

Previous studies used heat-shock to sparsely induce lacZ expression at early developmental time points and referred cell clusters that are located nearby to be in the same SOP lineages (Brewster and Bodmer, 1995, 1996). We started *nBitbow* lineage tracing with heat-shock at 3-4 hr AEL. The lineage relatedness test led to some conclusions the same as the previous studies did: 4 distinct lineages give rise to a pair of ldaA-lesA, ldaB-lesB, v'ada-v'esB, or v'pda-v'es2 neurons, respectively (Figure 3.5).

The lacZ-based lineage tracing approach may incorrectly determine neurons in different lineages as in the same lineage, if they are easily labeled at the same heat-shock time point. *nBitbow*, on the other hand, labels the lineage-unrelated neurons in distinct colors even if their progenitors are labeled at the same heat-shock time point. For instance, prior studies suggested that some of the dendritic arborization (da) neurons in the dorsal multidendritic (dmd) cluster were generated from one SOP and those in the ventral multidendritic (vmd) cluster were generated from another SOP (Figure 3.3A, shaded clusters) (Brewster and Bodmer, 1995, 1996). In contrast, our results showed that none of the da neurons from either dmd or vmd cluster are lineage related (Figure 3.6).

The lacZ-based lineage tracing approach may also incorrectly determine neurons in the same lineage as in different lineages, if they migrate away from each other. *nBitbow*, on the other hand, relies on color identify but not spatial proximity that avoids this type of error. For instance, the 5 external sensory (es) neurons (desC, lesC, v'esA, vesA and vesB) had been previously concluded as the only neurons generated from 5 SOPs. Our lineage relatedness test revealed that each of the 5 es neurons were lineage-related to either a da or a tracheal dendrite (td) neuron

(ddaD-desC, ltd-lesC, vdaA-v'esA, vdaC-vesB, and vdaD-vesA, Figure 3.3C-D). This finding is in agreement with the results mentioned above that dda or vda neurons in the dmd or vmd clusters, respectively, are not lineage-related to each other, but are lineage-related to the des or ves neurons, respectively (Figure 3.3C-D and Figure 3.6).

Estimating the birth-timing of neurons by *nBitbow*

One inherent benefit of using *nBitbow* for lineage mapping is its efficiency. *nBitbow* does not require very sparse labeling. Indeed, all samples expressing any FP colors were utilized in the analysis. This allowed us to efficiently map the complete PNS lineages using only 25 larvae for each heat-shock time point.

Comparing experiments done with 3-4 hr AEL heat-shock to those done with 5-6 hr AEL heat-shock, we found that even though a lot more neurons were labeled (Figure 3.2A), the overall percentage of neuron pairs that were labeled in matching colors decreased from 28.80% to 23.98%, respectively. Consistently, the lineage relatedness tests indicated that the ddaD-desC, v'pda-v'es2, v'td2-vchA/vchB/vesC, v'esA-vdaA, and vdaD-vesA neuron pairs no longer appeared to be lineage-related when heat-shock was applied at 5-6 hr AEL (Figure 3.4, middle and right panels). Interestingly, while the frequency of color matching of the v'ada-v'esB pair or the vdaC-vesB pair dropped significantly in the experiments done with 5-6 hr AEL heat-shock, that of the ldaA-lesA pair or the two es neurons in the v'es2 group remained unchanged (Figure 3.7). These observations suggest that at least one of the neurons in the v'ada-v'esB or the vdaC-vesB lineage finish its final cell division earlier than those in the ldaA-lesA or the v'es2 lineage.

Taken together, the birth-timing of individual lineages can be estimated by comparing the color matching frequency between earlier and later heat-shock time points.

Different combinations of *cis*-regulatory elements determine the expression of the terminal selector gene *dar1* in different lineages

Neurons assume distinct morphologies that can be categorized into multipolar, bipolar, and unipolar subtypes (Cajal, 1995; Wang et al., 2015). We previously found that *dar1* is selectively expressed in post-mitotic multipolar neurons and is necessary and sufficient for the multipolar morphology (Wang et al., 2015), thus functioning as a terminal selector for multipolar neuronal morphology (Hobert, 2008). With a refined PNS neuron lineage map, we can now investigate whether distinct *cis*-regulatory elements control the expression of *dar1* in multipolar neurons that are generated through distinct lineage patterns (e.g., da/es, da/es/es, or solo-da) (Figure 3.4).

We first created GFP-reporter *Drosophila* lines to identify the minimal genomic region that specifies *dar1* expression in multipolar neurons in the PNS. We found that an approximately 500 base-pair (bp) region located about 950 bp upstream from the *dar1* transcription start site was sufficient for driving GFP expression in most multipolar neurons, in particular nearly all da neurons except vdaD (Figure 3.8A-B and 3.9A). Interestingly, this 500-bp fragment also drives GFP expression in all bipolar ch neurons, but rarely in bipolar es neurons (Figure 3.8B). Moreover, consistent with the fact that *dar1* is absent in the larval CNS, which only contains non-multipolar neurons, this 500-bp fragment only drove GFP expression in a few neurons in the entire CNS, which was similar to a control driver that did not contain any *dar1* fragment (Figure 3.9B). These observations collectively suggest that this 500-bp fragment drives *dar1* expression in multipolar neurons while additional regulatory mechanisms prevent *dar1* expression in ch neurons.

Next, we set to determine whether this 500-bp fragment contains *cis*-regulatory elements that specifies *dar1* expression in certain lineage patterns of da neurons. To do so, we synthesized 9 overlapping DNA fragments of ~100 bp each to tile the entire 500-bp (Figure 3.9A). We then generated 9 reporter *Drosophila* lines, in each of which GFP was driven by one of the ~100 bp fragments. We then quantified the GFP expression pattern in da neurons (Figure 3.8C). We found that except fragments 4 and 5, all the other ~100-bp fragments drove GFP expression in at least one da neuron, indicating that they contain at least one *cis*-regulatory element. We also found that none of the 100-bp *cis*-regulatory fragments drove GFP expression in any ldaA, ddaB, ddaE, ddaF or vpda neurons, which suggests that *dar1* expression in these neurons requires combinations of these *cis*-regulatory elements. Next, we examined whether any particular combination of *cis*-regulatory elements drives GFP expression in da neurons generated with the same lineage pattern. We found that a region tiled by fragments 3, 6, 7 and 8 drove common GFP expression in ldaB and vdaD, both of which are generated with the da/es lineage pattern. None of the other combinations of *cis*-regulatory elements drove a common GFP expression pattern between any two da neurons.

These results suggest that da neurons generated through the same lineage pattern do not necessarily achieve their morphologies through a common set of *cis*-regulatory elements. Instead, different combinations of *cis*-regulatory elements determine the basic morphological types in different lineages.

Discussion

Our findings demonstrate that the novel *nBitbow* and the lineage relatedness test are proper tools for mapping neuronal lineages and estimating the birth-timing of neurons in the *Drosophila*

nervous system. Providing limited unique color choices in a transgenic animal, previous multi-spectral labeling methods were constrained to study lineages that contain large number of cells forming physically connected clones (Loulier et al., 2014). *nBitbow* overcomes this limitation by generating ~30 reliably detectable FP combination colors. The different frequency of expressing each color becomes an advantage for lineage tracing because our lineage relatedness test weights in the rarely generated color in a modified κ statistics to reveal the lineage relationship between two neurons.

Mapping lineages by *nBitbow* is much more efficient compared to previous method. For example, in a previous study, ~5000 embryos were examined to identify the lineage relationships in the *Drosophila* larval PNS. This is because in order to reliably count the frequency of neighboring cells expressing a lacZ marker that was induced by heat-shock in a single progenitor cell, labeling needs to be extremely sparse (Brewster and Bodmer, 1995, 1996). Using *nBitbow*, we achieved a similar goal with 40 larvae (23 for heatshock at 3-4 hr AEL and 17 for heatshock at 5-6 hr AEL). In addition, we took advantage of the fact that each larval PNS neuron is identifiable by its cell body position and the morphology of proximal dendrites (Bodmer and Jan, 1987; Grueber et al., 2002; Jan and Jan, 1982), and combined neuronal morphology staining with *nBitbow*'s multi-color nuclear labeling to assign each identified neuron to a lineage.

nBitbow's ability to generate many more unique colors also overcomes a fundamental limitation of the previous methods. With limited color choices, previous monochromic or multicolor labeling methods rely on physical proximity when determining whether two or more cells belong to the same lineage. This may generate false negative or false positive results; for instance, cells that migrate far from their sisters may be missed as in distinct lineages, or cells that locate close to it cluster boundary may be included in the neighboring lineages. Our method

minimizes these errors by providing reliable statistics to determine whether two cells are lineage-related based solely on *nBitbow* color but not on their physical locations. For instance, we discovered that even though da neurons in the vmd or dmd clusters are physically very close to each other, they are all generated by distinct progenitor cells (Figure 3.6). Interestingly, each of these da neurons was found to be lineage-related to a non-multipolar neuron that locates further away (Figure 3.3C-D).

Initiating *nBitbow* labeling at different developmental time points permitted convenient birth-timing analysis in the context of lineage-relationship among PNS neurons (Figure 3.4). We found that several PNS neuronal pairs that were identified as lineage-related in experiments with an earlier heat-shock time point were identified as lineage-unrelated in experiments with a later heat-shock time point. This suggests that none of the neurons in those lineages were born at the earlier time point so that they inherited the same colors from their mother SOPs when heat-chock was applied. On the other hand, one of the neurons in any of these lineages became to complete its last cell division at the later time point so that its color is distinct from its sister neuron. However, this method could not be used to determine the birth-timing of those are the sole neurons in their lineages. Since the *nBitbow* expresses bright nuclear targeted FPs, it is possible that the birth-timing of these neurons can be revealed by time lapse imaging in living larvae.

The success of our PNS neuronal lineage mapping created new opportunities for studying other biological aspects in the context of lineage development. For instance, it lays the foundation for studying whether particular molecular mechanisms are specified in neurons arising from different lineage patterns. Our results suggest that the transcriptional control of *dar1* gene in different da neuron lineages is complex. We speculate that distinct transcription factors are recruited to control *dar1* expression in different da neuron lineages, but common factors

might also be used in certain subsets of da neurons. Profiling the expression pattern of transcription factors in the context of da neuron lineages may reveal the regulatory mechanisms underlying neuronal morphogenesis in different lineages.

In summary, we expect these new tools to greatly increase the efficiency and accuracy for studying *Drosophila* lineage development beyond the nervous system. These new tools also bring the potentials of combining lineage mapping with other fields of research to answer complex questions in developmental biology.

3.4 Materials and Methods

The nBitbow construct and transgenic Drosophila lines

cDNAs encoding the following FPs were used: mAmetrine, mTFP, mNeonGreen, mKusabira-Orange2, and tdKatushka2 (Ai et al., 2008; Ai et al., 2006; Sakaue-Sawano et al., 2008; Shaner et al., 2013; Shcherbo et al., 2009). Human histone 2B protein (hH2B) was fused in frame to the N-terminus of individual FPs (hH2B-FP). Individual incompatible FRT sequence pairs (FRT^{F3}, FRT^{F14}, FRT^{545}, FRT^{F13}, or FRT^{5T2}) were then placed in the opposing direction on both ends of the hH2B-FP sequence (Cai et al., 2013; Mcleod et al., 1986; Schlake and Bode, 1994; Turan et al., 2010; Volkert and Broach, 1986). And then each of the five FRT-H2B-FP-invFRT cassettes were assembled into the pJFRC-MUH backbone vector (Addgene, Inc.) by standard cloning method, so that the expression of each cassette is under the control of an upstream activation sequence (UAS) and an p10 poly-adenylation (p10pA) sequence (Pfeiffer et al., 2012). The final *nBitbow* targeting plasmid was assembled by Gibson assembly (Gibson et al., 2009) into the same pJFRC-MUH backbone and was integrated into *Drosophila melanogaster* genome docking site VK00027 (BestGene, Inc.) using the ΦC31 integrase-mediated transgenesis systems

(Bateman et al., 2006b; Bischof et al., 2007; Groth et al., 2004; Markstein et al., 2008; Venken et al., 2006b).

nBitbow sample preparation and imaging

nBitbow transgenic flies, *nBitbow*$^{20355\text{-}2M3}$, was crossed with flies that carry heat-shock-inducible FLP^{122} and elav-Gal4, and raised at 23 °C for 2 days. To induce FP expression in the larval PNS, embryos were collected within consecutive 1-hour windows on day 3, and kept at 23 °C until heat shock at 2-3, 3-4, 4-5, 5-6, or 6-7 hr AEL. To induce FP expression in the larval CNS, 1st instar larvae were heat-shocked on 1 day AEL. The heat shock was performed by heating the embryo-containing agar-plate on the surface of a 70 °C heat-block for 1.5 min, followed by a 30 min heat chamber incubation at 37 °C. The plate was then transferred back to the 23 °C incubator for the next 4 days.

Late 3rd instar larvae were dissected to make fillet preparations in 1x hemolymph-like 3.1 saline buffer (Feng et al., 2004), immediately followed by fixation in 4% paraformaldehyde in 1x PBS for 20 min at room temperature (RT) with gentle shaking. Larval fillets were transferred to 1.5 ml Eppendorf tubes wrapped in tinfoil to prevent possible photobleaching by ambient lights. The samples were washed 3 times with 0.1% Triton X-100 in 1x PBS, 15 min each at RT, on a nutator, and then incubated in 5% normal donkey serum containing 0.1% Triton X-100 in 1x PBS for 30 min at RT. Alexa Fluor® 647 AffiniPure Goat Anti-Horseradish Peroxidase antibody (1:500, Jackson Immuno Research) was added to the samples for overnight incubation at 4 °C with gentle shaking. Samples were washed 3 times as described above. Fillets were placed on poly-L-lysine-coated coverslips and mounted with ProLong Diamond Antifade mountant

(Invitrogen™). Samples were left dry in the dark overnight at RT and imaged by confocal imaging on the following day or kept at 4 °C for up to a week until imaging.

nBitbow samples were imaged with a Zeiss LSM780 laser scanning confocal microscope. PNS data were collected from abdominal segments 2 to 7 (A2-A7). Fiji with customized plugin scripts was used to process raw images for FP spectral unmixing (Schindelin et al., 2012). Individual FP signals assuming the shape of a nucleus in the soma were identified on a single z-plane. If a particular FP signal were observed in a neuron, it is recorded as an "1" in the color code; if that FP's signal is not observed, it is then recorded as a "0". Color code of each neuron was recorded manually to create a data sheet for each experimental condition, which were subsequently analyzed computationally and statistically.

Quantification of lineage relatedness

The goal of our statistical methods was to systematically identify neurons that share a common lineage and those do not share a common lineage with any others. A key aspect of this test is the ability to score the lineage relatedness for a pair of two neurons based on the color codes recorded from the *nBitbow* experiments. To do this, we implemented a modified version of the Cohen's Kappa (κ) to quantify the degree of color-code agreement between two neurons, which is defined as:

$$\kappa = \frac{p_0 - p_e}{1 - p_e} \ , \qquad (1)$$

where p_0 and p_e are the degree of color code agreement between the two neurons calculated by observation and by chance, respectively.

To calculate the κ value for each neuron pair, we first calculate the probability of a neuron n that expresses a particular color c, $P_{n,c}$:

$$P_{n,c} = \frac{M_c}{N}, \quad (2)$$

where, M_c is the total observation that a neuron expresses color c, and N is the total number of neurons. As shown in Figure 2D, the percentage of neuron expressed any fluorescent color was relatively low (~6% maximum). We therefore hypothesize that most of the null-color (00000) neurons were the result of no Flp recombination at all, instead of due to the same FP being recombined even times. As a result, we estimated the κ in the cases that at least one of the neurons in a comparing pair needs to express at least one FP to avoid the false identification of null-color expressing neurons being lineage related. Based on this assumption, we can estimate the p_e value between neurons i and j (i.e., $p_e^{i,j}$), in which at least one of them expresses at least one FP. The $p_e^{i,j}$ value can be calculated by summing the products of the $P_{n,c}$ for both neurons for all the non-null colors (denoted from 1 to C):

$$p_e^{i,j} = \sum_1^C (P_{i,c}) \times (P_{j,c}) . \quad (3)$$

To calculate the p_0 value of the corresponding neuron pair $p_0^{i,j}$, we again, only considered the cases in which at least one of the neurons expressed at least one FP:

$$p_0^{i,j} = \frac{N_{i,j}^c}{M_{i,j}}, \quad (4)$$

where, $N_{i,j}^c$ is the total observations that both neurons expressed a same non-null colors color and $M_{i,j}$ is the total observations that either neuron expressed a non-null color.

Finally, we acquired the observed κ values for all the neuron pairs using their p_e and p_0 values following equation (1). An analysis of this equation reveals that if any two neurons always have perfectly matched colors (i.e., $p_0 = 1$), they will have a $\kappa = 1$. If two neurons' colors are matched exactly as would be expected by chance (i.e., $p_0 = p_e$), then they will have a

$\kappa = 0$. In this way, a higher κ value indicates a higher probability that the two neurons are labeled in the same color not by chance (i.e., lineage-related).

Statistical analysis of lineage relatedness

We designed a statistical test to determine whether the experimentally observed κ value of a neuron pair is significantly higher than that by chance. To estimate the κ value distribution from labeling a particular neuron pair by random colors, we established a randomization process, starting with generating a raw color matrix where every row represents an individual PNS hemi-segment, and each column represents a neuron within that hemi-segment. The κ values were calculated for all possible combinations of neuron pairs within the data. Next, the raw color matrix was randomized by shuffling the colors each neuron expressing any non-00000 null-color. This ensures that the neurons receiving a color in the randomized data will have also had a color in the real data. We reason that this randomization process is more accurate than a total randomization process because each neuron pair remains the same total chance to match colors as in the real experiments, in which the ambiguous 00000 null-color are excluded from being assigning as a matched color (see above). After the color randomization, the κ values were calculated for all possible combinations of neuron pairs within the data. This randomization process was repeated 100,000 times for each neuron pair to generate a distribution of κ values that were compared to the κ value obtained from the experimental observation. The number of times that the random κ value was greater than or equal to the observed κ value was counted and then divided by 100,000 to generate a p-value to estimate whether the experimentally observed κ value is significantly larger than those calculated by random color assignment. Finally, the p-values was adjusted for multiple hypothesis testing by calculating a false discovery rate (FDR)

using the Python statsmodels package (https://www.statsmodels.org/dev/generated/statsmodels.stats.multitest.multipletests.html). The Benjamini/Hochberg (non-negative) method was used for FDR evaluation (Benjamini and Hochberg, 1995).

It is important to run a separate test for each neuron pair because certain neurons expressed a color more often than others. This allowed us to normalize the high expressing neurons in a way that they did not just have a better κ value by chance.

The implementation of our lineage relatedness statistical model is available at https://github.com/MikeVeling/Process-Brainbow-Data.

The complete lineages map of PNS neurons was generated by the Cytoscape Software package (version 3.7.1., https://cytoscape.org/index.html).

dar1 cis-reporter constructs and transgenic fly generation

Genomic DNA (gDNA) of the *white*^{1118} strain of *Drosophila melanogaster* was extracted by standard method, and used as template for amplifying the 500 bp and 100 bp *cis*-regulatory elements with restriction sites (BamHI and EcoRI) added to the 5' and 3' end, respectively. The amplified DNA fragments were each cloned into the gateway entry vector (pBP-ENTR/D-TOPO) via restriction digestion and T4 ligation reaction. Subsequently the Invitrogen™ Gateway® LR clonase® II system was used to integrate the *cis*-element entry vectors into the destine backbone vector pBPGUw, which carries a minimal promoter to allow expressing Gal4 in the presence of active *cis*-regulatory element(s) (Pfeiffer et al., 2008; Pfeiffer et al., 2010; Swanson et al., 2008). Control transgene was made in the same backbone vector without adding any *cis*-regulatory element into the gateway entry vector. Purified plasmids were integrated into

Drosophila genome at the attP40 docking site using the ΦC31 integrase-mediated transgenesis systems (Bateman et al., 2006b; Bischof et al., 2007; Groth et al., 2004; Markstein et al., 2008; Venken et al., 2006b).

Sample preparation and imaging for dar1 expression reporters

dar1 cis-element-Gal4 transgenic flies were mated with UAS-GFP reporter flies (UAS-GFP^{VK33} or UAS-lacZ.nls::GFP) at 25 °C. The late 3rd instar larvae from the cross were dissected to make fillet preparations, fixed, washed, and blocked for immunostaining as described above for *nBitbow* samples. Primary antibodies chicken anti-GFP (Aves, 1:1000 dilution) and rat anti-Elav (Developmental Studies Hybridoma Bank, 1:100 dilution) were added to larval fillets for overnight incubation at 4 °C. Samples were then washed 3 times and then incubated with secondary antibodies for overnight incubation at 4 °C. The secondary antibodies used were Alexa Fluor® 488 AffiniPure Donkey Anti-Chicken IgY (IgG) (H+L), Rhodamine Red™-X (RRX) AffiniPure Donkey Anti-Rat IgG (H+L), and Alexa Fluor® 647 AffiniPure Goat Anti-Horseradish Peroxidase (Jackson Immuno Research, 1:500 dilution). After being washed 3 times, the samples were placed on poly-l-lysine coated coverslips for ethanol dehydration at 30%, 50%, 70%, 95%, 100% (two times) ethanol for 5 minute each. After that, the samples were treated with 100% xylene twice for 10 minute each. The fillet samples were mounted with DPX mounting media (Electron Microscopy Sciences) and left dry in the dark for at least overnight at RT. Confocal imaging was performed with a Leica TCS SP5 confocal microscope. PNS neurons in segments A2 to A7 were imaged.

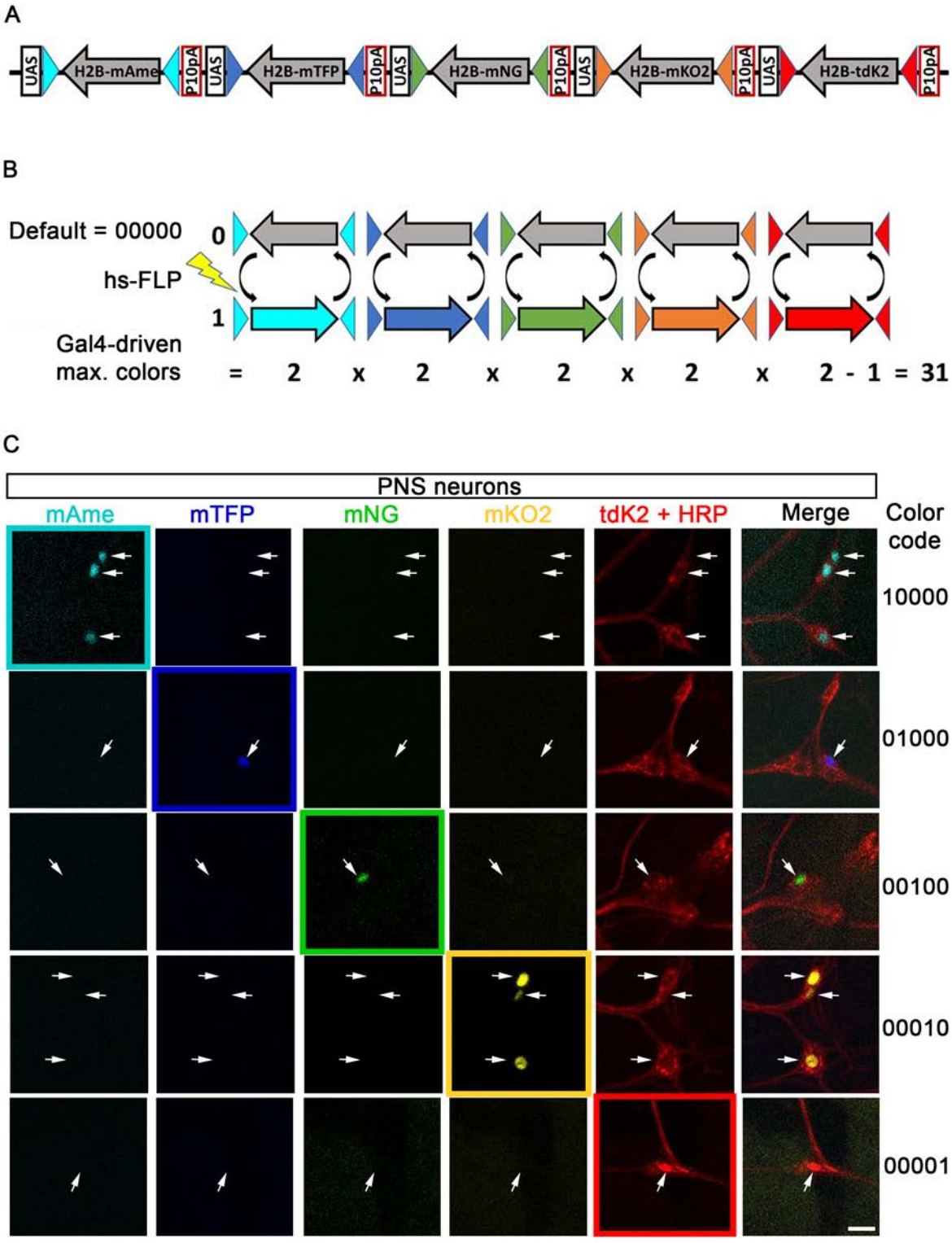

A
UAS
H2B-mAme
P10pA
UAS
H2B-mTFP
P10pA
UAS
H2B-mNG
P10pA
UAS
H2B-mKO2
P10pA
UAS
H2B-tdK2
P10pA
B
Default = 00000
hs-FLP
Gal4-driven
max. colors
0
1
= 2 x 2 x 2 x 2 x 2 - 1 = 31
C
PNS neurons
mAme
mTFP
mNG
mKO2
tdK2 + HRP
Merge
Color code
10000
01000
00100
00010
00001

Figure 3.1 Design and color-coding principles of *nBitbow*.

(**A**) Schematic of the *nBitbow* "spinning" design. The H2B fusion nuclear-FP (nucFP) open reading frames are positioned in the reverse direction as a default non-detectable color in the absence of FLP.
(**B**) Schematics of color-coding in *nBitbow*. Upon heat-shock-induced FLP expression, which causes recombination of FRT sites, each H2B-FP module can stochastically and independently spin into a forward (1, visible) or reversed (0, non-detectable) expression state. Maximum of 31 visible colors can be detected in the presence of a Gal4 driver.
(**C**) Spectral imaging and linear unmixing are performed to identify the five-bit *nBitbow* color code for each cell, in which "1"s represent the FPs that are turned on and "0"s represent those that are not turned on. HRP: anti-HRP immunostaining, which specifically labels PNS neurons. Scale bar: 10 μm.

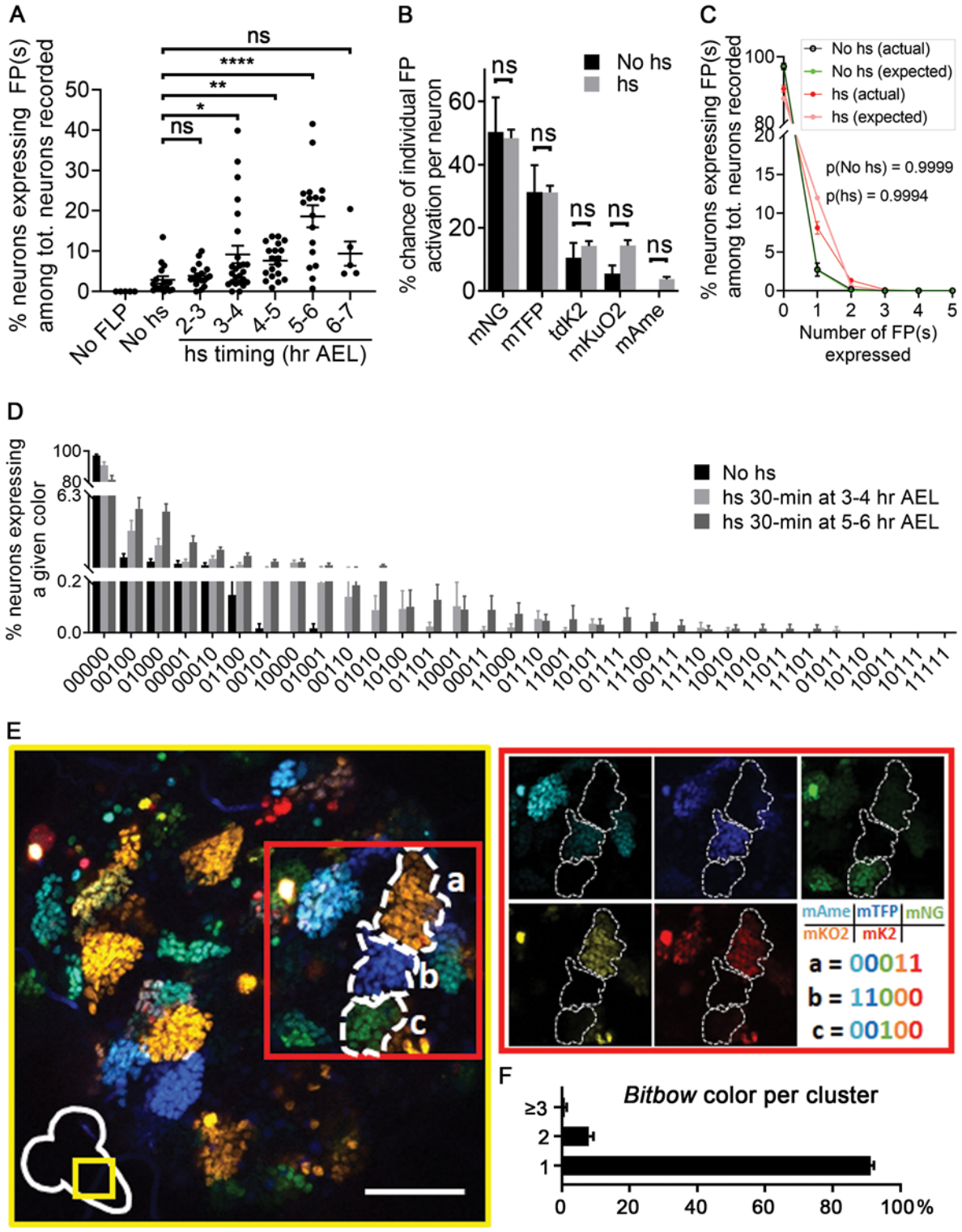

A
% neurons expressing FP(s) among tot. neurons recorded
ns
****
**
*
ns
No FLP
No hs
2-3
3-4
4-5
5-6
6-7
hs timing (hr AEL)
B
% chance of individual FP activation per neuron
No hs
hs
ns
mNG
mTFP
tdK2
mKuO2
mAme
C
% neurons expressing FP(s) among tot. neurons recorded
No hs (actual)
No hs (expected)
hs (actual)
hs (expected)
p(No hs) = 0.9999
p(hs) = 0.9994
Number of FP(s) expressed
D
% neurons expressing a given color
No hs
hs 30-min at 3-4 hr AEL
hs 30-min at 5-6 hr AEL
E
a
b
c
mAme
mTFP
mNG
mKO2
mK2
a = 00011
b = 11000
c = 00100
F
Bitbow color per cluster
≥3
2
1
100%

Figure 3.2 Labeling and lineage tracing efficacy of *nBitbow* in *Drosophila* nervous system.

(**A**) Quantification of the labeling coverage of *nBitbow* by heat-shock FLP induction in the PNS at various time points during early embryonic development. Sample numbers (larvae): no hs, 16; 2-3 hr AEL, 18; 3-4 hr AEL, 25; 4-5 hr AEL, 19; 5-6 hr AEL, 17; 6-7 hr AEL, 5. P-values were calculated by Dunn's multiple comparisons test. ns: $p > 0.05$, *: $0.01 < p \leq 0.05$, **: $0.001 < p \leq 0.01$, ***: $0.001 < p \leq 0.001$, and ****: $p < 0.0001$.
(**B**) Comparison of the turn-on efficiency of each FRT-nucFP-FRT module in the PNS. Heat-shock (hs) data are the combined data from hs at 2-3, 3-4, 4-5, 5-6, and 6-7 hr AELs. Sample numbers (larvae): no hs, 16; hs, 81. P-values were calculated by multiple comparisons using the Holm-Sidak method.
(**C**) The actual FP frequency distribution is not different from the theoretical distribution ("expected") as the number of activated FP increases in the PNS. This indicates that the recombination of each FRT-nucFP-FRT module is independent to each other. Sample numbers (larvae): no hs, 15; hs, 81. P-values were calculated by the Chi-square goodness-of-fit test for Poisson distribution.
(**D**) 27 color codes were observed with different frequencies in the PNS from a *Drosophila* line that carries only one *nBitbow* cassette. Sample numbers (larvae): no hs, 15; 3-4 hr AEL, 25; 5-6 hr AEL, 17.
(**E**) Representative images of *nBitbow* labeling in thoracic segments in the CNS of 3rd instar larvae with embryonic heat-shock FLP induction. Most of the cell clusters (i.e. lineage clones) were labeled by the same color. 193 clusters were analyzed. Scale bar: 50 μm.
(**F**) Proportion of thoracic lineage clones labeled by one, two or more *Bitbow* color tags, quantified across n=193 clusters. P-values were calculated using unpaired two-tailed t-test and α of 0.05 is used as the cutoff for significance. Error bars: standard error of mean.

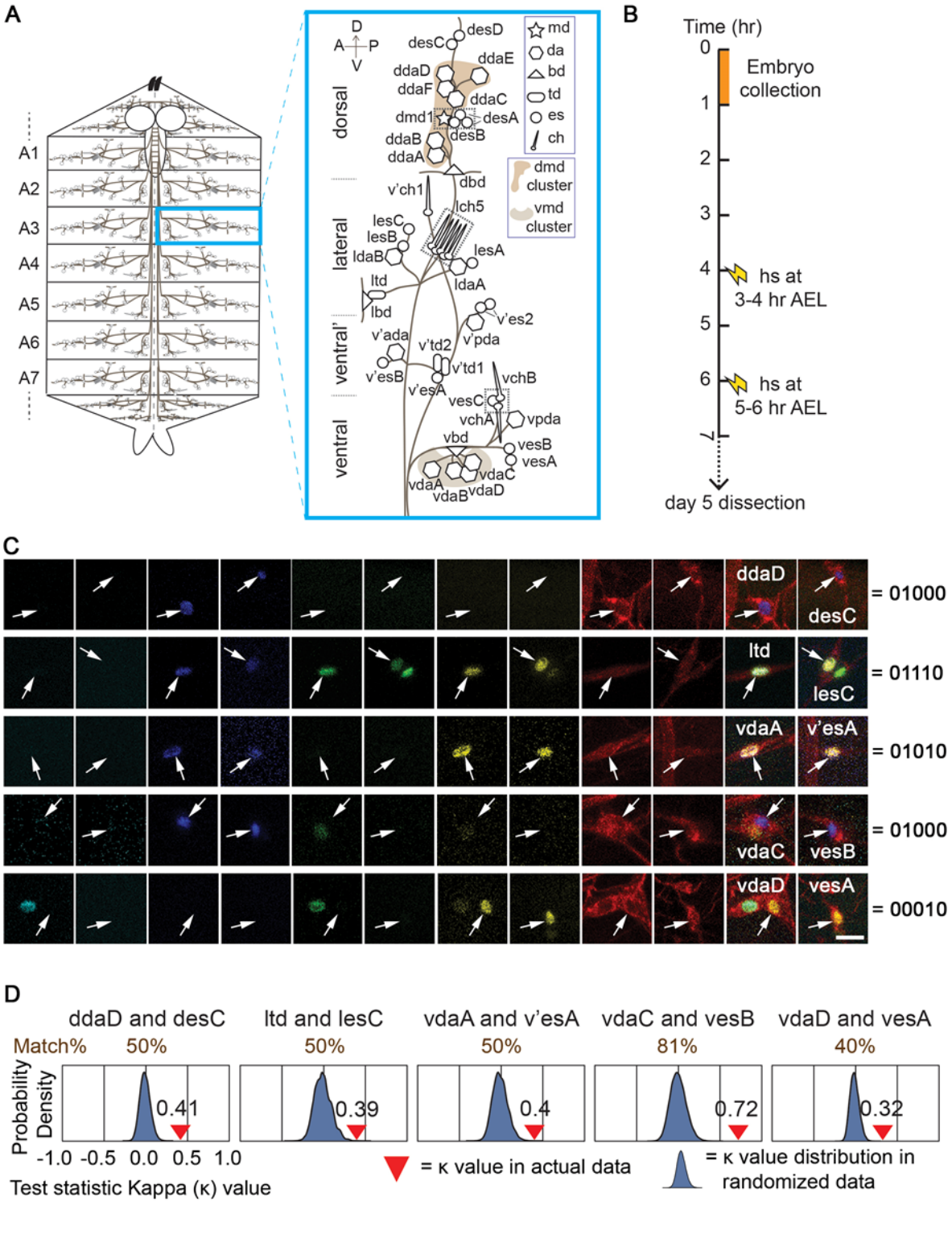

A
A1
A2
A3
A4
A5
A6
A7
D
A
P
V
dorsal
lateral
ventral'
ventral
desC
desD
ddaE
ddaD
ddaF
ddaC
dmd1
desA
desB
ddaB
ddaA
dbd
v'ch1
lch5
lesC
lesB
ldaB
lesA
ldaA
ltd
lbd
v'es2
v'ada
v'td2
v'pda
v'esB
v'td1
v'esA
vchB
vesC
vchA
vpda
vbd
vesB
vesA
vdaC
vdaA
vdaB
vdaD
md
da
bd
td
es
ch
dmd cluster
vmd cluster
B
Time (hr)
0
1
2
3
4
5
6
Embryo collection
hs at 3-4 hr AEL
hs at 5-6 hr AEL
day 5 dissection
C
ddaD
desC
= 01000
ltd
lesC
= 01110
vdaA
v'esA
= 01010
vdaC
vesB
= 01000
vdaD
vesA
= 00010
D
ddaD and desC
ltd and lesC
vdaA and v'esA
vdaC and vesB
vdaD and vesA
Match%
50%
50%
50%
81%
40%
Probability Density
0.41
0.39
0.4
0.72
0.32
-1.0 -0.5 0.0 0.5 1.0
Test statistic Kappa (κ) value
= κ value in actual data
= κ value distribution in randomized data

Figure 3.3 *nBitbow* efficiently identifies neuronal lineages of *Drosophila* PNS neurons.

(**A**) Schematic drawing of the distribution of PNS neurons in one hemi-segment of the larval body wall. In the PNS, multipolar neurons include the md, da, bipolar dendrite (bd), and td types, whereas bipolar neurons include the es and chordotonal (ch) types.
(**B**) Schematic drawing of the experimental steps.
(**C**) Representative fluorescent images that show matching color-codes of pairs of neurons previously thought to be independent to each other. These newly identified neuronal pairs are the five es neurons (desC, lesC, v'esA, vesA and vesB) and their lineage-related da or td neurons. These es neurons have been previously reported as the only neuron from individual SOPs (Brewster and Bodmer, 1995). Larvae were heat-shocked at 3-4 hr AEL. Scale bar: 10 μm.
(**D**) Statistical analysis confirms that these neuron pairs are lineage-related. The κ values calculated based on experimental observations (red arrows) are significantly higher (i.e., closer to "1") than those calculated based on a random color distribution (blue).

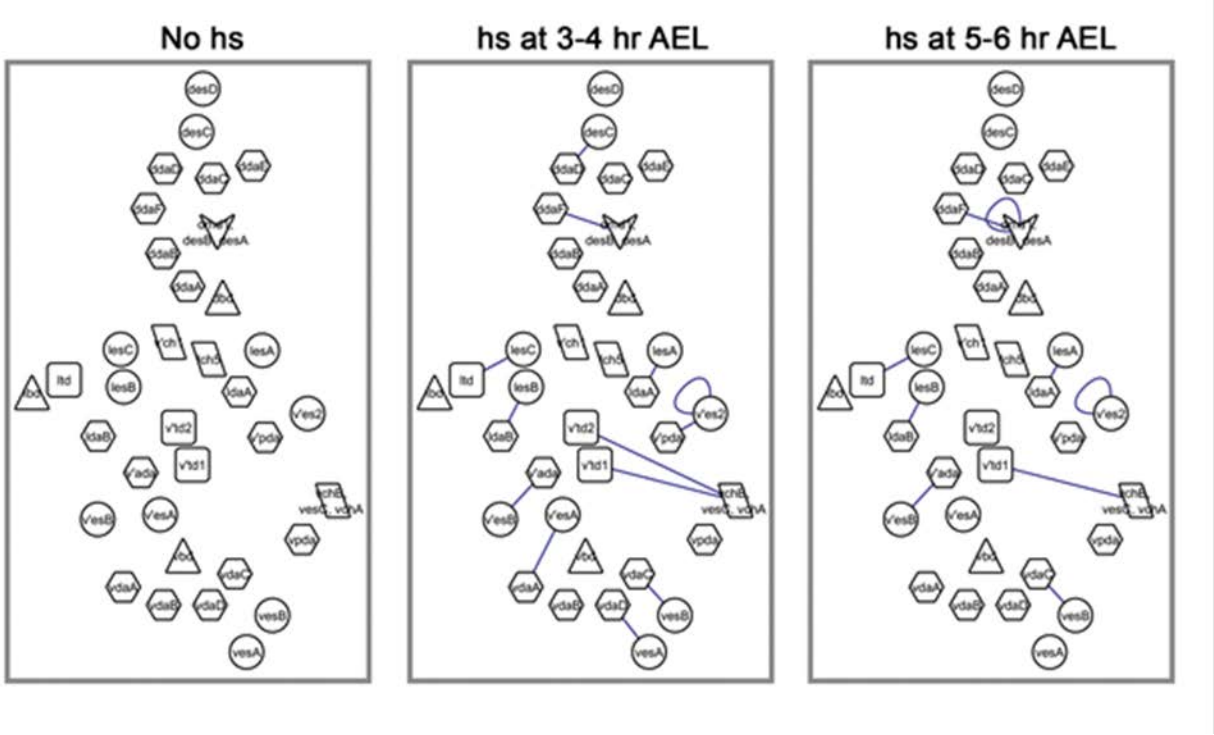


Figure 3.4 PNS lineage maps revealed by *nBitbow* at different developmental times.

Shown are neurons in a hemi-segment. These maps are based on the lineage relationships of all neurons determined by their calculated κ values from experiments with no heat-shock (left), heat-shock at 3-4 hr AEL (middle), and 5-6 hr AEL (right). Each line connects a pair of lineage-related neurons with ≤ 2% false discovery rate (FDR). Three groups of neurons that cannot be identified individually (dotted boxes in Figure 3A) are presented as single symbols in these maps: the arrow head includes four neurons—dmd1, desB, and 2 desA—which are located in close proximity; the parallelogram labeled as "lch5" includes 5 ch neurons; and the parallelogram labeled as "vchA, vchB, vesC" includes the three neurons indicated.

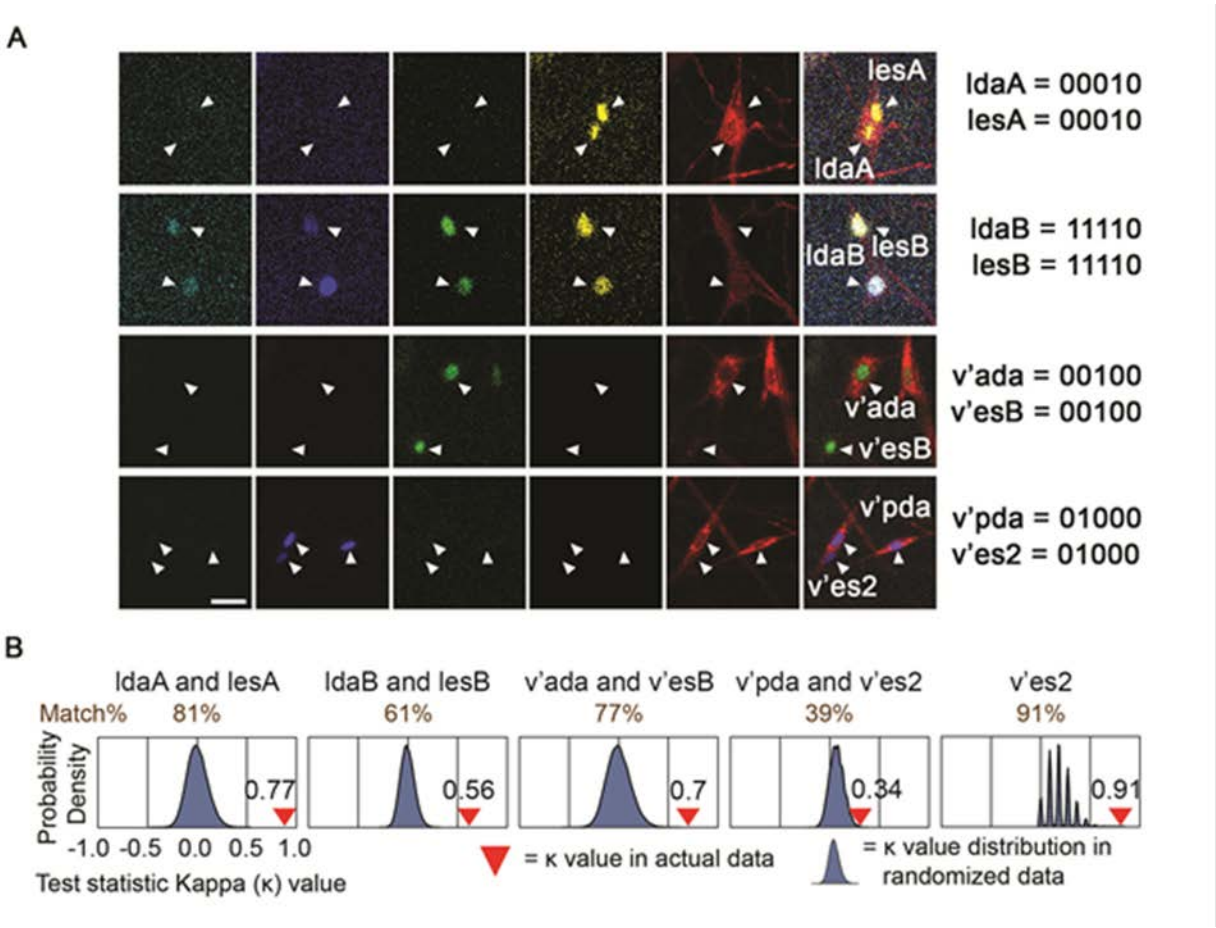


Figure 3.5 Lineage tracing by *nBitbow* confirms some previously reported lineages.

(**A**) Representative fluorescent images for the previously reported PNS neuron lineages ldaA-lesA, ldaB-lesB, v'ada-v'esB, and v'pda-v'es2 (Brewster and Bodmer, 1995). The color codes of the fluorescent proteins expressed in the neurons are shown on the right. Scale bar: 10 μm.
(**B**) The neuron pairs in these lineages have significantly higher positive κ values calculated from the experimental observations than those calculated from the randomized model in the relatedness tests.

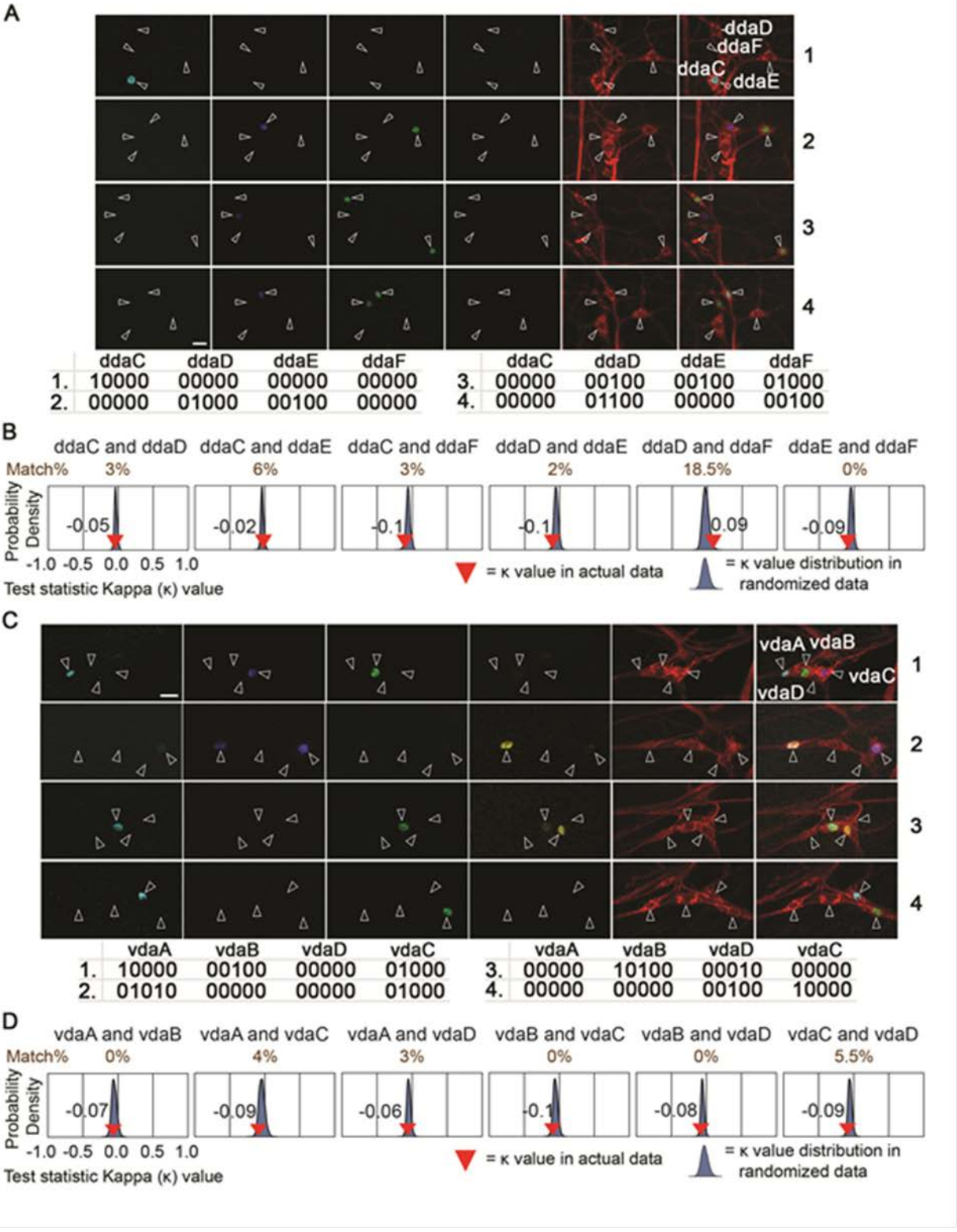

A
ddaD
ddaF
ddaC
ddaE
1
2
3
4
ddaC ddaD ddaE ddaF
1. 10000 00000 00000 00000
2. 00000 01000 00100 00000
3. 00000 00100 00100 01000
4. 00000 01100 00000 00100
B
ddaC and ddaD
ddaC and ddaE
ddaC and ddaF
ddaD and ddaE
ddaD and ddaF
ddaE and ddaF
Match%
3%
6%
3%
2%
18.5%
0%
Probability Density
-0.05
-0.02
-0.1
-0.1
0.09
-0.09
-1.0 -0.5 0.0 0.5 1.0
Test statistic Kappa (κ) value
= κ value in actual data
= κ value distribution in randomized data
C
vdaA vdaB
vdaC
vdaD
1
2
3
4
vdaA vdaB vdaD vdaC
1. 10000 00100 00000 01000
2. 01010 00000 00000 01000
3. 00000 10100 00010 00000
4. 00000 00000 00100 10000
D
vdaA and vdaB
vdaA and vdaC
vdaA and vdaD
vdaB and vdaC
vdaB and vdaD
vdaC and vdaD
Match%
0%
4%
3%
0%
0%
5.5%
Probability Density
-0.07
-0.09
-0.06
-0.1
-0.08
-0.09
-1.0 -0.5 0.0 0.5 1.0
Test statistic Kappa (κ) value
= κ value in actual data
= κ value distribution in randomized data

Figure 3.6 Lineage tracing by *nBitbow* rejects some previously reported lineages.

(**A**) Representative fluorescent images for the previously reported lineage-related neurons in the dmd cluster (Brewster and Bodmer, 1995). The color codes of the fluorescent proteins expressed in the neurons are shown at the bottom. Scale bar: 10 μm.
(**B**) The κ values of the neuron pairs in the dmd cluster are not significantly different from those calculated with the randomized model in the relatedness tests.
(**C**) Representative fluorescent images for the previously reported lineage-related neurons in the vmd cluster (Brewster and Bodmer, 1995).
(**D**) The κ values of the neuron pairs in the vmd cluster are not significantly different from those calculated with the randomized model.

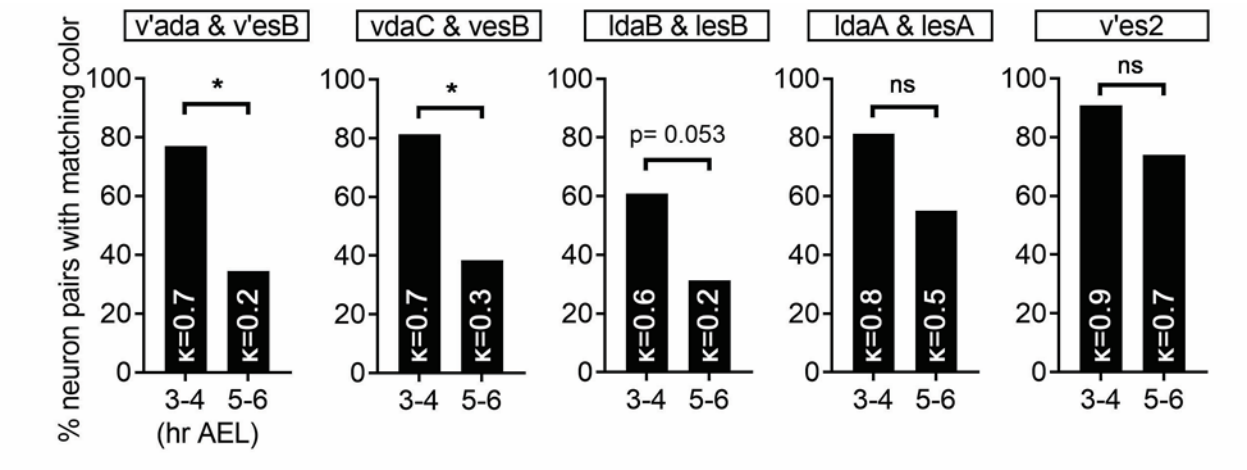


Figure 3.7 *nBitbow* provides an efficient way to compare the birth-time of neurons in different lineages.

The percentage of neuron pairs with matching colors decreases significantly for several lineages (e.g., v'ada-v'esB, vdaC-vesB, ldaB-lesB) but remains high for some lineages (e.g., the ldaA-lesA lineage, and two neurons in the v'es2 group), suggesting the former are closer to finishing their lineage development than the latter. The percentage of neuron pairs with matching colors is quantified by dividing the number of total neuron pairs that have the same colors to the number of total neuron pairs that are labeled by any color. All neuron pairs analyzed in this experiment are lineage-related, as determined by the relatedness test. *: $\alpha < 0.05$, Fisher's exact test.

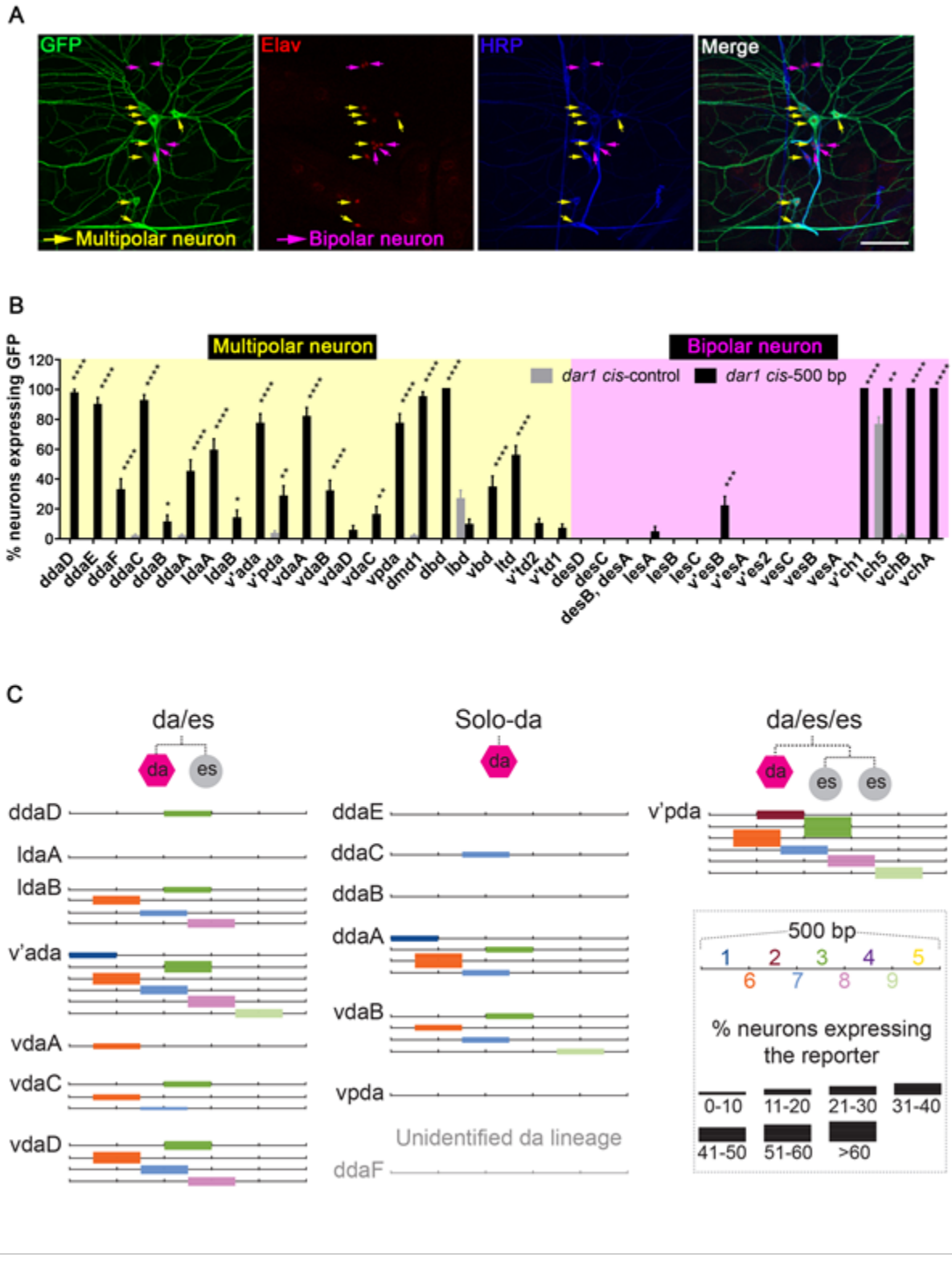

A
GFP
Elav
HRP
Merge
Multipolar neuron
Bipolar neuron
B
Multipolar neuron
Bipolar neuron
dar1 cis-control
dar1 cis-500 bp
% neurons expressing GFP
120
100
80
60
40
20
0
ddaD
ddaE
ddaF
ddaC
ddaB
ddaA
ldaA
ldaB
v'ada
v'pda
vdaA
vdaB
vdaD
vdaC
vpda
dmd1
dbd
lbd
vbd
ltd
v'td2
v'td1
desD
desC
desB, desA
lesA
lesB
lesC
v'esB
v'esA
v'es2
vesC
vesB
vesA
v'ch1
lch5
vchB
vchA
C
da/es
da
es
ddaD
ldaA
ldaB
v'ada
vdaA
vdaC
vdaD
Solo-da
da
ddaE
ddaC
ddaB
ddaA
vdaB
vpda
Unidentified da lineage
ddaF
da/es/es
da
es
es
v'pda
500 bp
1
2
3
4
5
6
7
8
9
% neurons expressing the reporter
0-10
11-20
21-30
31-40
41-50
51-60
>60

Figure 3.8 Multipolar neurons arising from different lineages express the morphological terminal selector gene *dar1* through different combinations of *cis*-regulatory elements.

(**A**) A 500-bp genomic DNA upstream of *dar1* transcription initiation site drives the expression of GFP-reporter in multipolar neurons (yellow arrows) but not in bipolar neurons (magenta arrows). Green: membrane-bound GFP reporter; red: pan-neuronal marker Elav; blue: anti-HRP. Scale bar: 50 μm.
(**B**) Quantification of the percentage of PNS neurons expressing GFP in the 500-bp driver line ("*dar1* cis-500 bp"). PNS neurons (lbd and lch5) are excluded in the following studies due to high non-specific reporter expression in the control transgenic animals ("*dar1* cis-control"). P-values were calculated by multiple comparisons using the Holm-Sidak method. *: $0.01 < p \leq 0.05$, **: $0.001 < p \leq 0.01$, ***: $0.001 < p \leq 0.001$, and ****: $p < 0.0001$. Error bars: standard error of mean.
(**C**) da neurons are categorized by three lineage patterns: da/es, da/es/es, and solo-da. The black lines represent the 500-bp genomic DNA fragment that drives reporter expression. Individual color block represents the ~100 bp fragments that drive reporter expression significantly in subsets of neurons. The thickness of the color blocks approximates the percentage of neurons expressing the reporter.

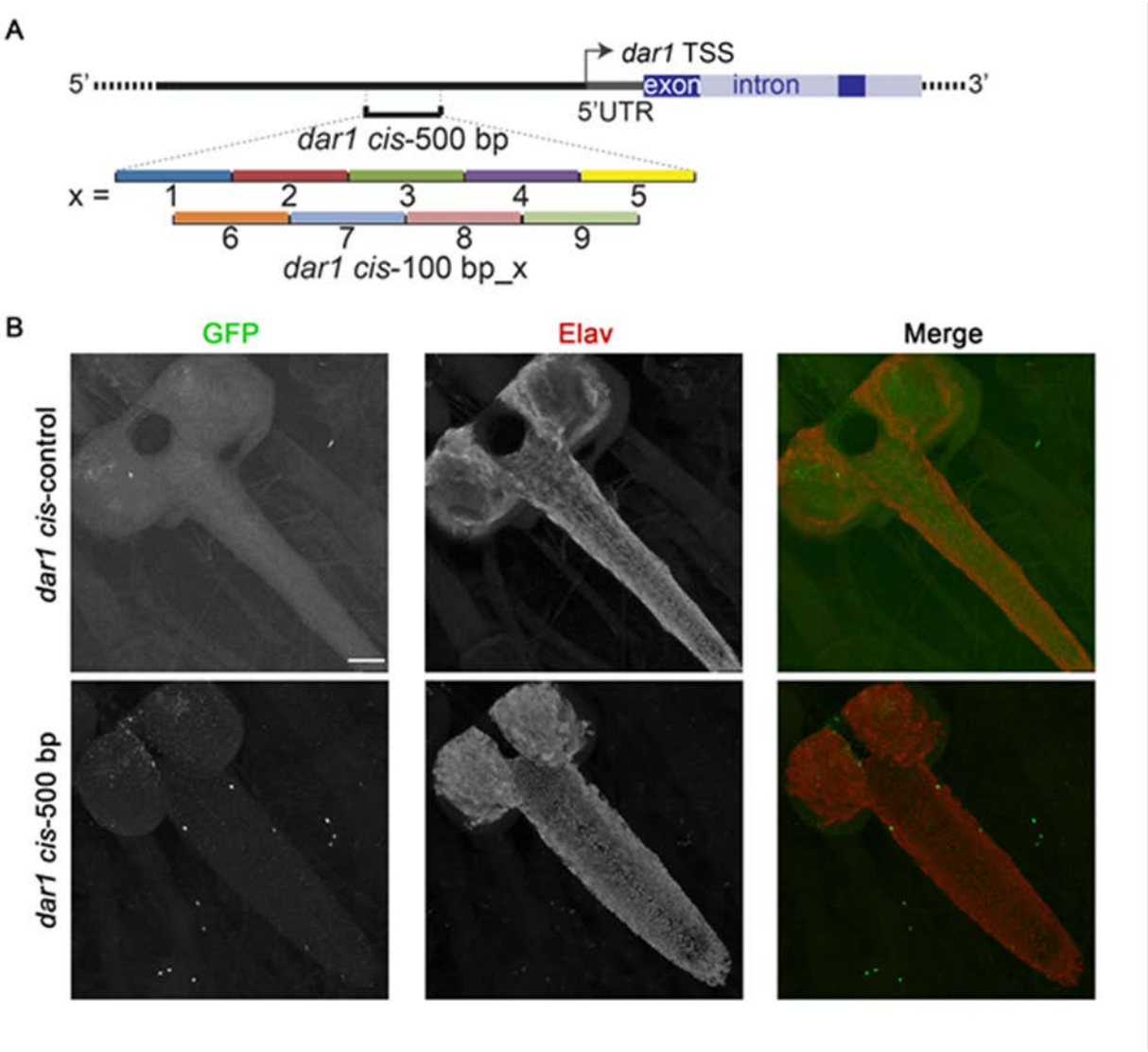


Figure 3.9 Identification of the cis-regulatory elements of *dar1* expression by using GFP reporters.

(**A**) Schematic drawing that shows the genomic locations of the 500-bp fragment that largely recapitulates *dar1* expression and the 100-bp fragments used to further identify the *cis*-regulatory elements. TSS: transcription start site.
(**B**) Both the control driver and the 500-bp *dar1* fragment drive the expression of the GFP-reporter only in a few neurons in the entire CNS, which contains only non-multipolar neurons. Scale bars: 50 μm.

Chapter 4 Functional interactions between Down syndrome genes in axon development

Co-authored with Gabriella Sterne, Hao Liu, and Bing Ye.

4.1 Abstract

The levels of Down syndrome cell adhesion molecule (Dscam) and amyloid precursor protein (APP) are increased in the brains of patients with Down syndrome (DS). Previous studies have shown that in *Drosophila* increased levels of Dscam cause overgrowth of presynaptic terminals, which requires Abelson tyrosine kinase (Abl). In this study, we show that overexpression of APP-like (Appl), the *Drosophila* homolog of APP, also causes overgrowth of presynaptic terminals. Appl overexpression requires Dscam to promote presynaptic overgrowth, while Dscam overexpression does not require Appl. Interestingly, Appl overexpression increased Dscam levels. These studies demonstrate an interaction between Dscam and Appl in the development of presynaptic terminals. They raise the possibility that these two DS genes function together to cause neurodevelopmental defects in DS, providing a hypothesis to test in mammals.

4.2 Introduction

The Down syndrome cell adhesion molecule (*dscam*) gene is located within the Down syndrome critical region (DSCR) on human chromosome 21 and is important for the development of neurons. Dscam plays many roles in neuron development, including dendritic growth, branching

and self-avoidance, as well as axon targeting and growth (Hattori et al., 2008; Hummel et al., 2003; Hutchinson et al., 2014; Kim et al., 2013; Koch et al., 2018; Lowe et al., 2018; Matthews et al., 2007; Millard et al., 2007; Millard et al., 2010). Recent studies in *Drosophila* revealed that the Dscam protein level determines the size of presynaptic arbor of sensory neurons (Kim et al., 2013). Interestingly, this function of Dscam is protein-level-dependent (Kim et al., 2013). Because Dscam levels are increased in the brains of Down syndrome (DS) patients, these findings lead to the hypothesis that the dysregulated Dscam levels in DS might cause changes in axon development. Moreover, the function of Dscam in promoting presynaptic arbor growth requires the activation of Abelson tyrosine kinase (Abl), and inhibiting Abl activity prevents axon overgrowth induced by Dscam overexpression (Sterne et al., 2015). These results revealed a Dscam-Abl signaling mechanism that could potentially be targeted for clinical treatment in DS. However, many protein-encoding genes of human chromosome 21, which may have overlapping functions in neuron, are overexpressed in DS. Thus, it is important to clarify whether different DS genes functionally interact with each other to affect neuronal development in DS.

The amyloid precursor protein (APP) gene, located outside the DSCR, encodes the precursor protein for the pathogenic β-amyloid (Aβ) peptides in Alzheimer's disease (Kang et al., 1987). While the processing of APP for the generation of Aβ have been extensively studied in the past two decades, less is known about the function of APP in development. It was previously suggested that both human APP and the *Drosophila* Homolog of APP (Appl) promote axonal arborization in *Drosophila* brain neurons, which also requires Abl (Guenette et al., 2017; Leyssen et al., 2005; Soldano et al., 2013). Given that Dscam and APP are functionally similar in promoting axonal growth and since both genes are overexpressed in DS, we asked whether Dscam and APP functionally interact to control axon terminal growth. Using *Drosophila* sensory

neurons to address this question, we observed that the effect of double overexpression of Dscam and Appl is additive. We found that Appl requires Dscam to promote axon terminal growth, while Dscam does not require Appl to promote axon terminal growth. Moreover, we observed that Dscam protein level is increased by Appl overexpression, and this upregulation of Dscam occurs at a post-transcriptional stage. Taken together, our studies provide a new mechanistic insight into how functionally overlapped DS genes can influent each other to act on axon terminal growth.

4.3 Results and discussion

Effect of increased Dscam and Appl on axon terminal growth is additive

To determine whether the function of Appl in axon terminal growth, which was identified in *Drosophila* brain neurons, behaves similar in the Class 4 dendritic arborization (C4da) sensory neurons, we first compared the presynaptic terminal size among control, loss of *appl*, and overexpression of Appl. We observed that loss of *appl* caused reduction of presynaptic terminal size while overexpressing Appl caused overgrowth, suggesting Appl plays a similarly role as Dscam in C4da neurons (Figure 4.1). Next, we examined whether overexpressing Dscam and Appl simultaneously results in more severe presynaptic overgrowth than overexpressing either one of them. Overexpression of both genes led to more severe presynaptic arbor overgrowth than overexpression of either gene (Figure 4.2). This observation led us to ask how Dscam and Appl genetically interact to control presynaptic arbor growth.

Appl requires Dscam to promote presynaptic arbor growth

To examine whether Dscam and Appl depend on each other to control presynaptic arbor growth, we performed epistasis experiments by overexpressing Appl with or without the loss of *dscam*. As expected, loss of *dscam* reduced the presynaptic terminal size, and Appl overexpression led to overgrow. Interestingly, overexpressing Appl in loss of *dscam* function failed to promote axon growth, suggesting Appl requires Dscam to promote presynaptic arbor growth (Figure 4.3).

We also performed the converse experiment. Loss of *appl* reduced the presynaptic terminal size, and Dscam overexpression led to overgrow. However, overexpressing Dscam in loss of *appl* function was sufficient to promote axon growth, with a similar magnitude of change as overexpressing Dscam in control background (Figure 4.4). This result indicates that Dscam does not require Appl. Taken together, these results suggest that Appl may act upstream of Dscam for promoting presynaptic arbor growth.

Appl overexpression increases Dscam protein levels in neurons

To further understand how Appl requires Dscam to promote presynaptic arbor growth, we examined whether Appl affects the protein level of Dscam. Surprisingly, the endogenous protein level of Dscam was increased by Appl overexpression but unaffected by loss of *appl* function in neurons (Figure 4.5). To determine if Appl alters Dscam level at the post-transcriptional stage, we used Gal4/UAS system to control gene expressions of GFP tagged *dscam* and V5 tagged *appl* independently while balancing the same number of Gal4 and UAS among all experimental conditions. Using antibody to against GFP tagged Dscam, we found that Dscam level was again increased when Appl was overexpressed, whereas V5 tagged Appl level remained the same between conditions (Figure 4.6). To further confirm Appl does not affect Dscam transcription, we used RT-qPCR to measure *dscam* mRNA levels in the absence of, or in the presence of extra,

Appl. We found that neither loss of *appl* nor overexpressing Appl altered the total mRNA level of *dscam*, indicating that Appl affects Dscam level at a post-transcriptional stage (Figure 4.7).

Discussion

Gene dosage imbalance is one of the major contributors to mental retardation in DS (Antonarakis, 2017; Asim et al., 2015; Rachidi and Lopes, 2007; Sinet et al., 1994) . This imbalance could lead to morphological defects of neurons during development, which may alter the brain circuity and result in intellectual disability (Forrest et al., 2018; Testa-Silva et al., 2012). Although different DS genes may play similar roles in specific aspects of neuronal development, few studies have been done to determine whether functionally similar DS genes interact.

Here, we demonstrated the functional interactions between *dscam* and *appl* genes in controlling presynaptic arbor growth. We found that Appl acts upstream of Dscam. Moreover, we showed that overexpression of Appl in neurons results in upregulation of Dscam protein level through a post-transcriptional regulation. Although we still do not know how exactly Appl affects Dscam expression, it is possible that the translation of *dscam* mRNA is enhanced or Dscam protein degradation is blocked when Appl is overexpressed. Further experiments are necessary to distinguish these biological processes. Moreover, our results provide a hypothesis to test whether APP affects Dscam protein levels in mammals. To do so, we can normalize *APP* gene number by crossing trisomy mouse models of DS with *APP* loss-of-function mice and then measure Dscam level.

In addition, several studies have suggested that Abl is required by Appl or Dscam to promote axon terminal growth, and Abl inhibitors can prevent axon overgrowth induced by

Dscam overexpression (Leyssen et al., 2005; Soldano et al., 2013; Sterne et al., 2015). In our studies, we showed that Appl requires Dscam to promote presynaptic arbor growth. If Abl were required by Appl to promote axon overgrowth, Abl would be a good therapeutic candidate to be targeted in DS. If not, we could identify other downstream effector(s) used by both Appl and Dscam. Further experiments are needed to answer these questions.

Overall, our finding is significant and show the necessity of understanding how multiple DS genes interact with each other to affect neuronal development and functions.

4.4 Materials and Methods

Fly strains

appl^{d} (BDSC #43632); UAS-Appl::V5 (this study); *Dscam*^{18} (Wang et al., 2002); *UAS-Dscam[TM2]::GFP (3.36.25)* (Wang et al., 2004)*; UAS-GFP::lacZ.nls (BDSC #6451 and #6452); nSyb-Gal4 (BDSC #51635);* and *UAS-mCD8::GFP* (Lee and Luo, 1999) were used in this study.

Generation of transgenic flies

Fly lines that express V5-tagged Appl driven by the UAS promoter was created in this study. The cDNA of *appl* sequence with restriction site (EcoRV) added to both the 5' and 3' ends was first cloned into the pAc5.1-V5/HisA plasmid (Doring et al., 2002; Lee et al., 2000; Park et al., 2006) with standard cloning method. Next, the Appl-V5/HisA DNA sequence with restriction sites (EcoRI and Acc65I) added to the 5' and 3' ends was cloned into the pUAST-attB plasmid (Bischof et al., 2007). The purified plasmid was then integrated into *Drosophila* genome at the attP40 (2nd chromosome) or attP2 (3rd chromosome) docking site using the ΦC31 integrase-

mediated transgenesis systems (Bateman et al., 2006a; Bischof et al., 2007; Groth et al., 2004; Markstein et al., 2008; Venken et al., 2006a) to generate pUAST-Appl-V5/HisA transgenic lines.

C4da axon terminal visualization and MARCM for single presynaptic terminal labeling

The axon terminals of all C4da neurons were visualized by the expression of membrane marker CD8::GFP, which was driven by the ppk-Gal4 driver. The additional combination of UAS-lacZ::GFP.nls, UAS-Appl::V5, and/or UAS-Dscam[TM2]::GFP (3.36.25) for axonal morphology determination were also driven by the same ppk-Gal4 driver, which was balanced with the equal number of UAS per experimental condition except in the wild-type. The MARCM technique (Lee and Luo, 1999) was used to generate homozygous for *appl*^{d} and *dscam*^{18}, or overexpression of Appl::V5 and Dscam[TM2]::GFP (3.36.25) in a single ddaC neuron expressing the membrane marker GFP::CD8 for visualization. P-values were calculated by ordinary One-way ANOVA test with Tukey's multiple comparison correction. ns: $p > 0.05$, *: $0.01 < p \leq 0.05$, **: $0.001 < p \leq 0.01$, ***: $0.001 < p \leq 0.001$, and ****: $p < 0.0001$.

Primary antibodies used for in vivo immunostaining were Chicken anti-GFP (1:1000 dilution, Avēs labs, Inc.). Antibodies were diluted in 0.1% Triton X-100 contained PBS solution. Secondary antibodies used for immunostaining were anti-chicken 488 (1:500 dilution, Jackson Immuno Research).

RT-qPCR

Total RNA was extracted and purified from the late 3rd instar of *Drosophila* larvae CNS using a standard Tri-zol protocol (Invitrogen). The wild-type and homozygous *appl*^{d} mutant were used for the loss of function qPCR comparison. nSyb-Gal4 crossed with either UAS-CD8::GFP or

UAS-Appl::V5 were used for overexpression qPCR comparison. First strand cDNA was synthesized using the SuperScript^{TM} III first-strand synthesis superMix (Invitrogen). cDNA from ~10 ng RNA was used for each real-time PCR reaction (10 µl), using the Power SYBR Green Master Mix (Thermo Scientific) with Applied Biosystems™ QuantStudio™ 6 Flex Real-Time PCR System (Thermo Scientific). After the cycle number at the threshold level of log-based fluorescence (Ct) had been collected for each sample, ΔCt for each test gene was calculated by subtracting the Ct number of the reference gene (*chmp1*) from that of the test gene (Ct_{test}-Ct_{chmp1}) (Yuan et al., 2006). This normalizes transcript levels of test genes to *chmp1*. The ΔCt of each test gene was statistically compared between wild-type and $appl^{d}$, or OE CD8::GFP and OE Appl::V5, and then converted to fold change. P-values were calculated by the Kruskal-Wallis test with Dunn's multiple comparison correction. ns, $p > 0.05$.

Primer sets used for qPCR were *Chmp1*, 5'-AAAGGCCAAGAAGGCGATTC-3' and 5'-GGGCAC TCATCCTGAGGTAGTT-3'; *Dscam* #1, 5'-CTTACGATTGTGCTCATTACTC-3' and 5'-CAGTT TCGATTTGTTCTGTTGG-3'; *Dscam* #2, 5'-ATCGAAACTGTTCAATGCAC-3' and 5'-CTT GAGTGTATCTGTGTTTCGG-3' (Kim et al., 2013).

Western blotting

Approximately ~20 CNS of the late 3rd instar larvae from wild-type, homozygous $appl^{d}$, or nSyb-Gal4 crossed with overexpression lines (i.e. UAS-CD8::GFP, UAS-Appl::V5, UAS-Dscam[TM2]::GFP, and/or UAS-GFP::lacZ.nls) were extracted and lysed in 40 µl of 2X lysis buffer containing 10% *β-mercaptoethanol*. Lysates were freeze/thawed 3 times between -80℃ and room temperature (RT) for 10 minute each condition, sonicated for 5 second each followed by heat boiling at 98℃ for 5 minutes. Samples were stored at -20℃ or process to next step.

Samples were quickly spinned down with maximum speed for 5 seconds. Individual samples were loaded 10 µl (or 15 µl) to the 7.5% SDS-PAGE gel, followed by gel runing at 100 V for 90 minutes. Next the gel was sandwiched with nitrocellular membrane (Thermo Fisher) and transferred in 5% methanol contained transfer buffer for 3 hours at 50 V (XCell II™ Blot Module, Invitrogen) in the cold room. Membrane was blocked in 5% milk contained 1X TBST for 1 hour at RT followed by primary antibody overnight incubation at 4℃ with gentle shaking. On the next day, membrane was washed 3 times with 1X TBST, 10 minute each, followed by secondary antibody incubation at RT for 1 hour. Membrane was washed 3 times as before and process for imaging using SuperSignal™ West Pico PLUS Chemiluminescent Substrate (Thermo Fisher) with the ChemiDoc™ Touch imaging system (Bio-Rad). P-values were calculated using the Mann-Whitney test. ns, $p > 0.05$; *, $0.01 < p \leq 0.05$; **, $0.001 < p \leq 0.01$.

Primary antibodies used for western blot were Mouse monoclonal anti-V5 (1:1000 dilution, Invitrogen Cat# xxxx), Mouse anti-Dscam (1:1000 dilution, gift from xxx), Mouse monoclonal anti-Aequorea Victoria GFP JL-8 (1:1000 dilution, Clontech), Rat anti-Elav-7E8A10 supernatant (1:500 dilution, DSHB). All primary antibodies were diluted in 5% milk contained 1X TBST.

Secondary antibodies used for western blot were anti-Mouse HRP and anti-Rat HRP (1:5000 dilution, Jackson Immuno Research) in 5% milk contained 1X TBST.

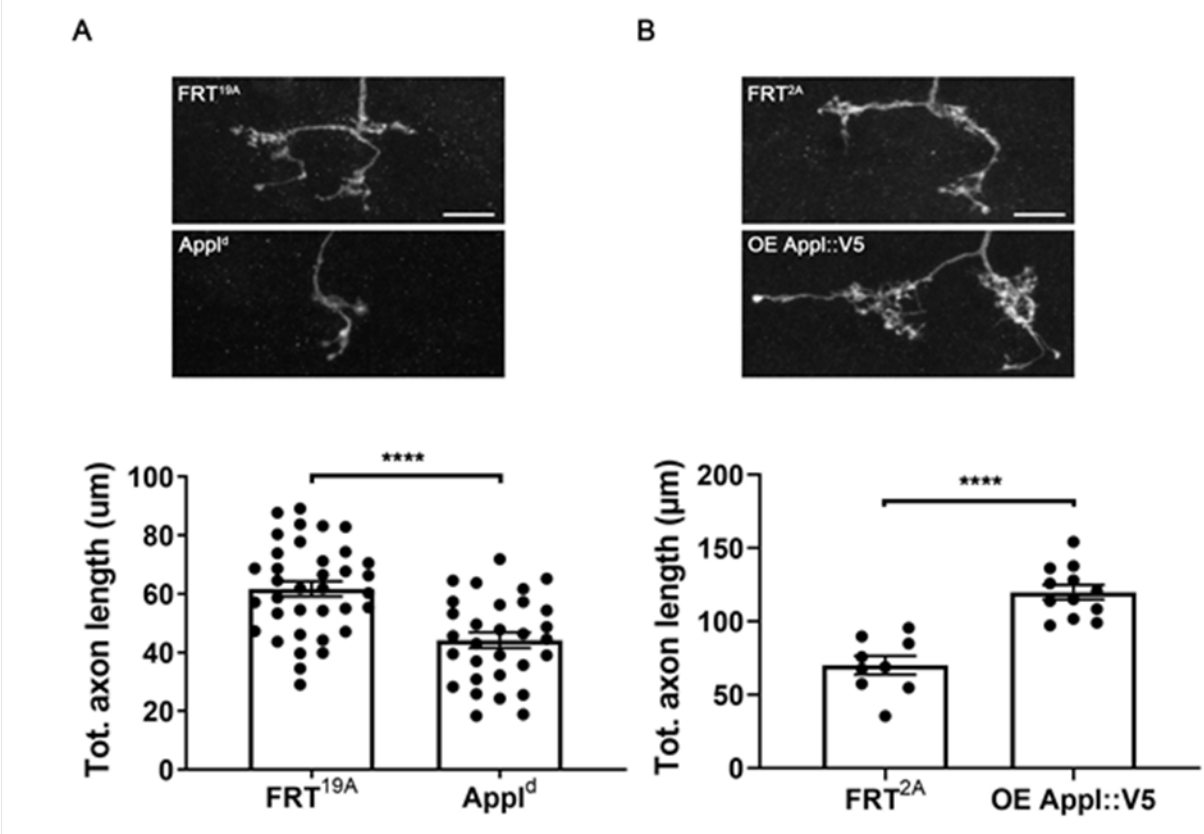


Figure 4.1 Appl promotes axon terminal growth in C4da sensory neurons.

(**A**-**B**) Loss of *appl* function reduces presynaptic arbor size as compared to control (**A**), whereas Appl overexpression increases presynaptic arbor size (**B)**. Scale bar, 10 µm. P-values were calculated by unpaired t-test. ****: $p < 0.0001$. Error bar: standard mean of error.

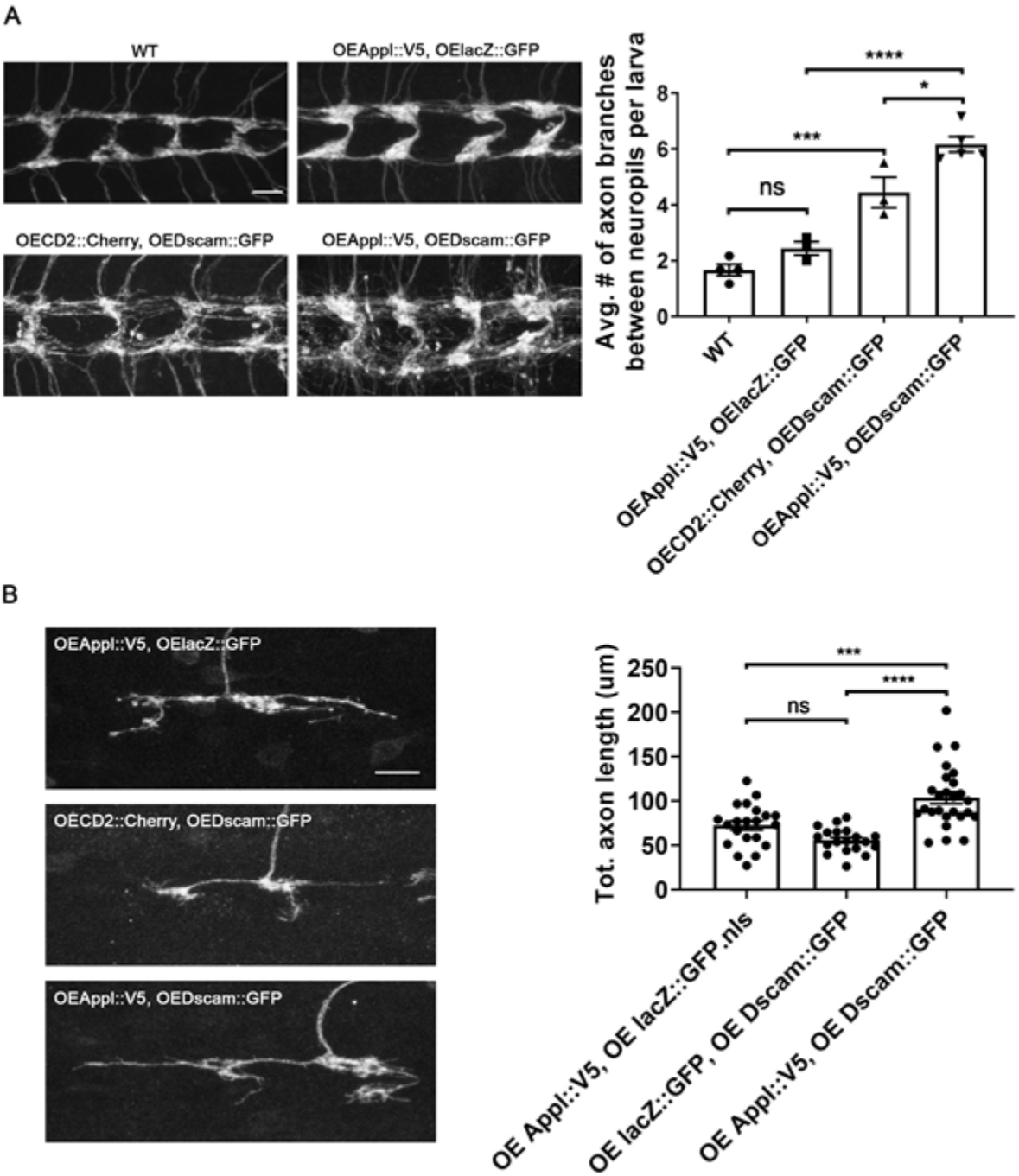

A
WT
OEAppl::V5, OElacZ::GFP
OECD2::Cherry, OEDscam::GFP
OEAppl::V5, OEDscam::GFP
Avg. # of axon branches between neuropils per larva
ns
***
****
*
WT
OEAppl::V5, OElacZ::GFP
OECD2::Cherry, OEDscam::GFP
OEAppl::V5, OEDscam::GFP
B
OEAppl::V5, OElacZ::GFP
OECD2::Cherry, OEDscam::GFP
OEAppl::V5, OEDscam::GFP
Tot. axon length (um)
ns
***
****
OE Appl::V5, OE lacZ::GFP.nls
OE lacZ::GFP, OE Dscam::GFP
OE Appl::V5, OE Dscam::GFP

Figure 4.2 Co-overexpression of Dscam and Appl shows additive effect on C4da presynaptic arbor growth.

(**A-B**) Dscam overexpression leads to increased presynaptic arbor growth as compared to wild-type (WT), and co-overexpression of Dscam and Appl enhances overgrowth more severe than overexpressing either one. Although Appl overexpression does not show significant overgrowth while looking at the overall C4da axon terminal in (**A**), it is confirmed that Appl overexpression increases presynaptic arbor size at the single cell level as shown in (**B**). Scale bar, 10 μm. P-values were calculated by ordinary One-way ANOVA test with Tukey's multiple comparison correction. ns: $p > 0.05$, *: $0.01 < p \leq 0.05$, **: $0.001 < p \leq 0.01$, ***: $0.001 < p \leq 0.001$, and ****: $p < 0.0001$. Error bar: standard mean of error.

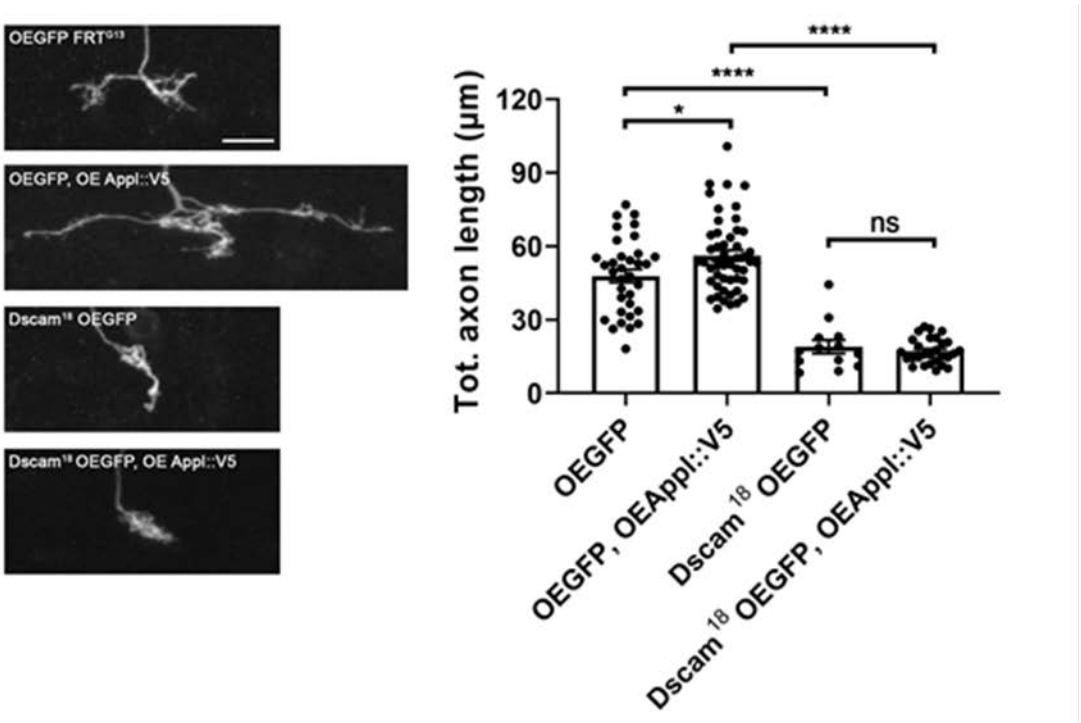


Figure 4.3 Appl requires Dscam to promote presynaptic arbor growth.

When compared to control, Appl overexpression increases presynaptic arbor size and loss of *dscam* function reduces the size. However, Appl overexpression in loss of *dscam* condition fails to induce presynaptic arbor growth. Scale bar, 10 μm. P-values were calculated by ordinary One-way ANOVA test with Tukey's multiple comparison correction. ns: $p > 0.05$, *: $0.01 < p \leq 0.05$, **: $0.001 < p \leq 0.01$, ***: $0.001 < p \leq 0.001$, and ****: $p < 0.0001$. Error bar: standard mean of error.

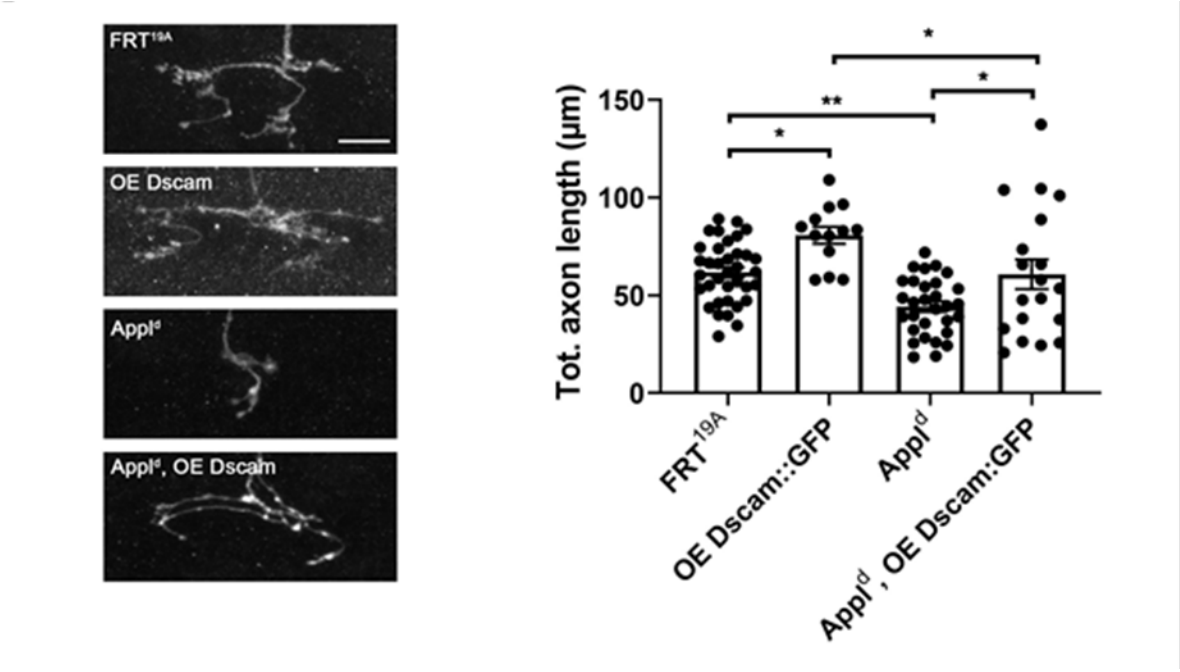


Figure 4.4 Dscam does not require Appl to promote presynaptic arbor growth.

When compared to control, Dscam overexpression increases presynaptic arbor size and loss of *appl* function reduces the size. However, Dscam overexpression in loss of *appl* function is able to induce presynaptic arbor growth significantly, and the magnitude of changes by Dscam overexpression in either control or loss of *appl* condition are very similar. Results of control and loss of *appl* are the same as those in Figure 4.1A. Scale bar, 10 µm. P-values were calculated by ordinary One-way ANOVA test with Tukey's multiple comparison correction. *: $0.01 < p \leq 0.05$, and **: $0.001 < p \leq 0.01$. Error bar: standard mean of error.

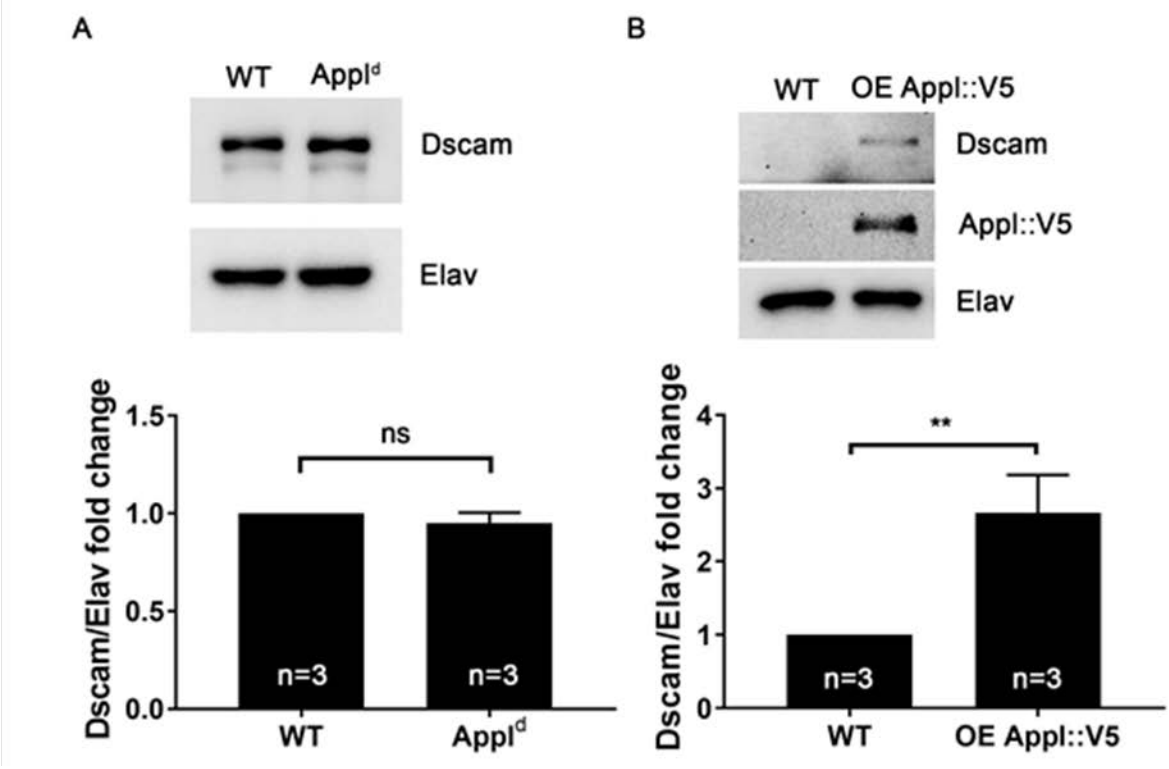


Figure 4.5 Appl overexpression increases endogenous Dscam levels in neurons.

Western blot results show that (**A**) loss of *appl* does not affect Dscam protein level as compared to WT. However, (**B**) Appl overexpression leads to increase of Dscam levels significantly than WT. P-values were calculated using the Mann-Whitney test. ns, $p > 0.05$; *, $0.01 < p \leq 0.05$; and **, $0.001 < p \leq 0.01$. Error bar: standard mean of error.

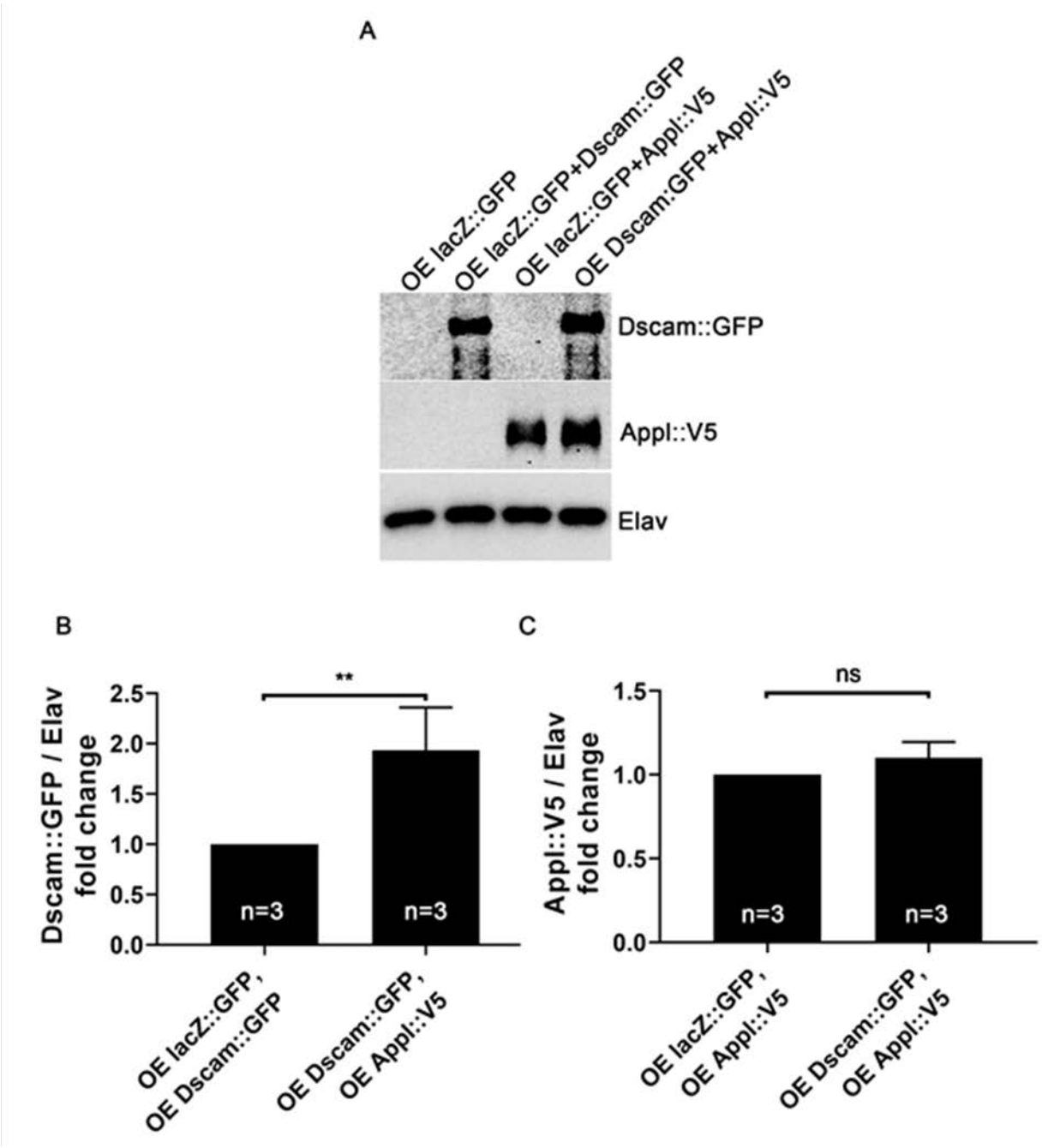


Figure 4.6 Dscam overexpression does not affect Appl levels in neurons.

(**A**) Western blot image of ectopic expression of Dscam, or Appl, or Dscam and Appl.
(**B**) Quantification shows Appl overexpression leads to increased Dscam level significantly as compared to control.
(**C**) Quantification shows Dscam overexpression has no effect on Appl levels as compared to control. P-values were calculated using the Mann-Whitney test. ns, $p > 0.05$; *, $0.01 < p \leq 0.05$; and **, $0.001 < p \leq 0.01$. Error bar: standard mean of error.

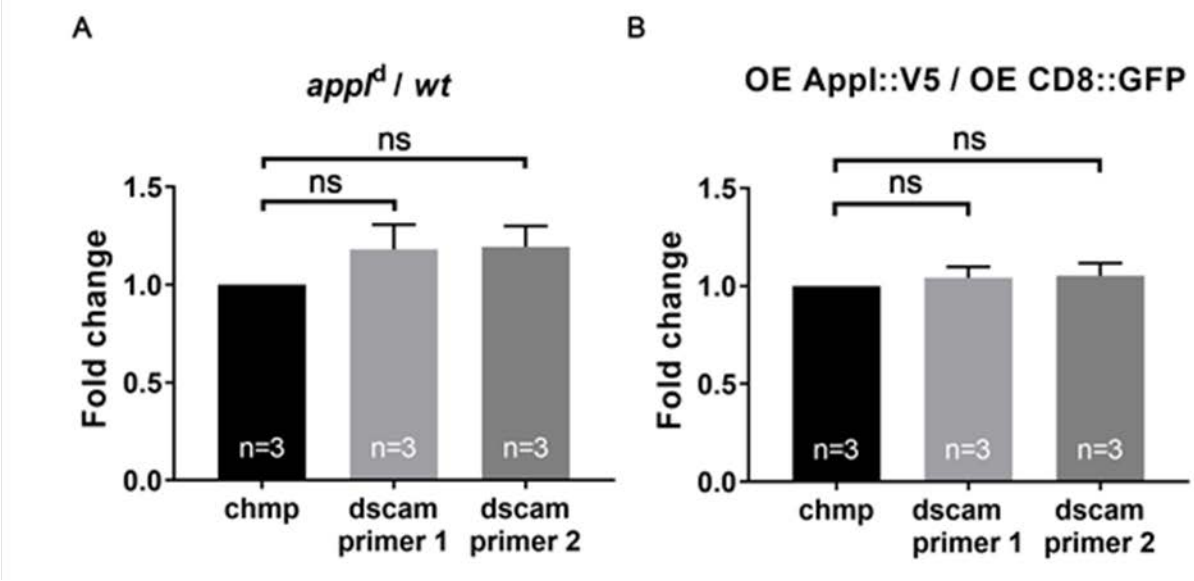


Figure 4.7 Appl does not regulate *dscam* transcript levels.

RT-qPCR results with two sets of *dscam* primers show no significant difference between (**A**) WT and loss of *appl*, or between (**B**) control and Appl overexpression. P-values were calculated by the Kruskal-Wallis test with Dunn's multiple comparison correction. ns, $p > 0.05$. Error bar: standard mean of error.

Chapter 5 Conclusions and future directions

Neuronal morphology formation is important for neural circuit development. How morphology of a neuron is determined can be considered in two distinct decision-making modules. One is the lineage fate that determines the inborn morphology of a neuron, which has been demonstrated in many studies using genetic approaches to manipulate the expression of lineage fate selectors. However, this module is insufficient to explain the complete morphological determination. Another module is the post-mitotic determination, which is independent from fate choice. This includes any intrinsic molecular programs, extrinsic cue stimulations, or neuronal activity that controls one or several features of neuron morphogenesis (e.g. outgrowth, elongation, branching).

Although studies of step by step formation in dendritic and axonal developments have been done intensively, the mechanisms of how various neurons adopt common morphologies is a gap in knowledge that has remained since the discovery of all neurons share basic morphologies (Cajal, 1995). The thesis work in studying the determination of basic morphologies has revealed a novel post-mitotic decision module, via the terminal selector gene *dar1*, in determining the multipolar morphology of neurons in the *Drosophila* nervous system. In general, it has been assumed that the formation of the basic morphological types of neurons is determined by the number of dendrites growing out from the cell body (the “outgrowth model”). Our finding, however, illustrated a new and instructive coupling mechanism, in which Dar1 controls the transcription level of some of the coupling factors, between the primary dendrites and the

nucleus that both factors are essential in the formation of multipolar morphology in neurons. Weaken this coupling interaction in multipolar neurons or loss of *dar1* function would lead to the nucleus to a different location in relation to dendrite and axon, without changing the neuronal identity, and thus reducing the number of primary dendrites connected from the cell body down to one. This indicated that the failure of proper nucleus localization can also switch the basic morphological types in post-mitotic neurons.

This study led to a new biological question of how the multipolar decision, via *dar1* gene activation, is selectively programmed in neurons from different lineages. Presumably, neurons across different lineages could use identical or different regulatory mechanism(s) to control the same morphological program. To answer how basic morphologies is regulated in the context of lineages. A full lineage map of multipolar neurons is necessary at first. To do so, a new multicolor labeling system – *Bitbow* – was created for mapping the complete *Drosophila* PNS lineages, which contains all multipolar neurons. *Bitbow* has several great advantages. First, it greatly improves the color pool diversity from a single genetic cassette. Second, along with a suit of statistical tests, it provides a more reliable way for distinguishing colors even in consider of the frequency of seeing individual colors. Using *Bitbow*, the refined PNS lineage map revealed that the da type multipolar neurons are born from individual lineages. Although da neurons undergo divergent development through different lineages, transgenic reporter system showed that da neurons use distinct combinations of *cis*-regulatory elements to control *dar1* expression to achieve the multipolar morphology, demonstrating a molecular convergence in the regulation of multipolar morphology.

In the module of post-mitotic determination of morphogenesis, many factors belonging to the same functional category (e.g. adhesion molecule, transcription factor) have been identified

that they can control the same morphological feature (e.g. outgrowth, elongation, branching) in neurons. However, it lacks a systematic way to understand whether functionally similar factors interact to promote the development of the same morphological feature, especially for investigation in neural disorders that involve multiple risk factors (e.g. Down syndrome, DS). Therefore, examining the effect of one risk factor at a time is incapable for understanding and predicting the morphological abnormality and the mechanism behind the abnormality. The last part of my thesis demonstrated that the two DS proteins Dscam and Appl clearly interact in the genetic and cellular levels, supporting a potential DS-specific mechanism between the two, as only in the overexpression of Appl affects Dscam and loss of either one does not alter the other one.

In summary, the thesis study is significant by providing the knowledge in the mechanism of basic morphological formation in neurons, and the genetic and cellular interactions of two DS risk factors in response to axon terminal development. This raises the concern that studying one risk factor at a time is insufficient to understand the morphological abnormality and the mechanisms behind it in diseases with multiple risk factors that control the same morphological features. This thesis study is innovated as we have successfully generated a new multicolor labeling tool together with a proper statistical method for lineage identification, which can be used in any tissues, and a new *Drosophila* PNS lineage map that can be applied to study neuronal properties in the context of PNS lineages. Below includes discussion about limitations, applications, or future directions related to each part of the thesis projects.

Dendrite–nucleus coupling in the morphogenesis of basic types

NudE is known to interact with the dynein-dynactin motors, which interact with the outer nuclear membrane (ONM) adaptor proteins Klarsicht (Klar) to form a bridge between microtubules and nucleus (Koizumi and Gleeson, 2009; Razafsky and Hodzic, 2009; Wainman et al., 2009). As I demonstrated that Dar1 requires NudE and NudC to promote multipolar morphology, it is interesting to know whether the same NudE and Klar bridging mechanism is used by Dar1 to promote the multipolar morphology (Figure 5.1). To continue dissecting the coupling mechanism between dendrites and nucleus, I would first perform loss of function studies *in vivo* to determine if the multipolar morphology of da neurons requires *klar*. If Klar is required in this case, I could visualize this interaction directly using a split GFP system by tagging specific GFP fragments onto Klar and either the large subunit Glued (Gl) or another subunit Dynamitin (Dmn) of the dynactin complex, respectively (Cabantous et al., 2013; Patterson et al., 2003). I would fuse the GFP fragments onto Gl and Dmn, which are known to interact with each other in the dynactin complex (Urnavicius et al., 2015) as positive control for the system. If the nucleus is coupled with the microtubules in the dendrites through this linkage, I would expect Klar to interact with Gl and Dmn, to form the dendrite-nucleus connection only when Dar1 is present. Because Dar1 appears to regulate nuclear coupling in multipolar neurons, I expect that loss of the Dar1 downstream activator NudC would also result in a lack of split GFP signal as determined by confocal microscopy. If Klar is not required for the multipolar morphology of da neurons, I will perform a screen with deficiency fly lines to identify new candidates (e.g. new ONM adaptor proteins in *Drosophila*) to test if they are required for the multipolar morphology in da neurons.

Applying nBitbow to lineage mapping in other tissues

One concern about applying nBitbow in other tissues is that while the nuclear *Bitbow* is sufficient for cell identification in the *Drosophila* PNS due to the fact that neurons can be readily identified by anti-HRP staining, it might be difficult to use in tissues where cells cannot be easily identified. The solution is to focus on mapping lineages within a subset of cells by using specific Gal4 drivers. For example, the ventral nerve cord (VNC) of *Drosophila* CNS also contains repeated segments that each contains about 30 neuroblasts giving rise to approximately 350 neurons (Bossing et al., 1996; Doe, 1992; Schmidt et al., 1997). Although there is no marker for the identification of every CNS neurons, markers that label subsets of cells, such as Gal4 drivers that express transgenes in specific cell types, allows the application of *nBitbow* to trace lineages within subsets of CNS neurons. Recent studies have identified a subset of larval interneurons, called Basin neurons (Basin-1, -2, -3, and -4), which receive synaptic inputs from nociceptors and mechanosensors (Ohyama et al., 2015). These neurons are speculated to be lineage-related, based on their similar cell body locations, morphologies, and projection patterns (Ohyama et al., 2015). Using *nBitbow* and the Basin-specific-driver R72F11-Gal4, with 1-hr heat-shock at 3-4 hr AEL, I observed that the color activation frequency was improved and the distribution was relatively high (Figure 5.2). Moreover, I found that the four Basins typically expressed the same colors, and were indeed significantly related to each other. These results demonstrate the feasibility of using *nBitbow* for lineage studies in the CNS of the *Drosophila* larva. Although the CNS demonstration here does not show the identity of individual Basins, additional cell-type-specific markers (e.g. Basin subtype-specific Gal4) (Ohyama et al., 2015) or UAS-membrane markers can be recombined with *nBitbow* to identify individual neurons. If Gal4 driver is weak, increasing Gal4 copies or immunostaining FPs would enhance *nBitbow* signals. If the expression of a Gal4 is dynamic, a cell-type-specific FLP with temporal expression in early developmental

stage can be used in combination with a constitutive Gal4. Alternatively, other binary expression systems (e.g. LexA/LexAop and QF/QUAS) can be combined with *nBitbow* to serve as cell-type-specific markers. Besides the nuclear localized-*Bitbow*, a membrane-*Bitbow* may be useful for cell identification.

Comparisons with other multicolor labeling systems

Different multicolor labeling systems have advantages and limitations for specific applications (Kretzschmar and Watt, 2012; Weissman and Pan, 2015). This is also true for *nBitbow*. First, the availability of drivers for activating colors through recombination limits the applicability of each system. For examples, *dBrainbow*, UAS-*Brainbows*, *LOLLIbow*, and MCFO use Cre recombinase to activate color selection, while *Flybows*, *TIE-DYE*, and our *nBitbow* use FLP recombinase; *Raeppli* uses FLP to activate an integrase, which in turn activate color selection (Boulina et al., 2013a; Hadjieconomou et al., 2011; Hampel et al., 2011a; Kanca et al., 2014; Nern et al., 2015; Richier and Salecker, 2015b; Worley et al., 2013). Because of *Raeppli* requires extra time to activate colors, it might not be suitable for studying lineages, at least those occurring at early developmental stages. Second, the subcellular localization and brightness of FPs are appropriate for specific purposes. For examples, *Flybows*, UAS-*Brainbows*, *LoLLIbow*, and *Raeppli* use membrane-bound FPs, allowing the visualization of fine morphological structures, such as dendritic spines or synapse, and can be used for identifying cells in certain circumstances. By contrast, *nBitbow* and *Raeppli* use nuclear FPs. Although they do not reveal cell morphology, they generally produce brighter FP signals, eliminating the need of immunostaining. Moreover, cells expressing nuclear FPs are easier to score than those expressing membrane FPs in tissues with a high density of cells. Third, the diversity of colors is

important for the successful application of multicolor labeling systems in large numbers of cells. The more color variants are available the less likely two random cells express the same color. *dBrainbow*, *Flybows*, UAS-*Brainbows*, *LOLLIbow*, and *Raeppli* provide 3 or 4 colors per construct, MCFO and TIE-DYE provide 7 colors, whereas *nBitbow* provides more than 20 colors per construct, making it a great candidate for lineage tracing of large numbers of cells. Last, the direct signal detection and stability of FPs affect the suitability for live imaging. For example, although MCFO provides more colors than other *Brainbow* variants, it requires immunostaining to enhance FP signals, precluding its use for live imaging. By contrast, both *nBitbow* and *LoLLIbow* can be used for live imaging. The *nBitbow* is probably more suitable for visualizing larger scales of lineage patterns and distribution because of its greater color diversity. The membrane-bound *LoLLIbow* is probably better for imaging fine details of cell morphology in a small number of cells due to its 3 color variants.

New opportunities resulted from lineage mapping by nBitbow

The success of the PNS lineage mapping created new opportunities for studying other aspects of neuronal development related to lineage development. For instance, it lays the foundation for studying whether particular molecular mechanisms are specified in neurons arising from different lineages. As a proof-of-concept, I applied the refined PNS lineage map to investigate how neurons activate the same terminal selector gene in different lineages. Using transgenic reporter system to identify *cis*-regulatory elements of *dar1* used in individual da neurons. The results suggest that the transcriptional control of *dar1* gene in da neurons vary between lineages, as some da share common *cis*-regulatory elements and some requires combinatory elements.

While Dar1 protein is always detected in post-mitotic da neurons, these *cis*-regulatory elements I identified appear to have lower frequency of reporter expression. One explanation is due to the effect of enhancer-core-promoter specificity, meaning that using a developmental gene enhancer with a housekeeping core-promoter may reduce the activity of the enhancer and vice versa (Zabidi et al., 2014; Zabidi and Stark, 2016). This possibility is unlikely because the core-promoter in the reporter system I selected is presumably favored by developmental over housekeeping genes (Pfeiffer et al., 2008). Another possibility is the docking site selected for the insertion of the reporter system may have chromosomal position effect on the activity of the enhancer. Although such chromosomal effect was identified in affecting gene expression (Feng et al., 2001; Hou et al., 2012; Sexton et al., 2012; Simonis et al., 2006; Ulianov et al., 2016), less is known about whether enhancer activity is influenced or not. This concern can be addressed by putting the same reporter system at different docking site of the genome for comparison. A third possibility for the low frequency expression is that additional regulatory region(s) is needed but not identified in our study, for subsets of da neurons, to enhance reporter expression. In fact, multiple enhancers, which are located close to or far away (including on different chromosomes) from the core-promoter of a gene can form a concentrated "super enhancer" for activating cell-type-specific expression of genes (Dowen et al., 2014; Monahan et al., 2019; Monahan et al., 2017; Spitz, 2016; Whyte et al., 2013). Nevertheless, our results suggest that the transcriptional control of *dar1* gene in different da neuron lineages is complex. I speculate that distinct transcription factors are recruited to control *dar1* expression in different da neuron lineages, but common factors might also be used in certain subsets of da neurons. Profiling the expression pattern of transcription factors in every single da neurons may reveal the regulatory mechanisms underlying neuronal morphogenesis in different lineages.

Besides morphological selection, other neuronal properties including electrophysiology, neurotransmission, and circuit connections can be compared between lineages.

Interaction of DS genes in controlling axon branching

To better understand how functional similar genes interaction to control the same morphological feature, I focused on two DS genes, *dscam* and *appl*, because each of them plays a role in axon terminal development and both are overexpressed in DS patients (Kim et al., 2013; Leyssen et al., 2005). As we reported that Dscam and Appl co-expression leads to an additive phenotype of axon terminal overgrowth as compared to overexpression of either one, and Appl overexpression increases Dscam protein level but loss of either one does not affect the other one. These findings point to a potential mechanism that may occur in DS brain, and traditional study by examining one DS gene would not be able to provide such mechanistic observation, bringing the necessity to investigate multiple gene interactions as many of them are dysregulated at the same time in DS.

One caveat of our study is that the overexpression of Dscam and Appl were driven by the Gal4/UAS system, which in general is robust. We observed that the overexpression of Dscam by one pan-neuronal Gal4 and one UAS-Dscam transgene results in an average of 3.3 fold more Dscam in the *Drosophila* brain (Figure 5.3). However, it is unclear how much Dscam and APP proteins are increased in DS brain when compared to normal brain. Future investigation from trisomy mice would be essential to provide such information, so that we could optimize the overexpressed protein level more similar to the physiological condition in DS when doing functional studies in different animal systems. Alternatively, we could generate transgenic flies that carry an extra copy of *dscam* and *appl* driven by their own endogenous promoter to study

axon terminal phenotype. For future directions, I plan to confirm whether Appl affects Dscam level is conserved in mammal. Since the Ts65Dn DS mice have three copies of functional Dscam and APP, I will normalize an APP gene number by crossing the Ts65Dn mice with the APP heterozygous mice and see if Dscam level would be reduced (Reeves et al., 1995; Zheng et al., 1995).

Previous study in mushroom body neurons suggested that Appl requires Abl to promote axon terminal growth (Leyssen et al., 2005). Similarly, we found that in C4da neurons Dscam requires Abl to promote axon terminal growth (Kim et al., 2013). These data led me to hypothesize that Appl may require Abl as well in C4da neurons (Figure 5.4). To address this question, I would use genetic approach by overexpressing Appl in control and in loss of *abl* function conditions for comparison. Moreover, we previously demonstrated that blocking Abl activity by nilotinib, a drug uses for leukemia treatment showing promising results in patients, suppresses the presynaptic overgrowth induced by Dscam overexpression (Kantarjian et al., 2007; Sterne et al., 2015). If Appl indeed required Abl, it would make Abl a potential drug target for preventing axon overgrowth induced by Dscam and Appl overexpression in DS. If Appl did not require Abl, I would prioritize a list of potential downstream effector(s) shared by Appl and Dscam based on literature, and examine their loss- and gain-of-function studies in axon phenotype.

Lastly, I would continue to dissect how Appl causes upregulation of Dscam when it's overexpressed (Figure 5.3). There are two major types of post-transcriptional regulation. One is protein synthesis and the other is protein degradation. To test whether Appl blocks Dscam degradation, I would measure the degradation rate of Dscam over time in the presence or absence of Appl in S2 cells treated with protein synthesis inhibitor (i.e. cycloheximide). If Dscam protein

level were decreased slower over time in the presence of Appl, it would suggest Appl affects Dscam level by preventing its degradation. To test whether Appl increases Dscam translation, I would measure Dscam synthesis rate in vivo using Translating Ribosome Affinity Purification sequencing (TRAP-seq) technique (Doyle et al., 2008; Heiman et al., 2008). In brief, I would overexpress a control marker or Appl in the CNS of a ribosome tagged fly line. I would then perform tagged ribosome immunoprecipitation followed by mRNA purification and measure the Ribosomal bounded Dscam mRNA level in control and in Appl overexpression (Heiman et al., 2014). Alternatively, I could measure Dscam synthesis rate over time in the presence or absence of Appl in S2 cells treated with degradation inhibitor (e.g. proteasome or lysosome inhibitor).

In summary, carrying out these experiments will continue to expand our understanding on the mechanisms underlie neuron morphogenesis, including how the dendrite-nucleus coupling machinery occurs in multipolar neurons, what specific factor(s) that "make decision" to decide the morphological selection via *dar1* in different lineages, and how functional overlapping genes interact to control axon morphology in DS.

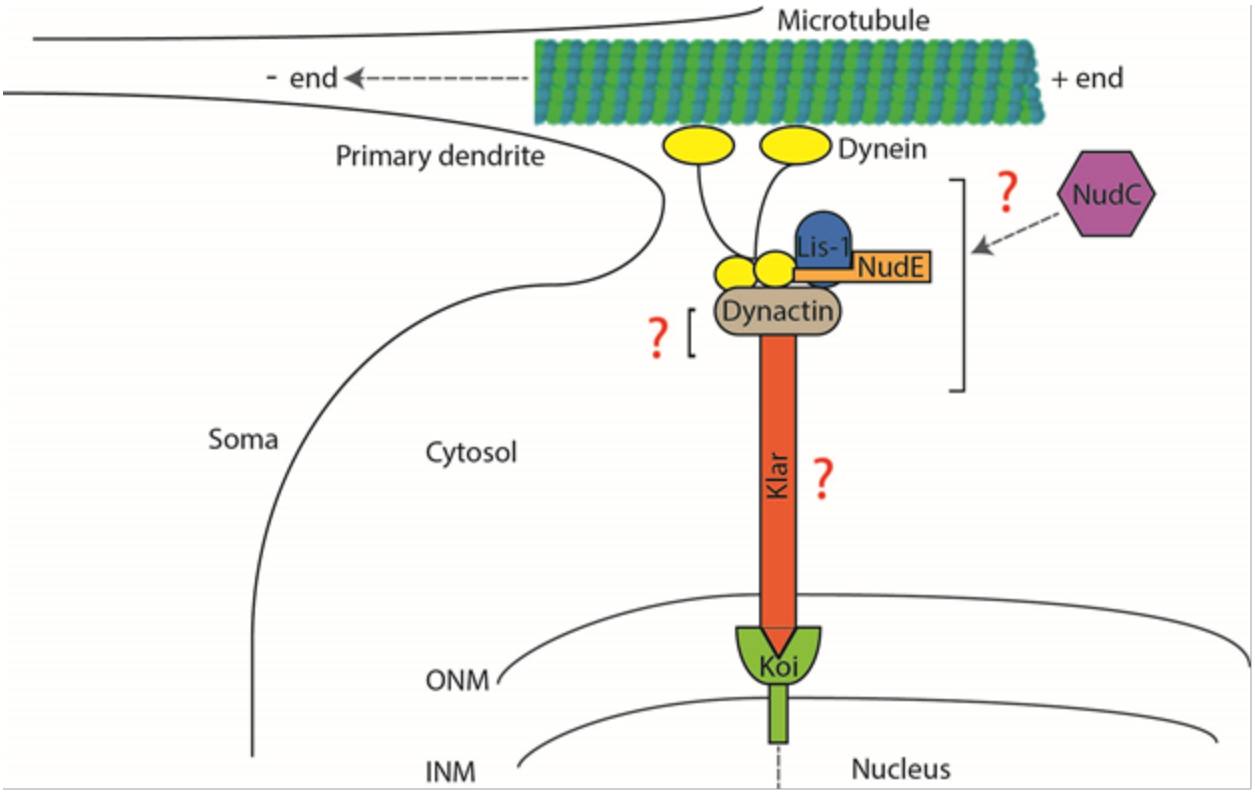


Figure 5.1 Proposed model of how dendrite-nucleus coupling occurs to promote formation of multipolar morphology in neurons.

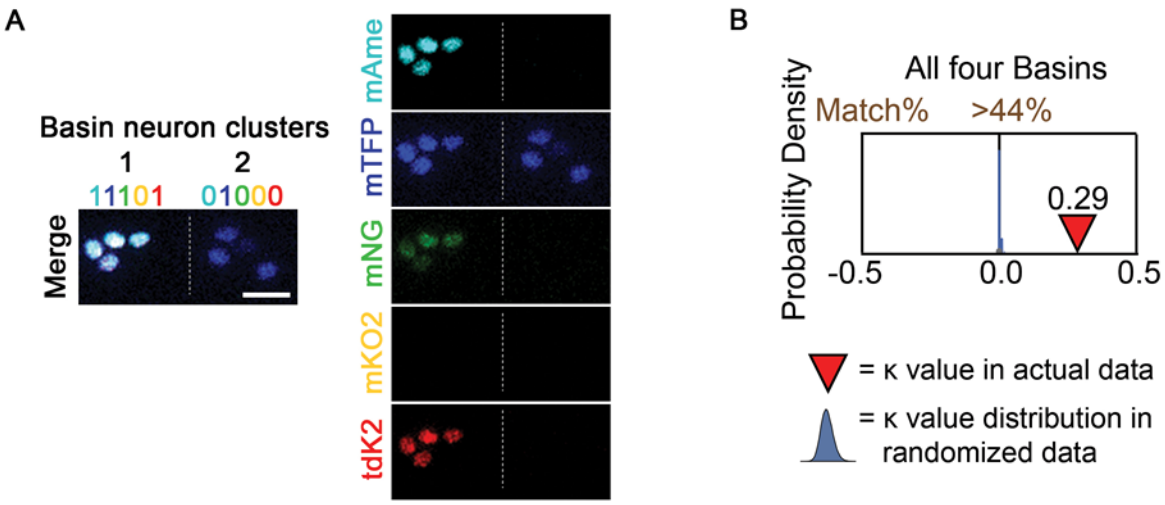


Figure 5.2 Lineage tracing of Basin neurons.

(**A**) Representative fluorescent images that show Basin neurons expressing the same color in a cluster that is different than the adjacent cluster. (**B**) The actual κ value is significantly different than the random distribution of colors in Basin neurons, suggesting these neurons are lineage related. Scale bar: 10 μm.

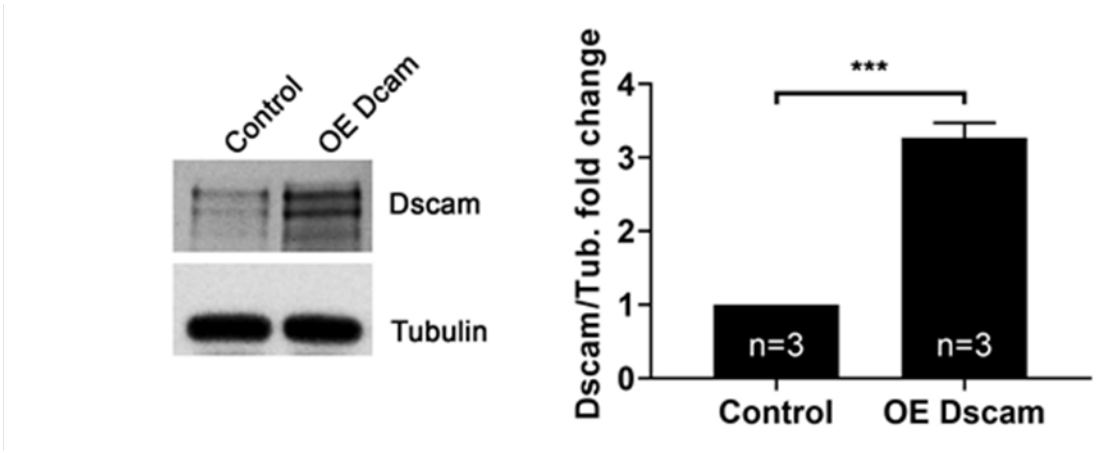


Figure 5.3 Dscam expression level driven by the Gal4/UAS system with 1:1 ratio.

One pan-neuronal Gal4 (nSyb-Gal4) was crossed with one UAS-CD8::GFP or one UAS-Dscam[TM2]::GFP for total Dscam fold change comparison. Dscam level is normalized to tubulin (Tub).

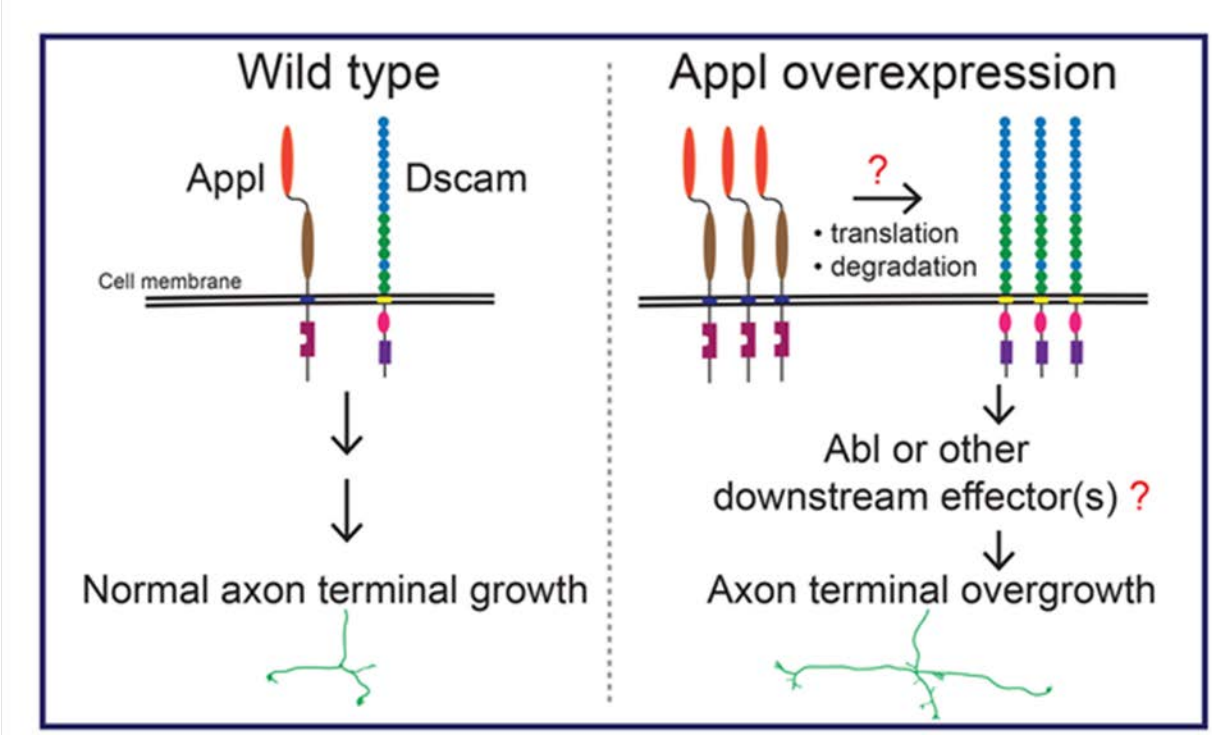


Figure 5.4 Working model of axon development in normal and Appl overexpression conditions.

Bibliography

Agarwala, K.L., Ganesh, S., Amano, K., Suzuki, T., and Yamakawa, K. (2001). DSCAM, a highly conserved gene in mammals, expressed in differentiating mouse brain. Biochem Biophys Res Commun *281*, 697-705.

Ai, H.W., Hazelwood, K.L., Davidson, M.W., and Campbell, R.E. (2008). Fluorescent protein FRET pairs for ratiometric imaging of dual biosensors. Nature methods *5*, 401-403.

Ai, H.W., Henderson, J.N., Remington, S.J., and Campbell, R.E. (2006). Directed evolution of a monomeric, bright and photostable version of Clavularia cyan fluorescent protein: structural characterization and applications in fluorescence imaging. Biochemical Journal *400*, 531-540.

Allen, M.J., Shan, X., Caruccio, P., Froggett, S.J., Moffat, K.G., and Murphey, R.K. (1999). Targeted Expression of Truncated Glued Disrupts Giant Fiber Synapse Formation in Drosophila. The Journal of Neuroscience *19*, 9374.

Altman, J. (1972). Postnatal development of the cerebellar cortex in the rat. II. Phases in the maturation of Purkinje cells and of the molecular layer. Journal of Comparative Neurology *145*, 399-463.

Antonarakis, S.E. (2017). Down syndrome and the complexity of genome dosage imbalance. Nature Reviews Genetics *18*, 147-163.

Artavanis-Tsakonas, S., and Simpson, P. (1991). Choosing a cell fate: a view from the Notch locus. Trends in Genetics *7*, 403-408.

Arthur, A.L., Yang, S.Z., Abellaneda, A.M., and Wildonger, J. (2015). Dendrite arborization requires the dynein cofactor NudE. Journal of Cell Science *128*, 2191.

Asim, A., Kumar, A., Muthuswamy, S., Jain, S., and Agarwal, S. (2015). "Down syndrome: an insight of the disease". Journal of Biomedical Science *22*.

Ayala, R., Shu, T., and Tsai, L.-H. (2007). Trekking across the Brain: The Journey of Neuronal Migration. Cell *128*, 29-43.

Baas, P.W., Black, M.M., and Banker, G.A. (1989). Changes in microtubule polarity orientation during the development of hippocampal neurons in culture. The Journal of Cell Biology *109*, 3085.

Barlow, G.M., Micales, B., Lyons, G.E., and Korenberg, J.R. (2001). Down syndrome cell adhesion molecule is conserved in mouse and highly expressed in the adult mouse brain. Cytogenet Cell Genet *94*, 155-162.

Bashaw, G.J., Kidd, T., Murray, D., Pawson, T., and Goodman, C.S. (2000). Repulsive axon guidance: Abelson and enabled play opposing roles downstream of the roundabout receptor. Cell *101*, 703-715.

Bateman, J.R., Lee, A.M., and Wu, C.T. (2006a). Site-specific transformation of Drosophila via phi C31 integrase-mediated cassette exchange. Genetics *173*, 769-777.

Bateman, J.R., Lee, A.M., and Wu, C.T. (2006b). Site-specific transformation of Drosophila via phiC31 integrase-mediated cassette exchange. Genetics *173*, 769-777.

Bear, J.E., and Gertler, F.B. (2009). Ena/VASP: towards resolving a pointed controversy at the barbed end. Journal of Cell Science *122*, 1947.

Bear, J.E., Svitkina, T.M., Krause, M., Schafer, D.A., Loureiro, J.J., Strasser, G.A., Maly, I.V., Chaga, O.Y., Cooper, J.A., Borisy, G.G., *et al.* (2002). Antagonism between Ena/VASP Proteins and Actin Filament Capping Regulates Fibroblast Motility. Cell *109*, 509-521.

Benjamini, Y., and Hochberg, Y. (1995). Controlling the False Discovery Rate - a Practical and Powerful Approach to Multiple Testing. J Roy Stat Soc B *57*, 289-300.

Bennett, V., and Baines, A.J. (2001). Spectrin and Ankyrin-Based Pathways: Metazoan Inventions for Integrating Cells Into Tissues. Physiological Reviews *81*, 1353-1392.
Birkholz, O., Rickert, C., Nowak, J., Coban, I.C., and Technau, G.M. (2015). Bridging the gap between postembryonic cell lineages and identified embryonic neuroblasts in the ventral nerve cord of Drosophila melanogaster. Biol Open *4*, 420-U432.
Bischof, J., Maeda, R.K., Hediger, M., Karch, F., and Basler, K. (2007). An optimized transgenesis system for Drosophila using germ-line-specific phi C31 integrases. Proceedings of the National Academy of Sciences of the United States of America *104*, 3312-3317.
Bixby, J.L., and Harris, W.A. (1991). Molecular Mechanisms of Axon Growth and Guidance. Annual Review of Cell Biology *7*, 117-159.
Blasius, T.L., Cai, D., Jih, G.T., Toret, C.P., and Verhey, K.J. (2007). Two binding partners cooperate to activate the molecular motor Kinesin-1. J Cell Biol *176*, 11-17.
Blochlinger, K., Bodmer, R., Jack, J., Jan, L.Y., and Jan, Y.N. (1988). Primary structure and expression of a product from cut, a locus involved in specifying sensory organ identity in Drosophila. Nature *333*, 629-635.
Blochlinger, K., Bodmer, R., Jan, L.Y., and Jan, Y.N. (1990). Patterns of expression of cut, a protein required for external sensory organ development in wild-type and cut mutant Drosophila embryos. Genes Dev *4*, 1322-1331.
Blochlinger, K., Jan, L.Y., and Jan, Y.N. (1991). Transformation of sensory organ identity by ectopic expression of Cut in Drosophila. Genes Dev *5*, 1124-1135.
Blochlinger, K., Jan, L.Y., and Jan, Y.N. (1993). Postembryonic patterns of expression of cut, a locus regulating sensory organ identity in Drosophila. Development *117*, 441-450.
Bodmer, R., Carretto, R., and Jan, Y.N. (1989). Neurogenesis of the peripheral nervous system in Drosophila embryos: DNA replication patterns and cell lineages. Neuron *3*, 21-32.
Bodmer, R., and Jan, Y.N. (1987). Morphological differentiation of the embryonic peripheral neurons in Drosophila. Roux's Arch Dev Biol *196*, 69-77.
Bossing, T., Udolph, G., Doe, C.Q., and Technau, G.M. (1996). The embryonic central nervous system lineages of Drosophila melanogaster .1. Neuroblast lineages derived from the ventral half of the neuroectoderm. Developmental biology *179*, 41-64.
Boulina, M., Samarajeewa, H., Baker, J.D., Kim, M.D., and Chiba, A. (2013a). Live imaging of multicolor-labeled cells in Drosophila. Development *140*, 1605-1613.
Boulina, M., Samarajeewa, H., Baker, J.D., Kim, M.D., and Chiba, A. (2013b). Live imaging of multicolor-labeled cells in Drosophila. Development *140*, 1605-1613.
Bovolenta, P., and Fernaud-Espinosa, I. (2000). Nervous system proteoglycans as modulators of neurite outgrowth. Prog Neurobiol *61*, 113-132.
Boylan, K.L.M., and Hays, T.S. (2002). The Gene for the Intermediate Chain Subunit of Cytoplasmic Dynein Is Essential in Drosophila. Genetics *162*, 1211.
Brand, M., Jarman, A.P., Jan, L.Y., and Jan, Y.N. (1993). asense is a Drosophila neural precursor gene and is capable of initiating sense organ formation. Development *119*, 1-17.
Brennaman, L.H., and Maness, P.F. (2010). NCAM in Neuropsychiatric and Neurodegenerative Disorders. In Structure and Function of the Neural Cell Adhesion Molecule NCAM, V. Berezin, ed. (New York, NY: Springer New York), pp. 299-317.
Brewster, R., and Bodmer, R. (1995). Origin and specification of type II sensory neurons in Drosophila. Development *121*, 2923-2936.
Brewster, R., and Bodmer, R. (1996). Cell lineage analysis of the Drosophila peripheral nervous system. Developmental genetics *18*, 50-63.

Brewster, R., Hardiman, K., Deo, M., Khan, S., and Bodmer, R. (2001). The selector gene cut represses a neural cell fate that is specified independently of the Achaete-Scute-Complex and atonal. Mech Dev *105*, 57-68.
Brose, K., Bland, K.S., Wang, K.H., Arnott, D., Henzel, W., Goodman, C.S., Tessier-Lavigne, M., and Kidd, T. (1999). Slit proteins bind Robo receptors and have an evolutionarily conserved role in repulsive axon guidance. Cell *96*, 795-806.
Cabantous, S., Nguyen, H.B., Pedelacq, J.-D., Koraïchi, F., Chaudhary, A., Ganguly, K., Lockard, M.A., Favre, G., Terwilliger, T.C., and Waldo, G.S. (2013). A New Protein-Protein Interaction Sensor Based on Tripartite Split-GFP Association. Scientific Reports *3*, 2854.
Cabrera, C.V. (1990). Lateral inhibition and cell fate during neurogenesis in Drosophila: the interactions between scute, Notch and Delta. Development *110*, 733.
Cai, D., Cohen, K.B., Luo, T., Lichtman, J.W., and Sanes, J.R. (2013). Improved tools for the Brainbow toolbox. Nature methods *10*, 540-547.
Cajal, R. (1995). Histology of the nervous system of man and vertebrates (Oxford University Press, USA).
Campuzano, S., and Modolell, J. (1992). Patterning of the Drosophila nervous system: the achaete-scute gene complex. Trends in Genetics *8*, 202-208.
Chen, B.E., Kondo, M., Garnier, A., Watson, F.L., Püettmann-Holgado, R., Lamar, D.R., and Schmucker, D. (2006). The Molecular Diversity of Dscam Is Functionally Required for Neuronal Wiring Specificity in Drosophila. Cell *125*, 607-620.
Chen, Xing J., Squarr, Anna J., Stephan, R., Chen, B., Higgins, Theresa E., Barry, David J., Martin, Morag C., Rosen, Michael K., Bogdan, S., and Way, M. (2014). Ena/VASP Proteins Cooperate with the WAVE Complex to Regulate the Actin Cytoskeleton. Developmental Cell *30*, 569-584.
Clark, I., Giniger, E., Ruohola-Baker, H., Jan, L.Y., and Jan, Y.N. (1994). Transient posterior localization of a kinesin fusion protein reflects anteroposterior polarity of the Drosophila oocyte. Current Biology *4*, 289-300.
Cohen, J. (1960). A Coefficient of Agreement for Nominal Scales. Educ Psychol Meas *20*, 37-46.
Corty, M.M., Matthews, B.J., and Grueber, W.B. (2009). Molecules and mechanisms of dendrite development in Drosophila. Development *136*, 1049-1061.
Crozatier, M., and Vincent, A. (2008). Control of multidendritic neuron differentiation in Drosophila: The role of Collier. Developmental Biology *315*, 232-242.
de Cuevas, M., Tao, T., and Goldstein, L.S. (1992). Evidence that the stalk of Drosophila kinesin heavy chain is an alpha-helical coiled coil. The Journal of Cell Biology *116*, 957.
Dickinson, R.E., and Duncan, W.C. (2010). The SLIT-ROBO pathway: a regulator of cell function with implications for the reproductive system. Reproduction (Cambridge, England) *139*, 697-704.
Doe, C.Q. (1992). Molecular markers for identified neuroblasts and ganglion mother cells in the Drosophila central nervous system. Development *116*, 855-863.
Domínguez, M., and Campuzano, S. (1993). asense, a member of the Drosophila achaete-scute complex, is a proneural and neural differentiation gene. The EMBO Journal *12*, 2049-2060.
Dong, X.T., Shen, K., and Bulow, H.E. (2015). Intrinsic and Extrinsic Mechanisms of Dendritic Morphogenesis. Annual Review of Physiology, Vol 77 *77*, 271-300.

Doring, F., Wischmeyer, E., Kuhnlein, R.P., Jackle, H., and Karschin, A. (2002). Inwardly rectifying K+ (Kir) channels in Drosophila - A crucial role of cellular milieu factors for Kir channel function. Journal of Biological Chemistry *277*, 25554-25561.
Dowen, Jill M., Fan, Zi P., Hnisz, D., Ren, G., Abraham, Brian J., Zhang, Lyndon N., Weintraub, Abraham S., Schuijers, J., Lee, Tong I., Zhao, K., *et al.* (2014). Control of Cell Identity Genes Occurs in Insulated Neighborhoods in Mammalian Chromosomes. Cell *159*, 374-387.
Doyle, J.P., Dougherty, J.D., Heiman, M., Schmidt, E.F., Stevens, T.R., Ma, G., Bupp, S., Shrestha, P., Shah, R.D., Doughty, M.L., *et al.* (2008). Application of a Translational Profiling Approach for the Comparative Analysis of CNS Cell Types. Cell *135*, 749-762.
Duffy, J.B. (2002). GAL4 system in Drosophila: a fly geneticist's Swiss army knife. Genesis *34*, 1-15.
Dwass, M. (1957). Modified Randomization Tests for Nonparametric Hypotheses. Ann Math Stat *28*, 181-187.
Evangelista, M., Pruyne, D., Amberg, D.C., Boone, C., and Bretscher, A. (2002). Formins direct Arp2/3-independent actin filament assembly to polarize cell growth in yeast. Nature Cell Biology *4*, 32-41.
Feng, Y.-Q., Lorincz, M.C., Fiering, S., Greally, J.M., and Bouhassira, E.E. (2001). Position Effects Are Influenced by the Orientation of a Transgene with Respect to Flanking Chromatin. Molecular and Cellular Biology *21*, 298.
Feng, Y.F., Ueda, A., and Wu, C.F. (2004). A modified minimal hemolymph-like solution, HL3.1, for physiological recordings at the neuromuscular junctions of normal and mutant Drosophila larvae. Journal of Neurogenetics *18*, 377-402.
Fichelson, P., and Gho, M. (2003). The glial cell undergoes apoptosis in the microchaete lineage of Drosophila. Development *130*, 123.
Fischer, J.A., Giniger, E., Maniatis, T., and Ptashne, M. (1988). GAL4 activates transcription in Drosophila. Nature *332*, 853-856.
Forrest, M.P., Parnell, E., and Penzes, P. (2018). Dendritic structural plasticity and neuropsychiatric disease. Nature Reviews Neuroscience *19*, 215-234.
Fox, R.M., Hanlon, C.D., and Andrew, D.J. (2010). The CrebA/Creb3-like transcription factors are major and direct regulators of secretory capacity. The Journal of Cell Biology *191*, 479.
Fujioka, M., Lear, B.C., Landgraf, M., Yusibova, G.L., Zhou, J., Riley, K.M., Patel, N.H., and Jaynes, J.B. (2003). Even-skipped, acting as a repressor, regulates axonal projections in Drosophila. Development *130*, 5385.
Galiano, Mauricio R., Jha, S., Ho, Tammy S.-Y., Zhang, C., Ogawa, Y., Chang, K.-J., Stankewich, Michael C., Mohler, Peter J., and Rasband, Matthew N. (2012). A Distal Axonal Cytoskeleton Forms an Intra-Axonal Boundary that Controls Axon Initial Segment Assembly. Cell *149*, 1125-1139.
Gao, F.B. (2007). Molecular and cellular mechanisms of dendritic morphogenesis. Curr Opin Neurobiol *17*, 525-532.
Garcia-Moreno, F., Vasistha, N.A., Begbie, J., and Molnar, Z. (2014). CLoNe is a new method to target single progenitors and study their progeny in mouse and chick. Development *141*, 1589-1598.
Gauger, A.K., and Goldstein, L.S. (1993). The Drosophila kinesin light chain. Primary structure and interaction with kinesin heavy chain. J Biol Chem *268*, 13657-13666.

Gehler, S., Shaw, A.E., Sarmiere, P.D., Bamburg, J.R., and Letourneau, P.C. (2004). Brain-Derived Neurotrophic Factor Regulation of Retinal Growth Cone Filopodial Dynamics Is Mediated through Actin Depolymerizing Factor/Cofilin. The Journal of Neuroscience *24*, 10741.
Ghabrial, A., Luschnig, S., Metzstein, M.M., and Krasnow, M.A. (2003). Branching Morphogenesis of the Drosophila Tracheal System. Annual Review of Cell and Developmental Biology *19*, 623-647.
Ghysen, A., and Dambly-Chaudiere, C. (1989). Genesis of the Drosophila peripheral nervous system. Trends in Genetics *5*, 251-255.
Ghysen, A., Dambly-Chaudiere, C., Jan, L.Y., and Jan, Y.N. (1993). Cell interactions and gene interactions in peripheral neurogenesis. Genes Dev *7*, 723-733.
Ghysen, A., and Okane, C. (1989). Neural Enhancer-Like Elements as Specific Cell Markers in Drosophila. Development *105*, 35-52.
Giancotti, F.G. (1997). Integrin signaling: specificity and control of cell survival and cell cycle progression. Curr Opin Cell Biol *9*, 691-700.
Gibson, D.G., Young, L., Chuang, R.Y., Venter, J.C., Hutchison, C.A., and Smith, H.O. (2009). Enzymatic assembly of DNA molecules up to several hundred kilobases. Nature methods *6*, 343-U341.
Gindhart, J.G., Desai, C.J., Beushausen, S., Zinn, K., and Goldstein, L.S.B. (1998). Kinesin Light Chains Are Essential for Axonal Transport in Drosophila. The Journal of Cell Biology *141*, 443.
Goldberg, J.L. (2003). How does an axon grow? Genes Dev *17*, 941-958.
Goldberg, J.L., Espinosa, J.S., Xu, Y., Davidson, N., Kovacs, G.T.A., and Barres, B.A. (2002). Retinal Ganglion Cells Do Not Extend Axons by Default: Promotion by Neurotrophic Signaling and Electrical Activity. Neuron *33*, 689-702.
Golic, K.G., and Lindquist, S. (1989). The Flp Recombinase of Yeast Catalyzes Site-Specific Recombination in the Drosophila Genome. Cell *59*, 499-509.
Groth, A.C., Fish, M., Nusse, R., and Calos, M.P. (2004). Construction of transgenic Drosophila by using the site-specific integrase from phage phi C31. Genetics *166*, 1775-1782.
Grueber, W.B., Jan, L.Y., and Jan, Y.N. (2002). Tiling of the Drosophila epidermis by multidendritic sensory neurons. Development *129*, 2867-2878.
Grueber, W.B., Jan, L.Y., and Jan, Y.N. (2003). Different levels of the homeodomain protein cut regulate distinct dendrite branching patterns of Drosophila multidendritic neurons. Cell *112*, 805-818.
Grueber, W.B., and Jan, Y.N. (2004). Dendritic development: lessons from Drosophila and related branches. Current Opinion in Neurobiology *14*, 74-82.
Grueber, W.B., Yang, C.H., Ye, B., and Jan, Y.N. (2005). The development of neuronal morphology in insects. Current Biology *15*, R730-R738.
Guenette, S., Strecker, P., and Kins, S. (2017). APP Protein Family Signaling at the Synapse: Insights from Intracellular APP-Binding Proteins. Frontiers in Molecular Neuroscience *10*.
Hadjieconomou, D., Rotkopf, S., Alexandre, C., Bell, D.M., Dickson, B.J., and Salecker, I. (2011). Flybow: genetic multicolor cell labeling for neural circuit analysis in Drosophila melanogaster. Nat Meth *8*, 260-266.
Hampel, S., Chung, P., McKellar, C.E., Hall, D., Looger, L.L., and Simpson, J.H. (2011a). Drosophila Brainbow: a recombinase-based fluorescence labeling technique to subdivide neural expression patterns. Nat Meth *8*, 253-259.

Hampel, S., Chung, P., McKellar, C.E., Hall, D., Looger, L.L., and Simpson, J.H. (2011b). Drosophila Brainbow: a recombinase-based fluorescence labeling technique to subdivide neural expression patterns. Nature Methods *8*, 253-U102.
Han, C., Jan, L.Y., and Jan, Y.N. (2011). Enhancer-driven membrane markers for analysis of nonautonomous mechanisms reveal neuron-glia interactions in Drosophila. Proceedings of the National Academy of Sciences of the United States of America *108*, 9673-9678.
Harris, W.A. (2001). Temporal Coordinates: The Genes that Fix Cell Fate with Birth Order. Developmental Cell *1*, 313-314.
Hartenstein, V., and Campos-Ortega, J.A. (1984). Early neurogenesis in wild-typeDrosophila melanogaster. Wilehm Roux Arch Dev Biol *193*, 308-325.
Hartenstein, V., Rudloff, E., and Campos-Ortega, J.A. (1987). The pattern of proliferation of the neuroblasts in the wild-type embryo of Drosophila melanogaster. Roux Arch Dev Biol *196*, 473-485.
Hatten, M.E. (1999). CENTRAL NERVOUS SYSTEM NEURONAL MIGRATION. Annual Review of Neuroscience *22*, 511-539.
Hattori, D., Millard, S.S., Wojtowicz, W.M., and Zipursky, S.L. (2008). Dscam-Mediated Cell Recognition Regulates Neural Circuit Formation. Annual Review of Cell and Developmental Biology *24*, 597-620.
Hattori, Y., Sugimura, K., and Uemura, T. (2007). Selective expression of Knot/Collier, a transcriptional regulator of the EBF/Olf-1 family, endows the Drosophila sensory system with neuronal class-specific elaborated dendritic patterns. Genes to Cells *12*, 1011-1022.
Hayashi, R., Wainwright, S.M., Liddell, S.J., Pinchin, S.M., Horswell, S., and Ish-Horowicz, D. (2014). A Genetic Screen Based on in Vivo RNA Imaging Reveals Centrosome-Independent Mechanisms for Localizing gurken Transcripts in Drosophila. G3: Genes|Genomes|Genetics *4*, 749.
Heiman, M., Kulicke, R., Fenster, R.J., Greengard, P., and Heintz, N. (2014). Cell type–specific mRNA purification by translating ribosome affinity purification (TRAP). Nature Protocols *9*, 1282.
Heiman, M., Schaefer, A., Gong, S., Peterson, J.D., Day, M., Ramsey, K.E., Suárez-Fariñas, M., Schwarz, C., Stephan, D.A., Surmeier, D.J., *et al.* (2008). A Translational Profiling Approach for the Molecular Characterization of CNS Cell Types. Cell *135*, 738-748.
Heitzler, P., Bourouis, M., Ruel, L., Carteret, C., and Simpson, P. (1996). Genes of the Enhancer of split and achaete-scute complexes are required for a regulatory loop between Notch and Delta during lateral signalling in Drosophila. Development *122*, 161.
Heitzler, P., and Simpson, P. (1991). The choice of cell fate in the epidermis of Drosophila. Cell *64*, 1083-1092.
Hinz, U., Giebel, B., and Campos-Ortega, J.A. (1994). The basic-helix-loop-helix domain of Drosophila lethal of scute protein is sufficient for proneural function and activates neurogenic genes. Cell *76*, 77-87.
Hippenmeyer, S., Youn, Y.H., Moon, H.M., Miyamichi, K., Zong, H., Wynshaw-Boris, A., and Luo, L. (2010). Genetic Mosaic Dissection of Lis1 and Ndel1 in Neuronal Migration. Neuron *68*, 695-709.
Hobert, O. (2008). Regulatory logic of neuronal diversity: terminal selector genes and selector motifs. Proceedings of the National Academy of Sciences of the United States of America *105*, 20067-20071.

Hopmann, R., and Miller, K.G. (2002). A Balance of Capping Protein and Profilin Functions Is Required to Regulate Actin Polymerization in Drosophila Bristle. Molecular Biology of the Cell *14*, 118-128.
Horiuchi, D., Collins, C.A., Bhat, P., Barkus, R.V., Diantonio, A., and Saxton, W.M. (2007). Control of a kinesin-cargo linkage mechanism by JNK pathway kinases. Curr Biol *17*, 1313-1317.
Horton, A.C., Racz, B., Monson, E.E., Lin, A.L., Weinberg, R.J., and Ehlers, M.D. (2005). Polarized secretory trafficking directs cargo for asymmetric dendrite growth and morphogenesis. Neuron *48*, 757-771.
Hou, C., Li, L., Qin, Zhaohui S., and Corces, Victor G. (2012). Gene Density, Transcription, and Insulators Contribute to the Partition of the Drosophila Genome into Physical Domains. Molecular Cell *48*, 471-484.
Huang, D.W., Sherman, B.T., and Lempicki, R.A. (2008). Systematic and integrative analysis of large gene lists using DAVID bioinformatics resources. Nature Protocols *4*, 44.
Hummel, T., Vasconcelos, M.L., Clemens, J.C., Fishilevich, Y., Vosshall, L.B., and Zipursky, S.L. (2003). Axonal targeting of olfactory receptor neurons in Drosophila is controlled by Dscam. Neuron *37*, 221-231.
Hurd, D.D., and Saxton, W.M. (1996). Kinesin Mutations Cause Motor Neuron Disease Phenotypes by Disrupting Fast Axonal Transport in Drosophila. Genetics *144*, 1075.
Hutagalung, A.H., and Novick, P.J. (2011). Role of Rab GTPases in Membrane Traffic and Cell Physiology. Physiological Reviews *91*, 119-149.
Hutchinson, K.M., Vonhoff, F., and Duch, C. (2014). Dscam1 Is Required for Normal Dendrite Growth and Branching But Not for Dendritic Spacing in Drosophila Motoneurons. Journal of Neuroscience *34*, 1924-1931.
Iwai, Y., Usui, T., Hirano, S., Steward, R., Takeichi, M., and Uemura, T. (1997). Axon Patterning Requires D N-cadherin, a Novel Neuronal Adhesion Receptor, in the Drosophila Embryonic CNS. Neuron *19*, 77-89.
Iwasa, J.H., and Mullins, R.D. (2007). Spatial and Temporal Relationships between Actin-Filament Nucleation, Capping, and Disassembly. Current Biology *17*, 395-406.
Iyer, S.C., Iyer, E.P.R., Meduri, R., Rubaharan, M., Kuntimaddi, A., Karamsetty, M., and Cox, D.N. (2013). Cut, via CrebA, transcriptionally regulates the COPII secretory pathway to direct dendrite development in Drosophila. Journal of Cell Science *126*, 4732-4745.
Jan, L.Y., and Jan, Y.N. (1982). Antibodies to Horseradish-Peroxidase as Specific Neuronal Markers in Drosophila and in Grasshopper Embryos. P Natl Acad Sci-Biol *79*, 2700-2704.
Jan, Y.N., and Jan, L.Y. (1994). Genetic control of cell fate specification in Drosophila peripheral nervous system. Annu Rev Genet *28*, 373-393.
Jan, Y.N., and Jan, L.Y. (2010). Branching out: mechanisms of dendritic arborization (vol 11, pg 316, 2010). Nature Reviews Neuroscience *11*.
Jarman, A.P., Grau, Y., Jan, L.Y., and Jan, Y.N. (1993). ATONAL IS A PRONEURAL GENE THAT DIRECTS CHORDOTONAL ORGAN FORMATION IN THE DROSOPHILA PERIPHERAL NERVOUS-SYSTEM. Cell *73*, 1307-1321.
Jarman, A.P., Grell, E.H., Ackerman, L., Jan, L.Y., and Jan, Y.N. (1994). Atonal is the proneural gene for Drosophila photoreceptors. Nature *369*, 398-400.
Jinushi-Nakao, S., Arvind, R., Amikura, R., Kinameri, E., Liu, A.W., and Moore, A.W. (2007). Knot/Collier and Cut Control Different Aspects of Dendrite Cytoskeleton and Synergize to Define Final Arbor Shape. Neuron *56*, 963-978.

Jones, F.S., and Jones, P.L. (2000). The tenascin family of ECM glycoproteins: structure, function, and regulation during embryonic development and tissue remodeling. Dev Dyn *218*, 235-259.
Kamiguchi, H., Hlavin, M.L., and Lemmon, V. (1998). Role of L1 in Neural Development: What the Knockouts Tell Us. Molecular and Cellular Neuroscience *12*, 48-55.
Kanca, O., Caussinus, E., Denes, A.S., Percival-Smith, A., and Affolter, M. (2014). Raeppli: a whole-tissue labeling tool for live imaging of Drosophila development. Development *141*, 472-480.
Kang, J., Lemaire, H.-G., Unterbeck, A., Salbaum, J.M., Masters, C.L., Grzeschik, K.-H., Multhaup, G., Beyreuther, K., and Müller-Hill, B. (1987). The precursor of Alzheimer's disease amyloid A4 protein resembles a cell-surface receptor. Nature *325*, 733-736.
Kantarjian, H.M., Giles, F., Gattermann, N., Bhalla, K., Alimena, G., Palandri, F., Ossenkoppele, G.J., Nicolini, F.E., O'Brien, S.G., Litzow, M., *et al.* (2007). Nilotinib (formerly AMN107), a highly selective BCR-ABL tyrosine kinase inhibitor, is effective in patients with Philadelphia chromosome-positive chronic myelogenous leukemia in chronic phase following imatinib resistance and intolerance. Blood *110*, 3540-3546.
Kelliher, M.T., Yue, Y., Ng, A., Kamiyama, D., Huang, B., Verhey, K.J., and Wildonger, J. (2018). Autoinhibition of kinesin-1 is essential to the dendrite-specific localization of Golgi outposts. The Journal of Cell Biology *217*, 2531.
Kim, J.H., Wang, X., Coolon, R., and Ye, B. (2013). Dscam Expression Levels Determine Presynaptic Arbor Sizes in Drosophila Sensory Neurons. Neuron *78*, 827-838.
Kim, M.D., Jan, L.Y., and Jan, Y.N. (2006). The bHLH-PAS protein Spineless is necessary for the diversification of dendrite morphology of Drosophila dendritic arborization neurons. Genes & Development *20*, 2806-2819.
Kiryushko, D., Berezin, V., and Bock, E. (2004). Regulators of neurite outgrowth: role of cell adhesion molecules. Ann N Y Acad Sci *1014*, 140-154.
Koch, M., Nicolas, M., Zschaetzsch, M., de Geest, N., Claeys, A., Yan, J.K., Morgan, M.J., Erfurth, M.L., Holt, M., Schmucker, D., *et al.* (2018). A Fat-Facets-Dscaml-JNK Pathway Enhances Axonal Growth in Development and after Injury. Frontiers in Cellular Neuroscience *11*.
Koizumi, H., and Gleeson, J.G. (2009). Sun Proteins Enlighten Nuclear Movement in Development. Neuron *64*, 147-149.
Korobova, F., and Svitkina, T. (2008). Arp2/3 Complex Is Important for Filopodia Formation, Growth Cone Motility, and Neuritogenesis in Neuronal Cells. Molecular Biology of the Cell *19*, 1561-1574.
Krause, M., Dent, E.W., Bear, J.E., Loureiro, J.J., and Gertler, F.B. (2003). Ena/VASP Proteins: Regulators of the Actin Cytoskeleton and Cell Migration. Annual Review of Cell and Developmental Biology *19*, 541-564.
Kretzschmar, K., and Watt, F.M. (2012). Lineage Tracing. Cell *148*, 33-45.
Lai, E.C., and Orgogozo, V. (2004). A hidden program in Drosophila peripheral neurogenesis revealed: fundamental principles underlying sensory organ diversity. Developmental Biology *269*, 1-17.
Lai, S.-L., and Lee, T. (2006). Genetic mosaic with dual binary transcriptional systems in Drosophila. Nature Neuroscience *9*, 703-709.
Lee, C.-H., Herman, T., Clandinin, T.R., Lee, R., and Zipursky, S.L. (2001). N-Cadherin Regulates Target Specificity in the Drosophila Visual System. Neuron *30*, 437-450.

Lee, D.F., Chen, C.C., Hsu, T.A., and Juang, J.L. (2000). A baculovirus superinfection system: Efficient vehicle for gene transfer into Drosophila S2 cells. Journal of Virology *74*, 11873-11880.
Lee, T., and Luo, L.Q. (1999). Mosaic analysis with a repressible cell marker for studies of gene function in neuronal morphogenesis. Neuron *22*, 451-461.
Leterrier, C., Vacher, H., Fache, M.-P., Ortoli, S.A., Castets, F., Autillo-Touati, A., and Dargent, B. (2011). End-binding proteins EB3 and EB1 link microtubules to ankyrin G in the axon initial segment. Proceedings of the National Academy of Sciences *108*, 8826.
Lewis Jr, T.L., Mao, T., Svoboda, K., and Arnold, D.B. (2009). Myosin-dependent targeting of transmembrane proteins to neuronal dendrites. Nature Neuroscience *12*, 568.
Lewis, T.L., Jr., Mao, T., and Arnold, D.B. (2011). A Role for Myosin VI in the Localization of Axonal Proteins. PLOS Biology *9*, e1001021.
Leyssen, M., Ayaz, D., Hebert, S.S., Reeve, S., De Strooper, B., and Hassan, B.A. (2005). Amyloid precursor protein promotes post-developmental neurite arborization in the Drosophila brain. Embo Journal *24*, 2944-2955.
Lhamo, T., and Ismat, A. (2015). The extracellular protease stl functions to inhibit migration of v'ch1 sensory neuron during Drosophila embryogenesis. Mechanisms of Development *137*, 1-10.
Li, H.S., Chen, J.H., Wu, W., Fagaly, T., Zhou, L., Yuan, W., Dupuis, S., Jiang, Z.H., Nash, W., Gick, C., *et al.* (1999). Vertebrate slit, a secreted ligand for the transmembrane protein roundabout, is a repellent for olfactory bulb axons. Cell *96*, 807-818.
Li, W., Wang, F., Menut, L., and Gao, F.-B. (2004). BTB/POZ-Zinc Finger Protein Abrupt Suppresses Dendritic Branching in a Neuronal Subtype-Specific and Dosage-Dependent Manner. Neuron *43*, 823-834.
Lindsay, R.M. (1988). Nerve growth factors (NGF, BDNF) enhance axonal regeneration but are not required for survival of adult sensory neurons. The Journal of Neuroscience *8*, 2394.
Lindsay, R.M., Thoenen, H., and Barde, Y.-A. (1985). Placode and neural crest-derived sensory neurons are responsive at early developmental stages to brain-derived neurotrophic factor. Developmental Biology *112*, 319-328.
Livet, J., Weissman, T.A., Kang, H., Draft, R.W., Lu, J., Bennis, R.A., Sanes, J.R., and Lichtman, J.W. (2007). Transgenic strategies for combinatorial expression of fluorescent proteins in the nervous system. Nature *450*, 56-62.
Loulier, K., Barry, R., Mahou, P., Le Franc, Y., Supatto, W., Matho, K.S., Ieng, S.H., Fouquet, S., Dupin, E., Benosman, R., *et al.* (2014). Multiplex Cell and Lineage Tracking with Combinatorial Labels. Neuron *81*, 505-520.
Lowe, S.A., Hodge, J.J.L., and Usowicz, M.M. (2018). A third copy of the Down syndrome cell adhesion molecule (Dscam) causes synaptic and locomotor dysfunction in Drosophila. Neurobiology of Disease *110*, 93-101.
Lowery, L.A., and Van Vactor, D. (2009). The trip of the tip: understanding the growth cone machinery. Nature reviews Molecular cell biology *10*, 332-343.
Luo, L. (2002). Actin Cytoskeleton Regulation in Neuronal Morphogenesis and Structural Plasticity. Annual Review of Cell and Developmental Biology *18*, 601-635.
Manning, L., and Doe, C.Q. (1999). Prospero distinguishes sibling cell fate without asymmetric localization in the Drosophila adult external sense organ lineage. Development *126*, 2063.
Markstein, M., Pitsouli, C., Villalta, C., Celniker, S.E., and Perrimon, N. (2008). Exploiting position effects and the gypsy retrovirus insulator to engineer precisely expressed transgenes. Nature Genetics *40*, 476-483.

Matsuda, S., Baluk, P., Shimizu, D., and Fujiwara, T. (1996). Dorsal root ganglion neuron development in chick and rat. Anatomy and Embryology *193*, 475-480.
Matthews, B.J., Kim, M.E., Flanagan, J.J., Hattori, D., Clemens, J.C., Zipursky, S.L., and Grueber, W.B. (2007). Dendrite self-avoidance is controlled by Dscam. Cell *129*, 593-604.
Matusek, T., Gombos, R., Szecsenyi, A., Sanchez-Soriano, N., Czibula, A., Pataki, C., Gedai, A., Prokop, A., Rasko, I., and Mihaly, J. (2008). Formin proteins of the DAAM subfamily play a role during axon growth. J Neurosci *28*, 13310-13319.
Mcleod, M., Craft, S., and Broach, J.R. (1986). Identification of the Crossover Site during Flp-Mediated Recombination in the Saccharomyces-Cerevisiae Plasmid 2-Mu-M Circle. Molecular and cellular biology *6*, 3357-3367.
Millard, S.S., Flanagan, J.J., Pappu, K.S., Wu, W., and Zipursky, S.L. (2007). Dscam2 mediates axonal tiling in the Drosophila visual system. Nature *447*, 720-U714.
Millard, S.S., Lu, Z.Y., Zipursky, S.L., and Meinertzhagen, I.A. (2010). Drosophila Dscam Proteins Regulate Postsynaptic Specificity at Multiple-Contact Synapses. Neuron *67*, 761-768.
Miyamoto, S., Teramoto, H., Gutkind, J.S., and Yamada, K.M. (1996). Integrins can collaborate with growth factors for phosphorylation of receptor tyrosine kinases and MAP kinase activation: roles of integrin aggregation and occupancy of receptors. J Cell Biol *135*, 1633-1642.
Monahan, K., Horta, A., and Lomvardas, S. (2019). LHX2- and LDB1-mediated trans interactions regulate olfactory receptor choice. Nature *565*, 448-453.
Monahan, K., Schieren, I., Cheung, J., Mumbey-Wafula, A., Monuki, E.S., and Lomvardas, S. (2017). Cooperative interactions enable singular olfactory receptor expression in mouse olfactory neurons. eLife *6*, e28620.
Moore, A.W., Jan, L.Y., and Jan, Y.N. (2002). hamlet, a binary genetic switch between single- and multiple-dendrite neuron morphology. Science *297*, 1355-1358.
Moore, A.W., Roegiers, F., Jan, L.Y., and Jan, Y.-N. (2004). Conversion of neurons and glia to external-cell fates in the external sensory organs of Drosophila hamlet mutants by a cousin-cousin cell-type respecification. Genes & development *18*, 623-628.
Mora, N., Almudi, I., Alsina, B., Corominas, M., and Serras, F. (2013). beta amyloid protein precursor-like (Appl) is a Ras1/MAPK-regulated gene required for axonal targeting in Drosophila photoreceptor neurons. J Cell Sci *126*, 53-59.
Morris, N.R. (2000). Nuclear Migration. The Journal of Cell Biology *148*, 1097.
Nadarajah, B., Brunstrom, J.E., Grutzendler, J., Wong, R.O.L., and Pearlman, A.L. (2001). Two modes of radial migration in early development of the cerebral cortex. Nature Neuroscience *4*, 143-150.
Nakazawa, H., Sada, T., Toriyama, M., Tago, K., Sugiura, T., Fukuda, M., and Inagaki, N. (2012). Rab33a Mediates Anterograde Vesicular Transport for Membrane Exocytosis and Axon Outgrowth. The Journal of Neuroscience *32*, 12712.
Nern, A., Pfeiffer, B.D., and Rubin, G.M. (2015). Optimized tools for multicolor stochastic labeling reveal diverse stereotyped cell arrangements in the fly visual system. Proceedings of the National Academy of Sciences of the United States of America *112*, E2967-E2976.
Nguyen, M.M., Stone, M.C., and Rolls, M.M. (2011). Microtubules are organized independently of the centrosome in Drosophila neurons. Neural development *6*, 38-38.
Nichols, T., and Holmes, A. (2007). Non-parametric procedures. Statistical Parametric Mapping: The Analysis of Functional Brain Images, 253-272.
Nichols, T.E., and Holmes, A.P. (2002). Nonparametric permutation tests for functional neuroimaging: A primer with examples. Hum Brain Mapp *15*, 1-25.

Niethammer, M., Smith, D.S., Ayala, R., Peng, J., Ko, J., Lee, M.-S., Morabito, M., and Tsai, L.-H. (2000). NUDEL Is a Novel Cdk5 Substrate that Associates with LIS1 and Cytoplasmic Dynein. Neuron *28*, 697-711.
Ohyama, T., Schneider-Mizell, C.M., Fetter, R.D., Aleman, J.V., Franconville, R., Rivera-Alba, M., Mensh, B.D., Branson, K.M., Simpson, J.H., Truman, J.W., *et al.* (2015). A multilevel multimodal circuit enhances action selection in Drosophila. Nature *520*, 633-639.
Orgogozo, V., and Grueber, W.B. (2005). FlyPNS, a database of the Drosophila embryonic and larval peripheral nervous system. BMC Developmental Biology *5*, 4.
Orgogozo, V., Schweisguth, F., and Bellaiche, Y. (2001). Lineage, cell polarity and inscuteable function in the peripheral nervous system of the Drosophila embryo. Development *128*, 631.
Ori-McKenney, Kassandra M., Jan, Lily Y., and Jan, Y.-N. (2012). Golgi Outposts Shape Dendrite Morphology by Functioning as Sites of Acentrosomal Microtubule Nucleation in Neurons. Neuron *76*, 921-930.
Pan, Y.A., Freundlich, T., Weissman, T.A., Schoppik, D., Wang, X.C., Zimmerman, S., Ciruna, B., Sanes, J.R., Lichtman, J.W., and Schier, A.F. (2013). Zebrabow: multispectral cell labeling for cell tracing and lineage analysis in zebrafish. Development *140*, 2835-2846.
Papaioannou, V.E. (2016). Concepts of Cell Lineage in Mammalian Embryos. Curr Top Dev Biol *117*, 185-197.
Park, J.H., Attardo, G.M., Hansen, I.A., and Raikhel, A.S. (2006). GATA factor translation is the final downstream step in the amino acid/target-of-rapamycin-mediated vitellogenin gene expression in the anautogenous mosquito Aedes aegypti. Journal of Biological Chemistry *281*, 11167-11176.
Parks, A.L., and Muskavitch, M.A. (1993). Delta Function Is Required for Bristle Organ Determination and Morphogenesis in Drosophila. Developmental Biology *157*, 484-496.
Patterson, K., Molofsky, A.B., Robinson, C., Acosta, S., Cater, C., and Fischer, J.A. (2003). The Functions of Klarsicht and Nuclear Lamin in Developmentally Regulated Nuclear Migrations of Photoreceptor Cells in the Drosophila Eye. Molecular Biology of the Cell *15*, 600-610.
Pfeiffer, B.D., Jenett, A., Hammonds, A.S., Ngo, T.T.B., Misra, S., Murphy, C., Scully, A., Carlson, J.W., Wan, K.H., Laverty, T.R., *et al.* (2008). Tools for neuroanatomy and neurogenetics in Drosophila. Proceedings of the National Academy of Sciences of the United States of America *105*, 9715-9720.
Pfeiffer, B.D., Ngo, T.T.B., Hibbard, K.L., Murphy, C., Jenett, A., Truman, J.W., and Rubin, G.M. (2010). Refinement of Tools for Targeted Gene Expression in Drosophila. Genetics *186*, 735-U488.
Pfeiffer, B.D., Truman, J.W., and Rubin, G.M. (2012). Using translational enhancers to increase transgene expression in Drosophila. Proceedings of the National Academy of Sciences of the United States of America *109*, 6626-6631.
Prakash, S., Caldwell, J.C., Eberl, D.F., and Clandinin, T.R. (2005). Drosophila N-cadherin mediates an attractive interaction between photoreceptor axons and their targets. Nature Neuroscience *8*, 443-450.
Pring, M., Evangelista, M., Boone, C., Yang, C., and Zigmond, S.H. (2003). Mechanism of Formin-Induced Nucleation of Actin Filaments. Biochemistry *42*, 486-496.
Rachidi, M., and Lopes, C. (2007). Mental retardation in Down syndrome: From gene dosage imbalance to molecular and cellular mechanisms. Neuroscience Research *59*, 349-369.

Raj, B., Wagner, D.E., McKenna, A., Pandey, S., Klein, A.M., Shendure, J., Gagnon, J.A., and Schier, A.F. (2018). Simultaneous single-cell profiling of lineages and cell types in the vertebrate brain. Nature biotechnology *36*, 442-+.
Rall, W. (1964). Theoretical significance of dendritic trees for neuronal input-output relations. In: The theoretical foundation of dendritic function: selected papers of Wilfrid Rall with commentaries (Cambridge, MA: MIT.).
Ramón y Cajal, S. (1995). Histology of the nervous system of man and vertebrates (New York: Oxford University Press).
Rauvala, H., and Peng, H.B. (1997). HB-GAM (heparin-binding growth-associated molecule) and heparin-type glycans in the development and plasticity of neuron-target contacts. Prog Neurobiol *52*, 127-144.
Razafsky, D., and Hodzic, D. (2009). Bringing KASH under the SUN: the many faces of nucleo-cytoskeletal connections. Journal of Cell Biology *186*, 461-472.
Reeves, R.H., Irving, N.G., Moran, T.H., Wohn, A., Kitt, C., Sisodia, S.S., Schmidt, C., Bronson, R.T., and Davisson, M.T. (1995). A mouse model for Down syndrome exhibits learning and behaviour deficits. Nature Genetics *11*, 177-184.
Reiner, O., Carrozzo, R., Shen, Y., Wehnert, M., Faustinella, F., Dobyns, W.B., Caskey, C.T., and Ledbetter, D.H. (1993). Isolation of a Miller–Dicker lissencephaly gene containing G protein β-subunit-like repeats. Nature *364*, 717-721.
Richier, B., and Salecker, I. (2015a). Versatile genetic paintbrushes: Brainbow technologies. Wiley Interdisciplinary Reviews-Developmental Biology *4*, 161-180.
Richier, B., and Salecker, I. (2015b). Versatile genetic paintbrushes: Brainbow technologies. Wiley Interdiscip Rev Dev Biol *4*, 161-180.
Rodriguez, I., Hernandez, R., Modolell, J., and Ruiz-Gomez, M. (1990). Competence to develop sensory organs is temporally and spatially regulated in Drosophila epidermal primordia. Embo j *9*, 3583-3592.
Rohatgi, R., Ma, L., Miki, H., Lopez, M., Kirchhausen, T., Takenawa, T., and Kirschner, M.W. (1999). The interaction between N-WASP and the Arp2/3 complex links Cdc42-dependent signals to actin assembly. Cell *97*, 221-231.
Romani, S., Campuzano, S., Macagno, E.R., and Modolell, J. (1989). Expression of achaete and scute genes in Drosophila imaginal discs and their function in sensory organ development. Genes Dev *3*, 997-1007.
Rothberg, J.M., Hartley, D.A., Walther, Z., and Artavanis-Tsakonas, S. (1988). slit: an EGF-homologous locus of D. melanogaster involved in the development of the embryonic central nervous system. Cell *55*, 1047-1059.
Sakaue-Sawano, A., Kurokawa, H., Morimura, T., Hanyu, A., Hama, H., Osawa, H., Kashiwagi, S., Fukami, K., Miyata, T., Miyoshi, H., *et al.* (2008). Visualizing spatiotemporal dynamics of multicellular cell-cycle progression. Cell *132*, 487-498.
Salzberg, A., Develyn, D., Schulze, K.L., Lee, J.K., Strumpf, D., Tsai, L., and Bellen, H.J. (1994). MUTATIONS AFFECTING THE PATTERN OF THE PNS IN DROSOPHILA REVEAL NOVEL ASPECTS OF NEURONAL DEVELOPMENT. Neuron *13*, 269-287.
Sann, S., Wang, Z., Brown, H., and Jin, Y. (2009). Roles of endosomal trafficking in neurite outgrowth and guidance. Trends Cell Biol *19*, 317-324.
Satoh, D., Sato, D., Tsuyama, T., Saito, M., Ohkura, H., Rolls, M.M., Ishikawa, F., and Uemura, T. (2008). Spatial control of branching within dendritic arbors by dynein-dependent transport of Rab5-endosomes. Nat Cell Biol *10*, 1164-1171.

Schindelin, J., Arganda-Carreras, I., Frise, E., Kaynig, V., Longair, M., Pietzsch, T., Preibisch, S., Rueden, C., Saalfeld, S., Schmid, B., *et al.* (2012). Fiji: an open-source platform for biological-image analysis. Nature methods *9*, 676-682.
Schlake, T., and Bode, J. (1994). Use of Mutated Flp Recognition Target (Frt) Sites for the Exchange of Expression Cassettes at Defined Chromosomal Loci. Biochemistry *33*, 12746-12751.
Schmidt, H., Rickert, C., Bossing, T., Vef, O., Urban, J., and Technau, G.M. (1997). The embryonic central nervous system lineages of Drosophila melanogaster .2. Neuroblast lineages derived from the dorsal part of the neuroectoderm. Developmental biology *189*, 186-204.
Schmidt, S.T., Zimmerman, S.M., Wang, J.B., Kini, S.K., and Quake, S.R. (2017). Quantitative Analysis of Synthetic Cell Lineage Tracing Using Nuclease Barcoding. Acs Synth Biol *6*, 936-942.
Schmidt-Rhaesa, A., Harzsch, S., and Purschke, G. (2015). Structure and Evolution of Invertebrate Nervous Systems (Oxford: Oxford University Press).
Schroer, T.A., Steuer, E.R., and Sheetz, M.P. (1989). Cytoplasmic dynein is a minus end-directed motor for membranous organelles. Cell *56*, 937-946.
Schweisguth, F., Gho, M., and Lecourtois, M. (1996). Control of cell fate choices by lateral signaling in the adult peripheral nervous system of Drosophila melanogaster. Developmental Genetics *18*, 28-39.
Seeger, M., Tear, G., Ferres-Marco, D., and Goodman, C.S. (1993). Mutations affecting growth cone guidance in Drosophila: genes necessary for guidance toward or away from the midline. Neuron *10*, 409-426.
Seno, T., Ikeno, T., Mennya, K., Kurishita, M., Sakae, N., Sato, M., Takada, H., and Konishi, Y. (2016). Kinesin-1 sorting in axons controls the differential retraction of arbor terminals. Journal of Cell Science *129*, 3499.
Sexton, T., Yaffe, E., Kenigsberg, E., Bantignies, F., Leblanc, B., Hoichman, M., Parrinello, H., Tanay, A., and Cavalli, G. (2012). Three-Dimensional Folding and Functional Organization Principles of the Drosophila Genome. Cell *148*, 458-472.
Shaner, N.C., Lambert, G.G., Chammas, A., Ni, Y.H., Cranfill, P.J., Baird, M.A., Sell, B.R., Allen, J.R., Day, R.N., Israelsson, M., *et al.* (2013). A bright monomeric green fluorescent protein derived from Branchiostoma lanceolatum. Nature methods *10*, 407-+.
Shcherbo, D., Murphy, C.S., Ermakova, G.V., Solovieva, E.A., Chepurnykh, T.V., Shcheglov, A.S., Verkhusha, V.V., Pletnev, V.Z., Hazelwood, K.L., Roche, P.M., *et al.* (2009). Far-red fluorescent tags for protein imaging in living tissues. Biochemical Journal *418*, 567-574.
Sherman, L.S., Struve, J.N., Rangwala, R., Wallingford, N.M., Tuohy, T.M.F., and Kuntz Iv, C. (2002). Hyaluronate-based extracellular matrix: Keeping glia in their place. Glia *38*, 93-102.
Shu, T., Ayala, R., Nguyen, M.-D., Xie, Z., Gleeson, J.G., and Tsai, L.-H. (2004). Ndel1 Operates in a Common Pathway with LIS1 and Cytoplasmic Dynein to Regulate Cortical Neuronal Positioning. Neuron *44*, 263-277.
Siegal, M.L., and Hartl, D.L. (1996). Transgene Coplacement and high efficiency site-specific recombination with the Cre/loxP system in Drosophila. Genetics *144*, 715-726.
Simonis, M., Klous, P., Splinter, E., Moshkin, Y., Willemsen, R., de Wit, E., van Steensel, B., and de Laat, W. (2006). Nuclear organization of active and inactive chromatin domains uncovered by chromosome conformation capture–on-chip (4C). Nature Genetics *38*, 1348-1354.
Sinet, P.M., Theophile, D., Rahmani, Z., Chettouh, Z., Blouin, J.L., Prieur, M., Noel, B., and Delabar, J.M. (1994). MAPPING OF THE DOWN-SYNDROME PHENOTYPE ON

CHROMOSOME-21 AT THE MOLECULAR-LEVEL. Biomedicine & Pharmacotherapy *48*, 247-252.
Singhania, A., and Grueber, W.B. (2014). Development of the embryonic and larval peripheral nervous system of Drosophila. Wiley Interdisciplinary Reviews-Developmental Biology *3*, 193-210.
Smyth Gordon, K. (2004). Linear Models and Empirical Bayes Methods for Assessing Differential Expression in Microarray Experiments. In Statistical Applications in Genetics and Molecular Biology, pp. 1.
Soldano, A., Okray, Z., Janovska, P., Tmejova, K., Reynaud, E., Claeys, A., Yan, J.K., Atak, Z.K., De Strooper, B., Dura, J.M., *et al.* (2013). The Drosophila Homologue of the Amyloid Precursor Protein Is a Conserved Modulator of Wnt PCP Signaling. Plos Biology *11*.
Song, A.-h., Wang, D., Chen, G., Li, Y., Luo, J., Duan, S., and Poo, M.-m. (2009). A Selective Filter for Cytoplasmic Transport at the Axon Initial Segment. Cell *136*, 1148-1160.
Sosa, L.J., Caceres, A., Dupraz, S., Oksdath, M., Quiroga, S., and Lorenzo, A. (2017). The physiological role of the amyloid precursor protein as an adhesion molecule in the developing nervous system. J Neurochem *143*, 11-29.
Sosa, L.J., Postma, N.L., Estrada-Bernal, A., Hanna, M., Guo, R., Busciglio, J., and Pfenninger, K.H. (2013). Dosage of amyloid precursor protein affects axonal contact guidance in Down syndrome. The FASEB Journal *28*, 195-205.
Sotelo, C., and Dusart, I. (2009). Intrinsic versus extrinsic determinants during the development of Purkinje cell dendrites. Neuroscience *162*, 589-600.
Spanjaard, B., Hu, B., Mitic, N., Olivares-Chauvet, P., Janjuha, S., Ninov, N., and Junker, J.P. (2018). Simultaneous lineage tracing and cell-type identification using CRISPR-Cas9-induced genetic scars. Nature biotechnology *36*, 469-+.
Spitz, F. (2016). Gene regulation at a distance: From remote enhancers to 3D regulatory ensembles. Seminars in Cell & Developmental Biology *57*, 57-67.
Spruston, N. (2008). Pyramidal neurons: dendritic structure and synaptic integration. Nature Reviews Neuroscience *9*, 206-221.
Stent, G.S. (1985). The Role of Cell Lineage in Development. Philos T Roy Soc B *312*, 3-19.
Stepanova, T., Slemmer, J., Hoogenraad, C.C., Lansbergen, G., Dortland, B., De Zeeuw, C.I., Grosveld, F., van Cappellen, G., Akhmanova, A., and Galjart, N. (2003). Visualization of microtubule growth in cultured neurons via the use of EB3-GFP (end-binding protein 3-green fluorescent protein). J Neurosci *23*, 2655-2664.
Sterne, G.R., Kim, J.H., and Ye, B. (2015). Dysregulated Dscam levels act through Abelson tyrosine kinase to enlarge presynaptic arbors. Elife *4*.
Stone, M.C., Roegiers, F., and Rolls, M.M. (2008). Microtubules Have Opposite Orientation in Axons and Dendrites of Drosophila Neurons. Molecular Biology of the Cell *19*, 4122-4129.
Strausfeld, N.J. (1976). Atlas of an insect brain (Berlin ; New York: Springer-Verlag).
Stuart, G., Spruston, N., and Häusser, M. (1999). Dendrites (Oxford ; New York: Oxford University Press).
Sturtevant, A.H. (1929). The claret mutant type of Drosophila simulans: a study of chromosome elimination and of cell-lineage. Zeitschrift Fur Wissenschaftliche Zoologie *135*, 323-356.
Sugimura, K., Satoh, D., Estes, P., Crews, S., and Uemura, T. (2004). Development of Morphological Diversity of Dendrites in Drosophila by the BTB-Zinc Finger Protein Abrupt. Neuron *43*, 809-822.

Swanson, C.I., Hinrichs, T., Johnson, L.A., Zhao, Y., and Barolo, S. (2008). A directional recombination cloning system for restriction- and ligation-free construction of GFP, DsRed, and lacZ transgenic Drosophila reporters. Gene *408*, 180-186.
Taghert, P.H., Hewes, R.S., Park, J.H., Brien, M.A., Han, M., and Peck, M.E. (2001). Multiple Amidated Neuropeptides Are Required for Normal Circadian Locomotor Rhythms in Drosophila. The Journal of Neuroscience *21*, 6673.
Testa-Silva, G., Loebel, A., Giugliano, M., de Kock, C.P.J., Mansvelder, H.D., and Meredith, R.M. (2012). Hyperconnectivity and Slow Synapses during Early Development of Medial Prefrontal Cortex in a Mouse Model for Mental Retardation and Autism. Cerebral Cortex *22*, 1333-1342.
Truman, J.W., and Bate, M. (1988). Spatial and temporal patterns of neurogenesis in the central nervous system of Drosophila melanogaster. Developmental biology *125*, 145-157.
Tsai, J.-W., Bremner, K.H., and Vallee, R.B. (2007). Dual subcellular roles for LIS1 and dynein in radial neuronal migration in live brain tissue. Nature Neuroscience *10*, 970.
Tsai, J.-W., Chen, Y., Kriegstein, A.R., and Vallee, R.B. (2005). LIS1 RNA interference blocks neural stem cell division, morphogenesis, and motility at multiple stages. The Journal of Cell Biology *170*, 935.
Turan, S., Kuehle, J., Schambach, A., Baum, C., and Bode, J. (2010). Multiplexing RMCE: Versatile Extensions of the Flp-Recombinase-Mediated Cassette-Exchange Technology. Journal of Molecular Biology *402*, 52-69.
Ulianov, S.V., Khrameeva, E.E., Gavrilov, A.A., Flyamer, I.M., Kos, P., Mikhaleva, E.A., Penin, A.A., Logacheva, M.D., Imakaev, M.V., Chertovich, A., *et al.* (2016). Active chromatin and transcription play a key role in chromosome partitioning into topologically associating domains. Genome Research *26*, 70-84.
Urnavicius, L., Zhang, K., Diamant, A.G., Motz, C., Schlager, M.A., Yu, M., Patel, N.A., Robinson, C.V., and Carter, A.P. (2015). The structure of the dynactin complex and its interaction with dynein. Science *347*, 1441.
Vale, R.D., Schnapp, B.J., Mitchison, T., Steuer, E., Reese, T.S., and Sheetz, M.P. (1985). Different axoplasmic proteins generate movement in opposite directions along microtubules in vitro. Cell *43*, 623-632.
Venken, K.J.T., He, Y.C., Hoskins, R.A., and Bellen, H.J. (2006a). P acman : A BAC transgenic platform for targeted insertion of large DNA fragments in D-melanogaster. Science *314*, 1747-1751.
Venken, K.J.T., He, Y.C., Hoskins, R.A., and Bellen, H.J. (2006b). P[acman]: A BAC transgenic platform for targeted insertion of large DNA fragments in D-melanogaster. Science (New York, NY *314*, 1747-1751.
Verhey, K.J., and Hammond, J.W. (2009). Traffic control: regulation of kinesin motors. Nature Reviews Molecular Cell Biology *10*, 765.
Verheyen, E.M., and Cooley, L. (1994). Profilin mutations disrupt multiple actin-dependent processes during Drosophila development. Development *120*, 717.
Villarroel-Campos, D., Bronfman, F.C., and Gonzalez-Billault, C. (2016). Rab GTPase signaling in neurite outgrowth and axon specification. Cytoskeleton (Hoboken) *73*, 498-507.
Volkert, F.C., and Broach, J.R. (1986). Site-Specific Recombination Promotes Plasmid Amplification in Yeast. Cell *46*, 541-550.

Wainman, A., Creque, J., Williams, B., Williams, E.V., Bonaccorsi, S., Gatti, M., and Goldberg, M.L. (2009). Roles of the Drosophila NudE protein in kinetochore function and centrosome migration. Journal of Cell Science *122*, 1747-1758.
Wang, J., Ma, X.J., Yang, J.S., Zheng, X.Y., Zugates, C.T., Lee, C.H.J., and Lee, T. (2004). Transmembrane/juxtamembrane domain-dependent Dscam distribution and function during mushroom body neuronal morphogenesis. Neuron *43*, 663-672.
Wang, J., Zugates, C.T., Liang, I.H., Lee, C.H.J., and Lee, T.M. (2002). Drosophila Dscam is required for divergent segregation of sister branches and suppresses ectopic bifurcation of axons. Neuron *33*, 559-571.
Wang, T., Liu, Y., Xu, X.-H., Deng, C.-Y., Wu, K.-Y., Zhu, J., Fu, X.-Q., He, M., and Luo, Z.-G. (2011). Lgl1 Activation of Rab10 Promotes Axonal Membrane Trafficking Underlying Neuronal Polarization. Developmental Cell *21*, 431-444.
Wang, X., Kim, J.H., Bazzi, M., Robinson, S., Collins, C.A., and Ye, B. (2013). Bimodal Control of Dendritic and Axonal Growth by the Dual Leucine Zipper Kinase Pathway. Plos Biology *11*.
Wang, X., Zhang, M.W., Kim, J.H., Macara, A.M., Sterne, G., Yang, T., and Ye, B. (2015). The Kruppel-Like Factor Dar1 Determines Multipolar Neuron Morphology. J Neurosci *35*, 14251-14259.
Watanabe, K., Al-Bassam, S., Miyazaki, Y., Wandless, Thomas J., Webster, P., and Arnold, Don B. (2012). Networks of Polarized Actin Filaments in the Axon Initial Segment Provide a Mechanism for Sorting Axonal and Dendritic Proteins. Cell Reports *2*, 1546-1553.
Weissman, T.A., and Pan, Y.A. (2015). Brainbow: new resources and emerging biological applications for multicolor genetic labeling and analysis. Genetics *199*, 293-306.
Whyte, Warren A., Orlando, David A., Hnisz, D., Abraham, Brian J., Lin, Charles Y., Kagey, Michael H., Rahl, Peter B., Lee, Tong I., and Young, Richard A. (2013). Master Transcription Factors and Mediator Establish Super-Enhancers at Key Cell Identity Genes. Cell *153*, 307-319.
Winding, M., Kelliher, M.T., Lu, W., Wildonger, J., and Gelfand, V.I. (2016). Role of kinesin-1-based microtubule sliding in Drosophila nervous system development. Proc Natl Acad Sci U S A *113*, E4985-4994.
Wong, K., Ren, X.R., Huang, Y.Z., Xie, Y., Liu, G., Saito, H., Tang, H., Wen, L., Brady-Kalnay, S.M., Mei, L., *et al.* (2001). Signal transduction in neuronal migration: roles of GTPase activating proteins and the small GTPase Cdc42 in the Slit-Robo pathway. Cell *107*, 209-221.
Woodworth, M.B., Girskis, K.M., and Walsh, C.A. (2017). Building a lineage from single cells: genetic techniques for cell lineage tracking. Nature Reviews Genetics *18*, 230-244.
Worley, M.I., Setiawan, L., and Hariharan, I.K. (2013). TIE-DYE: a combinatorial marking system to visualize and genetically manipulate clones during development in Drosophila melanogaster. Development *140*, 3275-3284.
Xu, K., Zhong, G., and Zhuang, X. (2013). Actin, Spectrin, and Associated Proteins Form a Periodic Cytoskeletal Structure in Axons. Science *339*, 452.
Yamakawa, K., Huo, Y.-K., Haendel, M.A., Hubert, R., Chen, X.-N., Lyons, G.E., and Korenberg, J.R. (1998). DSCAM: A Novel Member of the Immunoglobulin Superfamily Maps in a Down Syndrome Region and is Involved in the Development of the Nervous System. Human Molecular Genetics *7*, 227-237.
Yang, L., and Bashaw, G.J. (2006). Son of sevenless directly links the Robo receptor to rac activation to control axon repulsion at the midline. Neuron *52*, 595-607.

Yang, L., Li, R., Kaneko, T., Takle, K., Morikawa, Rei K., Essex, L., Wang, X., Zhou, J., Emoto, K., Xiang, Y., *et al.* (2014). Trim9 Regulates Activity-Dependent Fine-Scale Topography in Drosophila. Current Biology *24*, 1024-1030.
Ye, B., Kim, J.H., Yang, L., McLachlan, I., Younger, S., Jan, L.Y., and Jan, Y.N. (2011). Differential Regulation of Dendritic and Axonal Development by the Novel Kruppel-Like Factor Dar1. Journal of Neuroscience *31*, 3309-3319.
Ye, B., Zhang, Y., Song, W., Younger, S.H., Jan, L.Y., and Jan, Y.N. (2007). Growing Dendrites and Axons Differ in Their Reliance on the Secretory Pathway. Cell *130*, 717-729.
Younossi-Hartenstein, A., and Hartenstein, V. (1997). Pattern, time of birth, and morphogenesis of sensillum progenitors in Drosophila. Microsc Res Tech *39*, 479-491.
Yuan, J.S., Reed, A., Chen, F., and Stewart, C.N. (2006). Statistical analysis of real-time PCR data. Bmc Bioinformatics *7*.
Zabidi, M.A., Arnold, C.D., Schernhuber, K., Pagani, M., Rath, M., Frank, O., and Stark, A. (2014). Enhancer–core-promoter specificity separates developmental and housekeeping gene regulation. Nature *518*, 556.
Zabidi, M.A., and Stark, A. (2016). Regulatory Enhancer–Core-Promoter Communication via Transcription Factors and Cofactors. Trends in Genetics *32*, 801-814.
Zhang, X., Lei, K., Yuan, X., Wu, X., Zhuang, Y., Xu, T., Xu, R., and Han, M. (2009). SUN1/2 and Syne/Nesprin-1/2 Complexes Connect Centrosome to the Nucleus during Neurogenesis and Neuronal Migration in Mice. Neuron *64*, 173-187.
Zheng, H., Jiang, M., Trumbauer, M.E., Sirinathsinghji, D.J.S., Hopkins, R., Smith, D.W., Heavens, R.P., Dawson, G.R., Boyce, S., Conner, M.W., *et al.* (1995). β-amyloid precursor protein-deficient mice show reactive gliosis and decreased locomotor activity. Cell *81*, 525-531.
Zheng, Y., Wildonger, J., Ye, B., Zhang, Y., Kita, A., Younger, S.H., Zimmerman, S., Jan, L.Y., and Jan, Y.N. (2008). Dynein is required for polarized dendritic transport and uniform microtubule orientation in axons. Nature Cell Biology *10*, 1172.
Zhu, H., and Luo, L. (2004). Diverse Functions of N-Cadherin in Dendritic and Axonal Terminal Arborization of Olfactory Projection Neurons. Neuron *42*, 63-75.
Zigman, W.B., Devenny, D.A., Krinsky-McHale, S.J., Jenkins, E.C., Urv, T.K., Wegiel, J., Schupf, N., and Silverman, W. (2008). Chapter 4 Alzheimer's Disease in Adults with Down Syndrome. In International Review of Research in Mental Retardation (Academic Press), pp. 103-145.